Functional characterization of the antimicrobial activity of synthetic callyaerins against *Mycobacterium tuberculosis*

Inaugural dissertation

for the attainment of the title of doctor
in the Faculty of Mathematics and Natural Sciences
at the Heinrich Heine University Düsseldorf

presented by

Yvonne Gröner

from Düsseldorf

Düsseldorf, March 2020

from the Institute of Pharmaceutical Biology and Biotechnology
at the Heinrich Heine University Düsseldorf

Published by permission of the
Faculty of Mathematics and Natural Sciences at
Heinrich Heine University Düsseldorf

Supervisor: Prof. Dr. Rainer Kalscheuer

Co-supervisor: Prof. Dr. Dr. h. c. Peter Proksch

Date of oral examination: May 27th, 2020

Abstract

Tuberculosis (TB), caused by *Mycobacterium tuberculosis (M. tuberculosis)*, is still one of the top ten causes of deaths worldwide. With 1.4 million deaths in 2018, TB is the leading cause of deaths from a single infectious pathogen. Drug resistance of *M. tuberculosis* represents a major challenge. In the last decades, extensively drug-resistant and totally drug-resistant phenotypes have emerged that nearly leave no treatment opportunities. This situation is exacerbated by the hesitance and diffidence in the development of new drugs. To control the global spread of TB, new drugs are urgently needed. Nature and its magnitude of products represent a rich source of new active compounds, underlined by a long history as antibiotics. Among the different classes of natural products, cyclic peptides stick out due to their three-dimensional structure, resulting in strong interaction with their molecular targets. Furthermore, cyclic peptides are relatively easy to synthesize overcoming the problem of product availability of many other natural products. In this study, a library of synthetic cyclic peptides belonging to the callyaerin family was investigated to elucidate their selective growth-inhibiting activity against *M. tuberculosis*. Besides revealing the indispensability of the cyclic structure, the bulky hydrophobic chemical properties of callyaerins were found to be essential for their activity. The strong growth inhibition of *M. tuberculosis* in low micromolar concentrations combined with a lack of cytotoxic side effects qualify callyaerins as new drug leads. By application of an affinity enrichment approach employing biotinylated callyaerins, hypoxic response protein 1 (Hrp1), a protein involved in bacterial dormancy, was identified as an interaction partner. Following contact with Hrp1, a protein cascade might be triggered resulting in reduced metabolism and suppressed replication of the bacteria and thereby causing a bacteriostatic effect of callyaerins. Furthermore, the membrane protein Rv2113 was identified as an essential determinant of activity and resistance, likely mediating cell wall permeation of callyaerins in *M. tuberculosis*. Heterologous expression of this membrane protein in other mycobacteria led to a strong sensitization against callyaerins. Rv2113 therefore might be exploited as a potential carrier system for callyaerin conjugates with compounds that otherwise fail to pass the complex cell wall structure of *M. tuberculosis*. In a proof of principle experiment, the exceptional selective activity of a fluorescent Cy3_CalA conjugate substantiated the capability of extending the callyaerin core structure with bulky moieties without impairing activity, paving the way for the design of multi-targeting pharmacophores. This study shows that callyaerins are not only interesting new drug

leads, but are also employable in further fields of application helping to embank the global spread of TB.

Table of Contents

Abbreviations

%	percent
% (v/v)	volume percent
% (w/v)	mass percent
°C	degree Celsius
µF	microfarad
µg	microgram
µL	microliter
µM	micromolar
µm	micrometer
16SrRNA	*16S ribosomal ribonucleic acid*
Å	Angstrom
ABC	ammonium bicarbonate
Abu	aminobutyric acid
ACF	Analytics Core Facility
ACN	acetonitrile
ADEPs	acyldepsipeptides
ADS	albumin dextrose salt
Aha	azidohomoalanine
AMR	antimicrobial resistance
approx.	approximately
apra	apramycin
Atc	anhydrotetracyline
ATP	adenosine triphosphate
BCG	Bacillus Calmette-Guérin
BDQ	bedaquiline
Bpa	benzophenone
bp	base pair
CalA	callyaerin A
CalB	callyaerin B
Cal-res	callyaerin-resistant
CBS	cystathionine-β-synthase
CCCP	carbonyl cyanide m-chlorophenyl hydrazone
CDC	Center for Disease Control and Prevention
CFU	colony-forming units
CID	collision-induced dissociation
ClpP	caseinolytic protease proteolytic subunit P
CLSI	Clinical and Laboratory Standard Institute
CO_2	carbon dioxide
CSS	Centre for Structural Studies
Ct	cycle threshold
CTAB	cetyltrimethylammonium bromide
Da	Dalton
DAA	diaminoacrylamide
DESY	‘Deutsches Elektronen-Synchrotron’
DMSO	dimethyl sulfoxide

DNA	deoxyribonucleic acid
DosR	dormancy regulon
dpi	days post-infection
DTT	dithiothreitol
E. coli	*Escherichia coli*
E. faecium	*Enterococcus faecium*
e.g.	exempli gratia, for example
EMB	ethambutol
EMBL	European Molecular Biological Laboratory
et al.	*et alia*
EV	empty vector
FA	formic acid
FBS	fetal bovine serum
FDA	Food and Drug Administration
fig.	figure
Fmoc	fluorenyl-methyloxycarbonyl
FTMS	fourier transform mass spectrometry
g	gram
GFP	green fluorescent protein
HCl	hydrochloric acid
His	histidine
HIV	human immunodeficiency virus
hrp1	*hypoxic response protein 1 (gene)*
Hrp1	hypoxic response protein 1
Hsp60	heat shock protein 60
Hz	Hertz
INFγ	interferon γ
INH	isoniazid
ITMS	ion trap mobility spectrometry
kan	kanamycin
kDa	kilodalton
kV	kilovolt
KZN	KwaZulu Natal
L	liter
LB	lysogeny broth
LC	liquid chromatography
LC-MS/MS	liquid chromatography tandem mass spectroscopy
M. bovis	*Mycobacterium bovis*
M. marinum	*Mycobacterium marinum*
M. smegmatis	*Mycobacterium smegmatis*
M. tuberculosis	*Mycobacterium tuberculosis*
MDR	multidrug-resistant
mg	milligram
MIC	minimal inhibitory concentration
min	minutes
mL	milliliter
mM	millimolar
mm	millimeter

MOI	multiplicity of infection
mRNA	messenger ribonucleic acid
MRSA	methicillin-resistant *Staphylococcus aureus*
ms	milliseconds
MS2	tandem mass spectrum
MTC	*Mycobacterium tuberculosis* complex
n	statistical sample size
nL	nanoliter
NaCl	sodium chloride
NAD	nicotinamide adenine dinucleotide
nat CalA	natural callyaerin A
nat CalB	natural callyaerin B
nm	nanometer
nM	nanomolar
OD	optical density
Ω	Ohm
PBS	phosphate-buffered saline
PCR	polymerase chain reaction
PEG3	triethylenglycol
PMA	phorbol-12-myristate-13-acetate
POA	pyrazinoic acid
ppm	parts-per-million
Pra	propargylglycine
PrGly	cycloproylglycine
PZA	pyrazinamide
qPCR	quantitative polymerase chain reaction
RD1	*genomic region of difference 1*
RG	research group
RIF	rifampicin
RNA	ribonucleic acid
Rpf	resuscitation-promoting factor
rpf	*resuscitation-promoting factor (gene)*
rpm	revolutions per minute
RpoB	RNA polymerase subunit β
rpoB	*RNA polymerase subunit β (gene)*
RR	rifampicin-resistant
RRDR	rifampicin resistance determining region
RT	room temperature
RT-qPCR	quantitative real-time polymerase chain reaction
S. aureus	*Staphylococcus aureus*
SAR	structure-activity relationship
SDS-PAGE	sodium dodecyl sulfate-polyacrylamide gel electrophoresis
SEM	standard error of the mean
SI	selectivity index
SPPS	solid-phase peptide synthesis
SRM	spontaneous resistant mutants
SSM	sputum smear microscopy
STREP	streptomycin

TB	tuberculosis
TDR	totally drug-resistant
Tle	*tert*-leucine
Tn Mut	transposon mutant
Tn Seq	transposon sequencing
TNFα	tumor necrosis factor α
Tri-FP	trifunctional fluorophosphonate
tRNA	transfer ribonucleic acid
UV	ultraviolet
V	Volt
WHO	World Health Organization
WT	wild type
XDR	extensively drug-resistant

1 Introduction

Bacterial human pathogens can cause life-threatening diseases. The discovery of antibiotics and the development of antimicrobial chemotherapy represent a major advance in controlling morbidity and mortality caused by bacterial infections. However, bacteria have acquired resistance against nearly all commonly used drugs. New drugs and treatment opportunities are urgently needed to cure infections caused by drug-resistant pathogens. Today, antimicrobial resistance (AMR) has become one of the major public health challenges predicted to cause up to ten million deaths per year by 2050 unless effective counter measures are rapidly implemented (O'Neill, 2016). The most critical drug-resistant bacteria, for which development of novel chemotherapeutic treatment options is most urgent, are highlighted in a priority list published by the World Health Organization (WHO) (Tacconelli *et al.*, 2018). Controlling tuberculosis (TB), caused by *Mycobacterium tuberculosis* (*M. tuberculosis*), represents a separate global health challenge. To control the global TB epidemic, the WHO has formulated 'The End TB Strategy' aiming to eliminate TB (WHO, 2015). In the following, an overview of *M. tuberculosis* and the TB disease is given. TB treatment and development of resistances are introduced starting with a short summary about the history of antibacterial drug development. Finally, natural products with a focus on cyclic peptides and callyaerins are described as a promising source for new lead structures and antibiotics against *M. tuberculosis*.

1.1 *Mycobacterium tuberculosis*

M. tuberculosis is the main causative agent of TB and was discovered in 1882 by Robert Koch (Sakula, 1983). The rod-shaped bacterium is characterized as being obligate aerobic, acid-fast and slow-growing with a generation time of approx. 20 hours. It belongs to the genus *Mycobacterium* that consists of approx. 170 species, most of them are environmental. Mycobacterial species able to cause TB in either humans or animals are summarized as *Mycobacterium tuberculosis* complex (MTC). Besides the most prominent pathogen *M. tuberculosis*, this group also consists of e.g. *Mycobacterium africanum*, *Mycobacterium canetti* and *Mycobacterium bovis (M. bovis)* (Niemann *et al.*, 2000). *M. bovis* only causes infections in animals, mainly in cows

(Phillips *et al.*, 2003). However, also the so-called non-tuberculous mycobacteria like *Mycobacterium abscessus* or *Mycobacterium marinum (M. marinum)* can cause disease such as skin infections, especially in immunocompromised people (Fedrizzi *et al.*, 2017). Evolution of today's successful pathogenic strains remains questionable, especially since *M. tuberculosis* has no environmental or animal reservoir (Gagneux, 2018). It is hypothesized that *M. tuberculosis* has co-evolved with its human host and thereby developed to the current pathogen by molecular adaption like downsizing of its genome due to loss of genes dispensable for pathogenicity (Veyrier *et al.*, 2011, Comas *et al.*, 2013). The unusual surface of the *M. tuberculosis* cells is caused by the specific composition of the lipid-rich cell wall. The cell wall compartment of *M. tuberculosi*s is composed of four main layers (I-IV). The innermost cytoplasm membrane (I) is followed by a complex of peptidoglycan and arabinogalactan building the periplasmic space (II) before connecting to the outer membrane (III), also called mycomembrane (Kalscheuer *et al.*, 2019). The mycomembrane is covalently connected to the components of the periplasmic space via mycolic acids. These long-chain fatty acids are divided into alpha-, keto- and methoxy-mycolic acids, which are involved in a wide spectrum of biological processes like pathogenicity, persistence and biofilm formation (Jackson, 2014). The integrity and composition of mycolic acids, arabinogalactan and peptidoglycan is essential for cell viability and cell wall permeability (Liu *et al.*, 1996). In addition, the inner and outer membrane are comprised of non-covalently linked glycophospholipids like phosphatidylinositol mannosides, lipomannan and lipoarabinomannan, which are known to modulate the host immune response (Jankute *et al.*, 2015). Last, the cell envelope consists of an outermost capsule (IV), that is only weakly connected to the mycomembrane (Kalscheuer *et al.*, 2019). In general, the mycobacterial cell envelope is highly linked to bacterial survival during infection and is associated with resistance to many common antibiotics (Jankute *et al.*, 2015). Due to its unique cell wall structure and ability to adapt to a wide spectrum of stresses, *M. tuberculosis* has become a successful pathogen that rapidly spreads via aerosols infecting a large number of human hosts and thereby became a global epidemic.

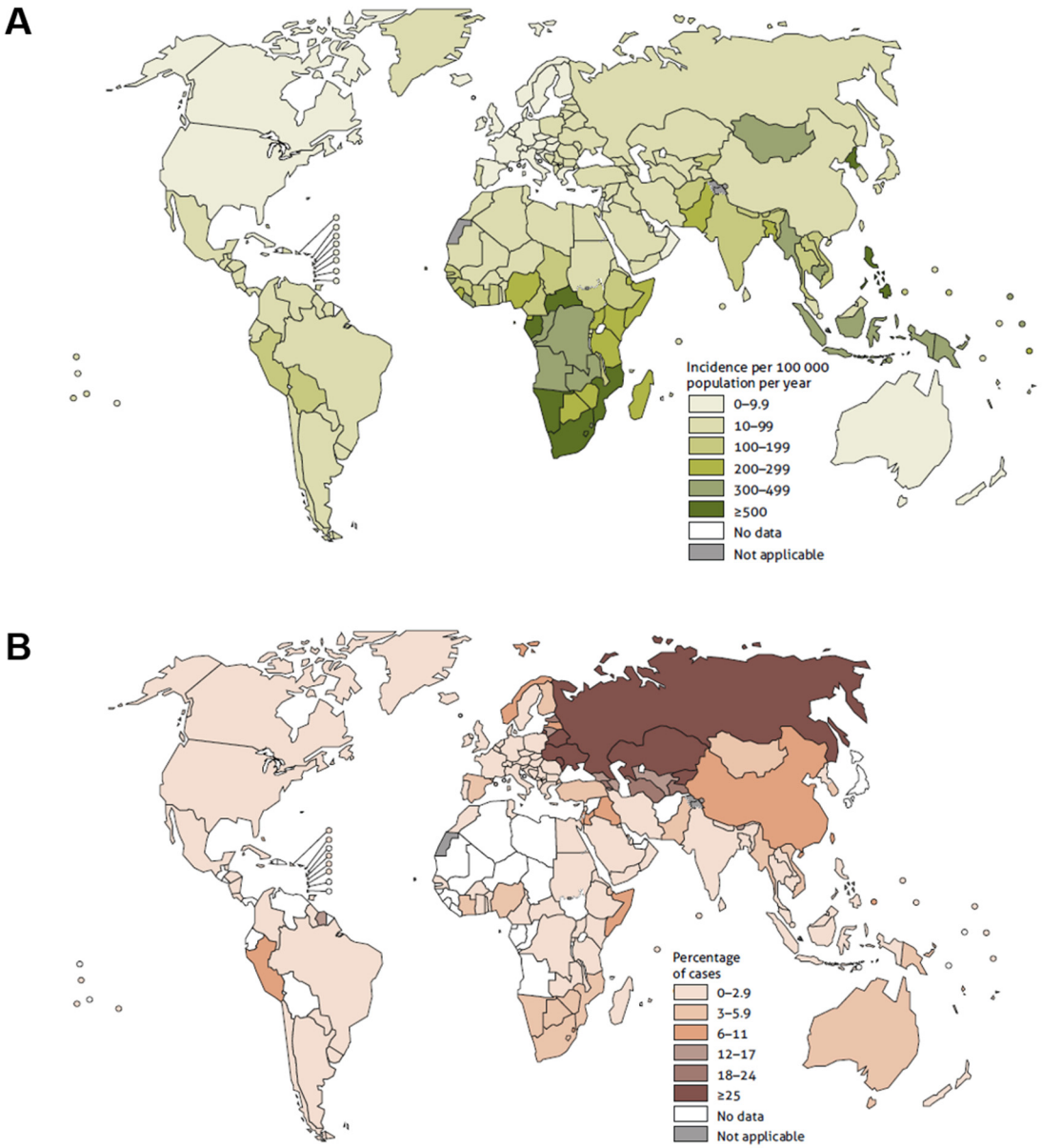

Figure 1: Estimated incidence rates of people infected with TB and drug-resistant TB in 2018. Ten million people fell ill with TB in 2018 with the highest numbers in South-East Asia, Africa and the Western Pacific (**A**). Half a million people have been newly infected with drug-resistant TB. Countries with the highest burden have been reported to be China, India and the Russian Federation (**B**). Figure and data from WHO, Global Tuberculosis Report (2019a).

1.1.1 Epidemiology and disease

According to the WHO, TB is still one of the top ten causes of death worldwide. In 2018, about ten million people fell ill with TB (fig. 1). Half a million estimated cases of rifampicin-resistant (RR) TB and multidrug-resistant (MDR) TB (see chapter 1.2.3) in 2018 have been reported by the WHO (fig. 1) (WHO, 2019a). With approx. 1.4 million deaths, TB is the leading cause of deaths from a single infectious agent (WHO, 2019a). Up to 251,000 deaths thereof are among human immunodeficiency virus (HIV)-positive people since the treatments of TB and HIV have been observed to negatively interfere with each other. Access to drugs and diagnostic tools needs to be substantially improved especially in high burden developing countries, making TB predominantly a disease of the poor (WHO, 2019a). It is estimated that approx. 1.7 billion people are infected with *M. tuberculosis*, but only up to 10% will develop an active disease during their lifetime. The remaining 90% will not develop a transmissible disease and stay asymptomatic supposedly due to a high human adaption to control TB (Barry *et al.*, 2009, Eldholm and Balloux, 2016). However, the immune response to *M. tuberculosis* does not lead to successful sterilization, maintaining the risk of developing an active disease even decades after primary infection due to reactivation of the dormant bacilli. Besides HIV, also immunodeficiency of other causes, malnutrition, diabetes and alcohol abuse can increase the risk for a TB disease (WHO, 2019a). People newly infected with *M. tuberculosis* are exposed to the highest risk of developing an active disease within the first 24 months. *M. tuberculosis* typically infects the lung but is also able to infect nearly any other tissue of the human body resulting in extrapulmonary TB. Today's understanding of the physical signs and characteristics of the pulmonary disease began with the description of Laennec in 1819 (reviewed in Daniel, 2006). *M. tuberculosis* is one of the most successful pathogens due to its transmission via aerosols. Once an individual inhales infectious droplets containing *M. tuberculosis*, the bacteria enter the lung followed by internalization by alveolar macrophages. Bacteria are sensed by macrophages due to the recognition of pathogen-associated molecular patterns by host cell pattern recognition receptors leading to phagocytosis of the pathogen (Queval *et al.*, 2017). Followed by decreasing pH inside the phagosome, the macrophage normally processes the fusion with a lysosome resulting in the biogenesis of the phagolysosome and pathogen destruction (Queval *et al.,* 2017). However, *M. tuberculosis* has evolved a broad spectrum of skills controlling the biogenesis of the phagolysosome and escaping host cell destruction. Besides controlling the pH of the phagosome, glycolipids of the *M. tuberculosis* cell wall are able to block progressive host cell events provoked by phosphatidylinositol-3-phosphate, a host membrane component essentially involved in

biogenesis of the phagolysosome (Roth, 2004). Once *M. tuberculo*sis is incorporated by a macrophage, the host immune response leads to the aggregation of further immune cells. Uninfected macrophages, T cells, neutrophils and fibroblasts surround infected macrophages resulting in the formation of a granuloma (fig. 2) (Queval *et al.*, 2017). Secreted cytokines of surrounding immune cells like interferon γ (INFγ) and tumor necrosis factor α (TNFα) lead to macrophage activation triggering the generation of reactive oxygen and nitrogen species. However, *M. tuberculosis* is able to persist in this toxic environment for decades remaining as a latent TB infection (Pieters, 2008). It is supposed that granulomas can bar different fates. While some granulomas continue to control the pathogen, others progress to release the bacilli resulting in an active disease (Huang *et al.*, 2019). Besides preserving in the phagosome, it was also shown that *M. tuberculosis* actively gains access to the cytosol by rupture of the phagosome (Simeone *et al.*, 2012). To escape host cell defense and to successfully disseminate, *M. tuberculosis* has found mechanisms to control host cell death by supporting both, apoptosis and necrosis. Once the macrophages and the entire granuloma architecture are destroyed, the inflammatory caseous center containing cell debris and pathogens is revealed. *M. tuberculosis* can be transmitted to surrounding tissues and organs. As a major consequence, upon cavity emergence in the lungs, the bacteria can be actively coughed out into the environment (Hunter, 2011).

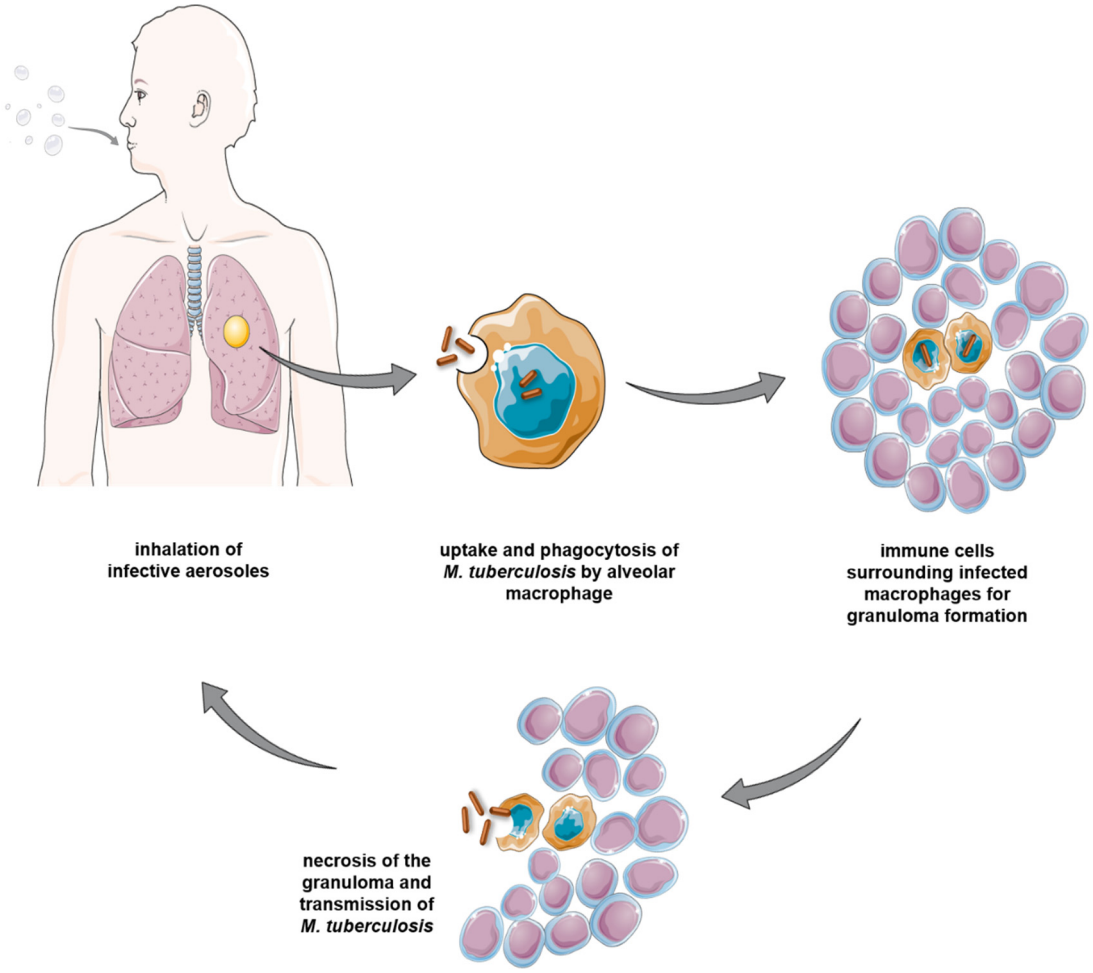

Figure 2: Infection, intracellular phagocytosis and transmission of *M. tuberculosis*. By inhaling infective aerosol, *M. tuberculosis* is transmitted from one host to another. In the lung tissue, *M. tuberculosis* is phagocytized by alveolar macrophages. Infected macrophages lead to the recruitment of other immune cells, surrounding the macrophage and building the granuloma. Necrosis of infected macrophages and the granuloma results in transmission of *M. tuberculosis* from the caseous center to further tissues via blood stream and expectoration to the environment. Figure adapted from Cambier *et al.* (2014).

Expectoration of infectious droplets leads to infection of other individuals. Since no successful immunization is established, *M. tuberculosis* is easily spread between individual hosts. Approx. 100 years ago, Albert Calmette and Camille Guérin started with the development of the only licensed TB vaccine by serial subcultures of *M. bovis* resulting in a complete loss of virulence. In 1940, most countries of Europe had established a vaccine routine using Bacillus Calmette-Guérin (BCG) for newborn and young children (Colditz *et al.*, 1995). However, vaccination showed disparate results and only low success has been reported, especially in adults resulting in lack of an efficient preventive TB vaccine nowadays (Luca and Mihaescu, 2013). Effective drugs for the treatment of TB were developed around 1940 (see chapter 1.2.2). The current treatment of drug-susceptible TB recommended by the WHO consists of the combinational therapy

of the four first-line drugs rifampicin (RIF), isoniazid (INH), ethambutol (EMB) and pyrazinamide (PZA) over a period of up to six months (see chapter 1.2.2). Besides drug resistance, also the ability of the bacillus to enter different metabolic states that are associated with a drug tolerant dormant phenotype complicate the treatment of TB (Mc. Dermott, 1958). Most antibiotics are only effective against actively growing cells of *M. tuberculosis*. Successful treatment of latent TB, which would prevent development of an active disease, remains challenging, especially since, to this day, dormancy of *M. tuberculosis* is not fully understood.

1.1.2 Dormancy of *M. tuberculosis*

As described previously, being exposed to infective aerosols containing *M. tuberculosis* can have different outcomes. While some people directly develop an active disease, the host immune system is also capable to control the pathogenic infection. In this case, fusion of the phagolysosome, granuloma formation and immune signaling lead to consumption of the bacteria. However, some bacteria survive within the granuloma without causing an active disease and thereby triggering a latent TB infection with absence of clinical symptoms. Phagocytosis of bacteria is accompanied by a dramatic change in environmental conditions like oxidative and nitrosative stress, acidification and starvation (Gengenbacher and Kaufmann, 2012). While the special cell wall of *M. tuberculosis* already facilitates the pathogen to tolerate low pH values, the bacteria additionally secrete ureases to neutralize the pH (Reyrat *et al.*, 1995). However, as a general response to those different stresses, the bacteria pass into a dormant state, characterized by a reduced metabolism and curbed replication. The entire molecular mechanism that triggers dormancy is not fully understood. A main factor that controls switching from active to dormant metabolism in *M. tuberculosis* is the dormancy regulon (DosR). DosR is controlled by a two-kinase system, DosS and DosT activating its response regulator (Park *et al.*, 2003, Dutta and Karakousis, 2014). DosR in *M. tuberculosis* controls 48 genes that are colocalized on the genome and can be clustered in nine blocks (Selvaraj *et al.*, 2012). The regulatory function of DosR is induced by several stresses that come along with phagocytosis, but especially by hypoxia (Dutta and Karakousis, 2014). While DosT most prominently interacts in the early stages of hypoxia and first activates DosR, DosS rather maintains the function of DosR (Gerasimova *et al.*, 2011). The maintained regulation of genes by DosR leads to a controlled reduction of metabolism and required energy levels and thereby allows

long-term survival in anaerobiosis (Bartek *et al.*, 2009). As described previously, nearly two billion people harbor a latent TB infection but, in consequence, only 10% will develop an active disease during their lifetime (WHO, 2019a). While secondary infections or autoimmune diseases increase the risk of developing an active disease on side of the host, the genetic mechanisms leading to a reactivated metabolism of *M. tuberculosis* are not fully understood. Restarting an active metabolism and switching to a replicative state is associated with resuscitation-promoting factors (Rpf). *M. tuberculosis* has five *rpf* genes encoding for RpfA to RpfE that stimulate regrowth and reactivation of the metabolism (Mukamolova *et al.*, 2002). Also, DosR and the controlled genes are predicted to interfere with successful recovery from dormancy state to an active metabolism and replication (Leistikow *et al.*, 2010). While dormancy describes a metabolic state of the bacteria, the term persistence is defined as the ability of bacteria to survive chemotherapeutic pressure without genetic modifications (McDermott, 1958). A direct connection between activation of DosR and persistence could be excluded, assuming that genes of DosR do not mediate drug tolerance in general (Bartek *et al.*, 2009). Nevertheless, treatment of latent TB infections bears a major challenge, since most drugs lose their activity against non-replicating bacteria.

1.2 Antibiotics and antimicrobial chemotherapy

To control infectious diseases caused by bacteria, antibiotics and chemotherapy are needed that hamper bacterial replication, control the spread of the infection and preferably lead to bacterial death. Antibiotics are defined as chemical agents, produced by living microorganisms that inhibit growth of bacteria or further microorganisms (Waksman, 1956). In this regard, synthetic compounds that inhibit bacterial growth are described as ‘antimicrobials’, both summarized as ‘antimicrobial drugs’. Antimicrobial chemotherapy can consist of both, antibiotics and antimicrobials. In the following, the history of antibiotics and antibacterial chemotherapy leading to the development of the current AMR crisis is described briefly before focusing on TB therapy and drug-resistant *M. tuberculosis*.

1.2.1 From the golden era of antibiotics to the antimicrobial resistance crisis

In 1929, penicillin was discovered by Alexander Fleming and was described as the first antibiotic that hampers bacterial growth (Fleming, 1929). Since then, the industrialization of penicillin, a β-lactam antibiotic, was driven forward, accompanied by the discovery of several currently used antibiotic classes, like aminoglycosides, sulfonamides and quinolones. The period from 1940 to 1970 is known as the golden era of antibiotics (Wohlleben *et al.*, 2016). Selma Waksman was the first to perform an analytical screen on soil microbes, that might exhibit antibacterial activity, yielding in the discovery of actinomycin produced by the actinomycete *Actinomyces antibioticus* (later renamed *Streptomyces antibioticus*) (Waksman and Woodruff, 1941). Antibiotics and antimicrobials have significantly changed the outcome of infectious diseases and led to extended life spans. With increased use, especially during World War II, resistance against penicillin developed rapidly. Trying to handle the problem of resistance, first the discovery of new β-lactam structural variants such as methicillin was pushed forward. Shortly after the introduction of methicillin in 1959, however, new resistance occurred (Ventola, 2015). Besides an intrinsic resistance against antibiotics and antimicrobials, bacteria engage several mechanisms to acquire resistance. Apart from direct modification of the target gene due to mutations or protection by methylation, resistance is also acquired by inactivation of the drug. This can either be caused by hydrolysis or modification like the conjugation of chemical groups such as acetylation (Blair *et al.*, 2015). Additionally, resistance is caused by the reduction of the intracellular concentration of the antimicrobial drugs due to reduced permeability or increased efflux (Blair *et al.*, 2015). The rapid spread of genes coding for multidrug efflux pumps across different bacterial species currently leads to the investigation of multidrug efflux pump inhibitors as a new strategy to target resistant bacteria (Pannek *et al.*, 2006). It was supposed that bacteria rapidly develop resistance against antibiotics since resistance genes from soil organisms can easily be spread to pathogenic bacteria. However, resistance has also been reported against linezolid, a synthetic antimicrobial (Eliopoulos *et al.*, 2004). The WHO has published a priority list for research and development of new antimicrobial drugs for resistant bacteria (Tacconelli *et al.*, 2018). The list suggests to especially focus on drug-resistant gram-negative bacteria like *Acinetobacter baumannii*, *Pseudomonas aeruginosa* and Enterobacteriaceae, grouped as ‘critical’ with the highest priority. Gram-positive bacteria like methicillin-resistant *Staphylococcus aureus* (MRSA, *S. aureus*) and vancomycin-resistant *Enterococcus faecium* (*E. faecium*) are classified as high priority pathogens (Tacconelli *et al.*, 2018). The overuse of antimicrobial drugs in chemotherapy, inappropriate prescribing and extensive agricultural use have forced

the development of resistant bacteria and lead to the reentering of a pre-antimicrobial drug era (Fernandes, 2006). Although the number of identified chemical structures is increasing, no new antimicrobial class has been identified since 1986 with the introduction of daptomycin as the first member of lipopeptides (Debono *et al.*, 1987, Raja *et al.*, 2003). Approaches to directly design new drugs for isolated individual bacterial targets often fail in *in vitro* and *in vivo* assays since permeability, globularity and charging of the compound plays an important role in reaching its target (Richter *et al.*, 2017). Nowadays, most pharma companies have left the field of antibiotic research and rather focus on developing treatments for chronic diseases ensuring a higher return on investment (Nathan and Goldberg, 2005). Drug-resistant bacteria are now present in hospitals and in the community and are rapidly spread globally supported by a modern lifestyle and globalization. Furthermore, drug-resistant bacteria have nowadays developed to a threat for everyone, not only for the young, old and immunocompromised (Fernandes, 2006). *M. tuberculosis* is excluded from the WHO priority list since drug-resistant TB has already independently been described as a global priority for research and development (WHO, 2019a). Current antimicrobial drugs used for TB therapy have been developed many years ago and need to be taken over a long period. Inappropriate intake and non-adherence to treatment regimens forces resistances to occur in *M. tuberculosis*, likewise, leading to an epidemic of drug-resistant TB (chapter 1.2.3).

1.2.2 Chemotherapy and drugs for the treatment of drug-susceptible TB

Without specialized chemotherapy, mortality rates among people suffering from TB are high. Since most of the drugs for successful treatment of drug-susceptible TB have been developed 60 to 80 years ago, the established therapy has remained static over the last years, consisting of four first-line drugs. The long-term treatment is based on a combinational therapy, which has a long history and aims to suppress the development of resistance that has been observed for monotherapy (Kerantzas and Jacobs, 2017). Starting with a daily dose of all four drugs in the ‘intensive phase’, INH, RIF, EMB and PZA are given over a period of two months. Treatment is then continued with an additional ‘continuation phase’ of four months by giving INH and RIF (Gilpin *et al.*, 2018). Furthermore, also ‘hard-to-treat’ phenotypes have been reported that required prolonged treatment up to two years (Jo *et al.*, 2014). Discovery of new drugs remains a

major challenge due to the high intrinsic resistance of *M. tuberculosis*. Their robust cell wall represents a strong natural permeability barrier that hampers many drugs from entering the bacteria (Janukte *et al.*, 2015). In addition, *M. tuberculosis* is a member of the order actinomycetales that also includes the genus *Streptomyces*. *Streptomyces* species are prominent for a wide production of secondary metabolites with antibiotic potential, leading to the hypothesis that *M. tuberculosis* might have inherited intrinsic defense mechanisms against some of those toxic compounds (Eldholm and Balloux, 2016). In the following, streptomycin (SRTEP) is introduced as the first antibiotic against *M. tuberculosis*. Additionally, the four first-line drugs for TB therapy are described.

Streptomycin

The discovery of bioactive compounds from bacteria of the order actinomycetales started with the isolation of actinomycin and streptothricin. However, none of them showed an adequate activity against *M. tuberculosis* (Waksman and Woodruff, 1941, Waksman and Woodruff, 1942). STREP (fig. 3A) was discovered in 1944 and 50 times more efficient against *M. tuberculosis* than the previous compounds (Schatz *et al.*, 1944). While up to this time TB was only treated with bed rest, fresh air and exposure to sunlight in the pre-antibiotic era, STREP represents a milestone for modern TB therapy. A comparative study of patients either treated with bed rest or STREP underlined the antibiotic success by increased survival rates up to 50%. However, almost simultaneously, resistance against the new antibiotic was observed, resulting in treatment failure (Crofton and Mitchison, 1948). STREP, as a member of aminoglycoside antibiotics, inhibits bacterial protein biosynthesis by binding to the 30 S ribosomal subunit via *16 S ribosomal ribonucleic acid* (1*6SrRNA*). Resistance of *M. tuberculosis* against STREP is mediated by mutations in the genes *16sRNA* or *rpsL* encoding for 30 S ribosomal protein S12 (Ruiz *et al.*, 2002).

Isoniazid

INH is a synthetic nicotinamide analog that was discovered in 1952 (Bernstein *et al.*, 1952, Fox, 1952). Previously used as an anticancer agent, INH was also found to be active against *M. tuberculosis* and was rapidly introduced into chemotherapy. However, high resistance rates have been reported for INH monotherapy by the British Medicine Journal (1952). INH is a prodrug (fig. 3B), that is activated after entering the bacterial cell by the catalase-peroxidase hemoprotein KatG. The emerging active form of the drug is an isonicotinoyl radical reacting with nicotinamide adenine dinucleotide (NAD) coenzymes forming an INH-NAD+ adduct (Johnsson and Schultz, 1994). The mode of action of INH, which inhibits the biosynthesis of mycolic acids and thereby hampers the

formation of the mycobacterial cell wall, was first demonstrated by Winder and colleagues (1970). Inhibition most likely is achieved by binding of the INH-NAD+ adduct to InhA (Rawat *et al.*, 2003, Rozwarski *et al.*, 1998). Especially in the first period of treatment, INH shows a strong killing effect on *M. tuberculosis* cells, which rapidly ceases to form a bacteriostatic plateau phase. Activity against dormant *M. tuberculosis* is missing, maybe due to lacking conversion into the active form of the prodrug, albeit INH-NAD+ is present in dormant bacteria (Raghunandanan *et al.*, 2018, Vilchèze and Jacobs, 2019).

Pyrazinamide

The nicotinamide analog PZA (fig. 3C) was discovered in 1952 and directly introduced into TB therapy (Yeager *et al.*, 1952, Schwartz, 1957). Besides shortening the course in combination therapy to six months, PZA has a sterilizing effect on both, actively replicating and dormant bacteria (Heifets and Lindholm-Levy, 1992). PZA is a prodrug that needs to be actively converted by the bacterial enzyme pyrazinamidase encoded by *pncA* (Scorpio and Zhang, 1996). The mode of action of the active form, pyrazinoic acid (POA) is still under discussion. It is thought that PZA interrupts several events like trans-translational processes, disruption of membrane energetics thus interfering with energy production, reduction of cytoplasmic pH or synthesis of coenzyme A (Zimhony *et al.*, 2007, Njire *et al.*, 2016). The latter has been proven by evidence of direct interaction of POA with PanD, an enzyme required for the biosynthesis of coenzyme A and thereby introducing PanD as a genetically and biophysically established target of PZA (Gopal *et al.*, 2017).

Rifampicin

Rifamycins, isolated from *Amycolatopsis rifamycinica*, were discovered in 1957 (reviewed in Sensi, 1983). Among different derivatives, rifamycin B has the strongest antimicrobial activity. However, rifamycins do not directly qualify as clinically applicable antibiotics due to poor absorbance in the gastrointestinal tract as well as low detectable blood levels following oral administration. Therefore, several modifications were introduced by chemical means concerning nearly every functional group of the natural compound resulting in the semisynthetic RIF (Sensi, 1983). The final structure of RIF (fig. 3D) combines high activity against *M. tuberculosis* as well as gram-positive and gram-negative bacteria, good oral absorption and low adverse reactions upon daily treatment resulting in the application in TB therapy since the late 1960s (Vall-Spinosa *et al.*, 1970). RIF was described to operate via a new mode of action by targeting the bacterial RNA polymerase (Wehrli and Staehelin, 1971). In detail, RIF directly targets

the deoxyribonucleic acid (DNA) dependent RNA polymerase subunit β (RpoB) and thereby inhibits the elongation of messenger RNA (mRNA). Resistance to RIF occurs by mutations in the target gene *rpoB*, more specifically in a specific region of 81 base pairs known as rifampicin resistance determining region (RRDR) (Telenti *et al.*, 1993, Goldstein, 2014). Application of RIF in both, intensive and continuation phases of treatment underlines the significance of this antibiotic in the therapy of drug-susceptible TB.

Ethambutol

By screening randomly selected synthetic compounds for their growth-inhibiting activity against *M. tuberculosis*, EMB was discovered in 1961 (Thomas *et al.*, 1961). The ethylenediamine derivative EMB (fig. 3E) targets the cell wall and inhibits arabinogalactan biosynthesis. Resistance is mediated by mutations in operonic genes coding for arabinosyltransferases, namely *embB* and *embC* (Mikusová *et al.*, 1995). It is assumed that EMB interferes early in the biosynthesis of arabinogalactan by inhibition of the conversion of glucose to monosaccharides (Silve *et al.*, 1993). In 2009, Goude *et al*. identified *embC* as a direct target of EMB (Goude *et al.*, 2009). Very recently, proteomic approaches revealed the upregulation of genes involved in energy metabolism and respiration under EMB pressure (Luciana *et al.*, 2019). Since mycobacterial resistance to EMB seems to be multifaceted, it is most likely that EMB has more than one direct intracellular target in *M. tuberculosis*. However, the detailed mode of action is still under discussion.

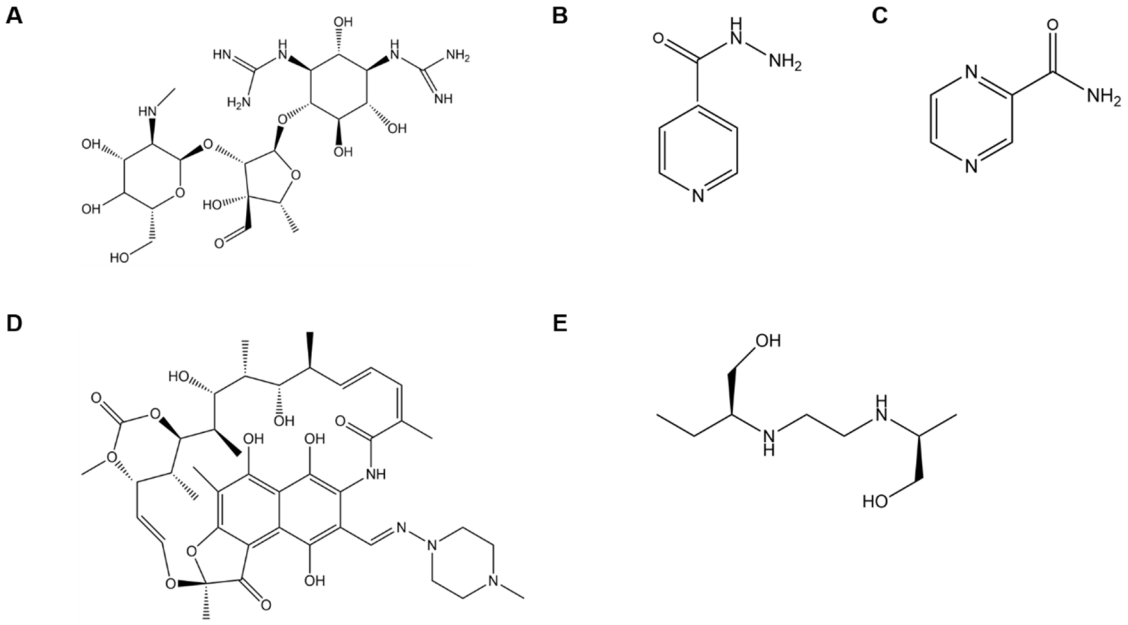

Figure 3: Streptomycin and first-line drugs used in TB therapy. STREP was the first identified antibiotic with anti-TB activity (**A**). First-line therapy of TB consist of the antimicrobial drugs INH (**B**), PZA (**C**) and EMB (**E**) as well as the semisynthetic compound RIF (**D**). Figure adapted from Hameed *et al.* (2018).

1.2.3 Drug resistance in *M. tuberculosis*

Therapy for treatment of drug-susceptible TB is well established and requires the correct intake of drug combinations over a long period of time (chapter 1.2.2). Inadequate application of drugs like suboptimal dosing and duration as well as missing monitoring of patients and therapy force resistance to occur in *M. tuberculosis* (Shenoi and Friedland, 2009). Drug resistance is a major challenge in treatment of TB. As described previously, in 2018, there have been approx. half a million cases of drug-resistant TB with 78% of the cases being MDR TB and only around 28% being treated (WHO, 2019a). The highest burden has been observed in countries of the former Soviet Union (fig. 1). Drug resistance in *M. tuberculosis* is divided into RR TB, MDR TB, extensively drug-resistant (XDR) TB and, very recently, the development of totally drug-resistant (TDR) TB was reported (Velayati *et al.*, 2009). While RR TB is defined as monoresistance to RIF, MDR TB is resistant to both, RIF and INH (WHO, 2019a). Resistance to RIF, in general, occurs due to mutations in the RRDR of the target gene. Resistance to INH is reported to be most common and can either be mediated by mutations in the enzyme activating the prodrug (KatG) or by mutations in *inhA* or its associated promoter region that leads to overexpression of the target gene (Ramaswamy *et al.*, 2003). The WHO and the Center for Disease Control and Prevention (CDC) defined XDR TB as resistance to RIF and INH

plus resistance to at least one fluoroquinolone and one injectable drug like amikacin, kanamycin or capreomycin (CDC, 2006). XDR TB is especially associated with HIV-coinfections and leads to high mortality rates (Gandhi *et al.*, 2006). The KwaZulu Natal (KZN) XDR strain family was reported to cause an outbreak of XDR TB in South Africa and has been studied to reveal several mutations causing resistance to a single drug excluding a general resistance mechanism like efflux (Ioerger *et al.*, 2009). TDR TB was introduced as a term for super extensively drug-resistant TB and harbors resistance against all first-line and nearly all second-line drugs (Velayati *et al.*, 2009, Velayati *et al.*, 2013).

In the last years, only three new drugs have reached the market for TB treatment: bedaquiline (BDQ), delamanid and pretomanid. Recently, two of them, BDQ and delamanid have been reported to be ineffective against TDR TB (Maeurer *et al.*, 2014). BDQ is a diarylquinoline with strong antimycobacterial properties underlying a new mode of action. BDQ inhibits the adenosine triphosphate (ATP) synthase in *M. tuberculosis* by targeting AtpE, which is part of the F0 subunit of the proton pump (Andries *et al.*, 2005). In 2013, the WHO recommended BDQ as a core drug in treatment of drug-resistant TB (WHO, 2013). While the treatment success of MDR TB patients improved by 75%, side effects like QT prolongation have been reported (Guglielmetti *et al.*, 2014, Pontali *et al.*, 2017). Additionally, resistance to BDQ has already been reported and associated with mutations in the gene *mmpL5* (Hartkoorn *et al.*, 2014). Delamanid was discovered in 2006 as an inhibitor of the mycobacterial synthesis of mycolic acids (Matsumoto *et al.*, 2006). It is recommended for treatment of drug-resistant TB since 2014, initially only for adults but later also for children and adolescents and is nowadays the drug of choice for treatment of patients under the age of six (WHO, 2016). However, also delamanid has been reported in the context of QT prolongation (Pontali *et al.*, 2017), and resistance in clinical isolates has been described with reference to mutations in the gene *ddn* (Fujiwara *et al.*, 2018). Most recently, pretomanid was approved in combinational treatment of adults suffering from pulmonary drug-resistant TB by the U.S. Food and Drug Administration (FDA, 2019). Pretomanid was previously known as PA-824 and described to inhibit both, drug-resistant and non-replicating *M. tuberculosis* (Stover *et al.*, 2000). Regarding the underlying mode of action, it is believed that pretomanid targets genes involved in cell wall processes as well as in the response to respiratory stress (Manjunatha *et al.*, 2009).

The emergence of highly transmissible MDR and XDR *M. tuberculosis* strains represents a major global health threat and prospective challenge. To control the global spread of TB, especially of drug-resistant TB, the WHO has devised a global strategy and targets for prevention aiming to end the global TB epidemic by 2035 (WHO, 2015).

To achieve this goal, better access to drug susceptibility testing and TB chemotherapy need to be provided. Most urgent, development of new drugs is needed to embank the spread of drug-resistant TB following different strategies. Besides the target-directed design of new antimicrobials, nature and its magnitude of products provide a rich source for new lead structures helping to control drug-resistant TB.

1.3 Natural products as a source for new antibiotic lead structures against *M. tuberculosis*

Natural products are secondary metabolites produced by living organisms like plants, bacteria, endophytic fungi, algae and marine organisms (Schmitz *et al.*, 1993, García *et al.*, 2012). Natural products and their analogs play a crucial role in modern chemotherapy for treatment of cancer and infectious diseases. Nearly 70% of all drugs that are currently used in clinics are natural products or analogs of natural structures (Newman and Cragg, 2012, Brown *et al.*, 2014). Focusing on *M. tuberculosis*, natural products and analogs like RIF, capreomycin or STREP are successfully used for years in first-line or second-line therapy, respectively. Natural products with specific activity against *M. tuberculosis* comprise compounds of several chemical classes like alkenes, quinones, alkaloids, terpenes, steroids, flavonoids and peptides (Copp and Pearce, 2007, García *et al.*, 2012). Targets of natural products in *M. tuberculosis* are e.g. fatty acid biosynthesis and amino acid synthesis like it was described for thiolactomycin (Slayden *et al.*, 1996) or chlorflavonin (Rehberg *et al.*, 2018), respectively. RNA polymerase is targeted not only by RIF but also by ripostatin, a secondary metabolite isolated from *Sorangium cellulosum* (Augustiniak *et al.*, 1996, Glaus and Altmann, 2012). With upcoming resistance, natural products provide new structural scaffolds with unprecedented mode of actions and bacterial targets that are not involved in mechanisms of resistance against currently used drugs, thus helping to overcome problems with existing treatments (Quan *et al.*, 2017). Among the class of peptides, especially cyclic peptides derived from nature represent a major source for new drugs that provide a high selective potency against *M. tuberculosis* including drug-resistant strains.

1.3.1 Cyclic peptides from nature as antibiotic lead structures against *M. tuberculosis*

Cyclic peptides occupy a central position as bioactive compounds and potential drugs since their structure provides many advantages with respect to their bioactivity. On the basis of their three-dimensional structure, peptides provide high specificity and strong interaction with their appropriate target (Henninot *et al.*, 2018). In general, they are reported to possess low cytotoxic side effects and low immunogenicity (McGregor, 2008). Cyclic peptides are relatively easy to synthesize by applying solid-phase peptide synthesis (SPPS) (Zhang *et al.*, 2019b), which represents a key advantage in overcoming the problem of product availability known for many natural products. According to Zhang *et al.* (2019b), cyclic peptides can be classified into four different categories, depending on their specific mode of ring closure. The first group of cyclic peptides is formed by a covalent linkage between the N- and C- terminus and is therefore described as 'head-to-tail' peptides. Ring closure of peptides can also occur between the sidechain and either the N- or C-terminus. These compounds are classified as 'head-to-sidechain' or 'tail-to-sidechain' cyclic peptides, respectively. The last group consists of peptides providing two functional sidechains that are connected covalently ('sidechain-to-sidechain').

Cyclic peptides provide a broad spectrum of bioactivity. They can operate as immunosuppressors like hymenistatin 1 (Pettit *et al.*, 1990, Cebrat *et al.*, 1996), provide lead structures for anti-cancer treatment such as stylassiamide X (Arai *et al.*, 2012) or exhibit anti-inflammatory activity as for instance stylissatin A (Kita *et al.*, 2013, Zhang *et al.*, 2019a). Furthermore, since the early times of antibiotic discovery, cyclic peptides are also known for their antimicrobial activity. In the following, cyclic peptides and their activity against *M. tuberculosis* are described, highlighting their great potential as potential drug leads for TB therapy.

Viomycin and Capreomycin

Viomycin was isolated from *Streptomyces floridae* in 1951 and exhibited strong activity against *M. tuberculosis* and moderate activity against several gram-positive and gram-negative bacteria (Bartz *et al.*, 1951). Viomycin, also known as tuberactinomycin B, was the first member of a class of antibiotics named tuberactinomycins (Barkei *et al.*, 2009). It was used in TB therapy until it was replaced by another member of tuberactinomycins, namely capreomycin (fig. 4A), due to its putatively lower cytotoxicity. Capreomycin was isolated in 1959 and described as a mixture of four metabolites (Herr, 1959, Herr Jr. and Redstone, 1966). Both tuberactinomycins interact with the bacterial

ribosome and target transfer RNA (tRNA) followed by inhibition of protein synthesis (Modolfll and Vázquez, 1977, Stanley *et al.*, 2010). Changes in the *16SrRNA* via *tlyA* inactivation confers resistance against capreomycin and viomycin (Johansen *et al.*, 2006). However, also other targets have been under discussion such as genes interacting on DNA level or genes involved in cell division (Fu and Shinnick, 2007). Capreomycin, used as a second-line antibiotic in TB therapy, was recently requested to be removed from the WHO list of essential medicines (WHO, 2019b) and is no longer recommended for the treatment of drug-resistant *M. tuberculosis* (WHO, 2019c).

Acyldepsipeptides

Acyldepsipeptides (ADEPs) were introduced as a new class of antibiotics in 2005 (Brötz-Oesterhelt *et al.*, 2005). However, related compounds have been isolated from *Streptomyces hawaiiensis* and already described in 1985 as a complex of structures named ‘A54556’ (Michel and Kastner, 1985). The essential core structure was identified as ‘factor A’ (fig. 4B). First, activity of ADEPs has been described against several gram-positive bacteria like *S. aureus* and *Enterococcus faecalis* including multidrug-resistant clinical isolates. ADEPs directly interact with the proteolytic core unit of caseinolytic proteases (ClpP) and thereby lead to uncontrolled proteolysis (Brötz-Oesterhelt *et al.*, 2005). A halogenated derivative, ADEP4, was additionally active against dormant *S. aureus* and showed synergistic killing of *S. aureus* biofilms in combinational treatment with RIF (Conlon *et al.*, 2013). Activity of ADEPs against *M. tuberculosis* and target validation was reported in 2012 (Ollinger *et al.*, 2012). In contrast to other bacteria, *M. tuberculosis* has two ClpP subunits, among which ClpP1 is essential for bacterial growth and virulence (Ollinger *et al.*, 2012, Famulla *et al.*, 2016). ClpP1 and ClpP2 together with further subunits ClpC1 and ClpC2 form a large ATP-dependent proteolytic complex (Akopian *et al.*, 2012). While the confirmed mode of action in *S. aureus* is based on target overactivation and nonspecific protein degradation (Kirstein *et al.*, 2009), ADEPs inhibit the mycobacterial Clp protease complex which leads to a loss of its essential function (Famulla *et al.*, 2016).

Lassomycin

Lassomycin was extracted from *Lentzea kentuckyensis* (Gavrish *et al.*, 2014). It belongs to the class of lasso peptides (fig. 4C), a subclass of peptides that are synthesized ribosomally and modified post-translationally (Arnison *et al.*, 2013). Gavrish and coworkers specifically screened for compounds active against *M. tuberculosis.* Lassomycin is highly active against several *M. tuberculosis* strains including drug-resistant clinical isolates. Additionally, activity could be observed against other

mycobacteria like *Mycobacterium smegmatis (M. smegmatis)* or *Mycobacterium avium*, while no growth inhibition of gram-positive and gram-negative bacteria could be detected. Studies on time-dependent killing of *M. tuberculosis* revealed a bactericidal effect on both, actively growing and dormant bacteria (Gavrish *et al.*, 2014). Sequencing of spontaneous resistant mutants (SRM) for target validation revealed mutations in the gene *clpC1* encoding a subunit of the ATPase complex mentioned above. Lassomycin leads to an increase of ClpC1 activity followed by intensification of ATP hydrolysis. While over activating the ATP hydrolysis of ClpC1, lassomycin induces a loss of the proteolytic activity (Gavrish *et al.*, 2014). Uncoupling these two functions of a target protein represents a new mode of action, distinguished from the mechanism of ADEPs. A first total synthesis of lassomycin and a lassomycin-amide derivative was published in 2016. However, both synthetic compounds lack the previously described activity against *M. tuberculosis* and consequently leave the synthesis a remaining challenge (Lear *et al.*, 2016, Martin-Gómez and Tulla-Puche, 2018).

Teixobactin

The cyclic depsipeptide teixobactin was isolated from the newly identified species *Eleftheria terrae* by applying iChip, a special approach described in 2010 that allows growth of so far unculturable bacteria (Nichols *et al.*, 2010, Ling *et al.*, 2015). Briefly, diluted soil samples are applied on a channel covered with semi-permeable membranes and incubated in the soil, allowing the diffusion of nutrients and growth factors and thereby mimicking the natural environment of the bacteria (Nichols *et al.*, 2010). Teixobactin is composed of eleven amino acids, including unusual enduracididine and methylphenylalanine (fig. 4D) (Guo *et al.*, 2018). It exhibits activity against many pathogenic microorganisms, gram-positive bacteria like *S. aureus*, *E. faecalis*, *Streptococcus pneumoni*a, *Clostridium difficile*, *Bacillus anthracis* and additionally *M. tuberculosis*. However, teixobactin was ineffective against most gram-negative bacteria. For *S. aureus*, a bactericidal effect could be shown with strong lysis and killing of the pathogen (Ling *et al.*, 2015). The lack of teixobactin-resistant mutants of *M. tuberculosis* or *S. aureus* on agar and by serial passaging underlined the strong lytic effect of the compound. The revealed mode of action is based on inhibition of bacterial cell wall synthesis by targeting lipid II and lipid III, both precursors of the cell wall components peptidoglycan or teichoic acid, respectively (Ling *et al.*, 2015). Recent synthetic approaches of teixobactin have been optimized to gram-scale yields, making it available for pharmacokinetic and clinical studies (Zong *et al.*, 2019).

Griselimycin

In the 1960s, a new structure named griselimycin was isolated from *Streptomyces* species and screened for antimycobacterial activity (Terlain and Thomas, 1971). However, griselimycin exhibited poor pharmacokinetic properties and studies on the compound were discontinued due to the increasing availability of other TB drugs. In the last years, this compound regained attention due to the reinvestigation by Sanofi (SATB-082) focusing on the activity against drug-resistant and dormant *M. tuberculosis*. Kling *et al.* investigated its antimycobacterial activity, accompanied by the establishment of a total synthesis and target evaluation (Kling *et al.*, 2015). Since the proline residue at position eight (fig. 4E) was the main site of degradation, structure-activity relationship (SAR) studies revealed that substitutions at this position led to increased stability and activity. Mouse models showed a bactericidal effect of the optimized compound cyclohexylgriselimycin and an accelerated synergistic killing in combination with RIF and PZA. A first hint regarding the target of griselimycins was revealed by a closer look at the gene cluster of *Streptomyces* (Broenstrup *et al.*, 2013). Thereby, a homolog region to *dnaN* was identified, encoding for the β-clamp of DNA polymerase III. This potential target was confirmed by SRM of *M. smegmatis* harboring mutations in the gene itself or the related promotor region, concluding that resistance is mediated by amplification of *dnaN* (Kling *et al.*, 2015).

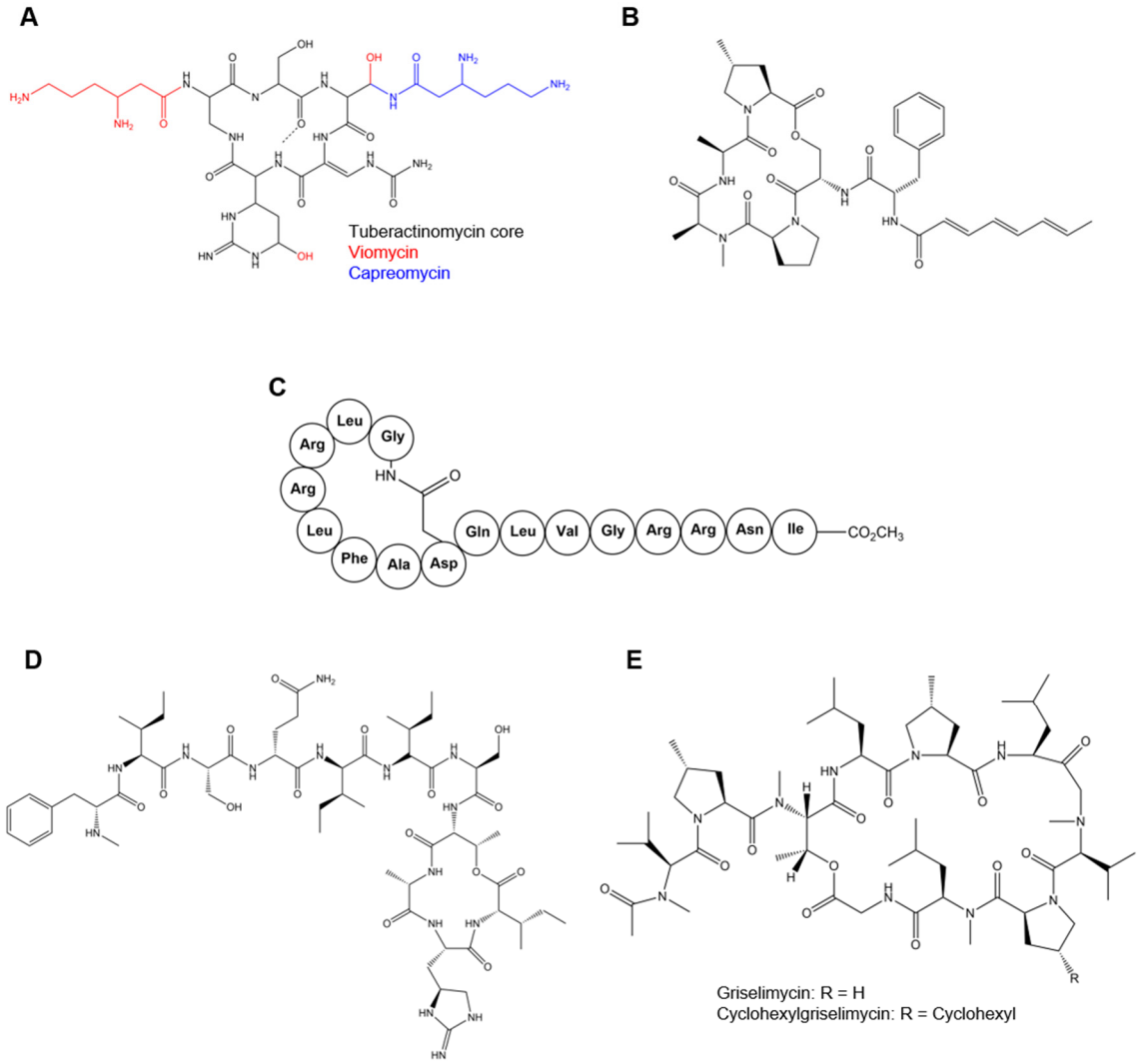

Figure 4: Natural occurring cyclic peptides that are active against *M. tuberculosis*. Viomycin and capreomycin belong to the class of tuberactinomycins (**A**). 'Factor A' is the core structure of ADEPs (**B**). ADEPs and lassomycin (**C**) both target an ATP-dependent proteolytic complex in mycobacteria. Teixobactin was obtained from a new bacterial species, isolated by applying iChip (**D**). The antimycobacterial activity of griselimycin was reinvestigated by Sanofi and Kling *et al.* (**E**). Figure adapted from Stanley *et al.* (2010), Brötz-Oesterhelt *et al.* (2005), Gavrish *et al.* (2014), Ling *et al.* (2015) and Kling *et al.* (2015).

1.4 Callyaerins: cyclic peptides from *Callyspongia aerizusa*

Callyaerins are a group of natural products first isolated and described by Ibrahim *et al.* (2008) and isolated from the Indonesian sponge *Callyspongia aerizusa.* By extraction of ethyl acetate soluble fractions, the structure of the natural products callyaerin A-H were successfully identified. The compounds are described as cyclic peptides, with a ring system of five to nine amino acids and a sidechain differing in length from two to five additional amino acids (Ibrahim *et al.*, 2010). Further cyclic peptides produced by *Callyspongia* species are e.g. phoriospongin A and B isolated from *Callyspongia bilamellata* (Capon *et al.*, 2002). Although they are missing a peptide sidechain, their described nematocidal activity highlights the promising bioactivity of compounds isolated from *Callyspongia* species.

Taking a closer look at the structure of callyaerins, a rare (*Z*)-2,3-diaminoacrylamide (DAA) moiety closes the ring and connects the sidechain resulting in their typical structure (see fig. 5). The special DAA moiety is also known from callynormine A, isolated from *Callyspongia abnormis* (Berer *et al.*, 2004). However, callynormine A is not active against *M. tuberculosis*. A more detailed chemical investigation and report about the bioactivity of callyaerins was published in 2015 (Daletos *et al.*, 2015). Additionally to the already known callyaerins A-H, the new callyaerins I-M were isolated and described. Peptides of the class of callyaerins consist of a high number of prolines including hydroxyprolines. They all have in common that their sidechain starts with a proline at position C1 (fig. 5A), while the remaining prolines are part of the ring structure. Further amino acids are typically hydrophobic, like isoleucine, leucine and phenylalanine (Ibrahim *et al.*, 2010, Daletos *et al.*, 2015). The natural callyaerins were screened for their activity against *M. tuberculosis* (fig. 5B). While most of the compounds were rather inactive, screenings with callyaerin A (CalA) and callyaerin B (CalB) against *M. tuberculosis* resulted in a minimal inhibitory concentration (MIC) of 2 and 5 µM, respectively. Further analysis of those two compounds revealed a cytotoxic effect of CalB. Summarizing the results from Daletos *et al*., the natural CalA was evaluated to be a promising lead structure for further studies. The two callyaerins active against *M. tuberculosis* share most of their amino acids and differ at one position in the ring structure and at two positions in the sidechain (compare fig. 5C and 5D), resulting in a shorter sidechain for CalB. Preliminary conclusions from the limited SAR data with the available natural callyaerins showed that the presence of hydrophobic amino acids in the ring structure is beneficial for general bioactivity and potentially increases membrane permeability of the compounds (Daletos *et al.*, 2015).

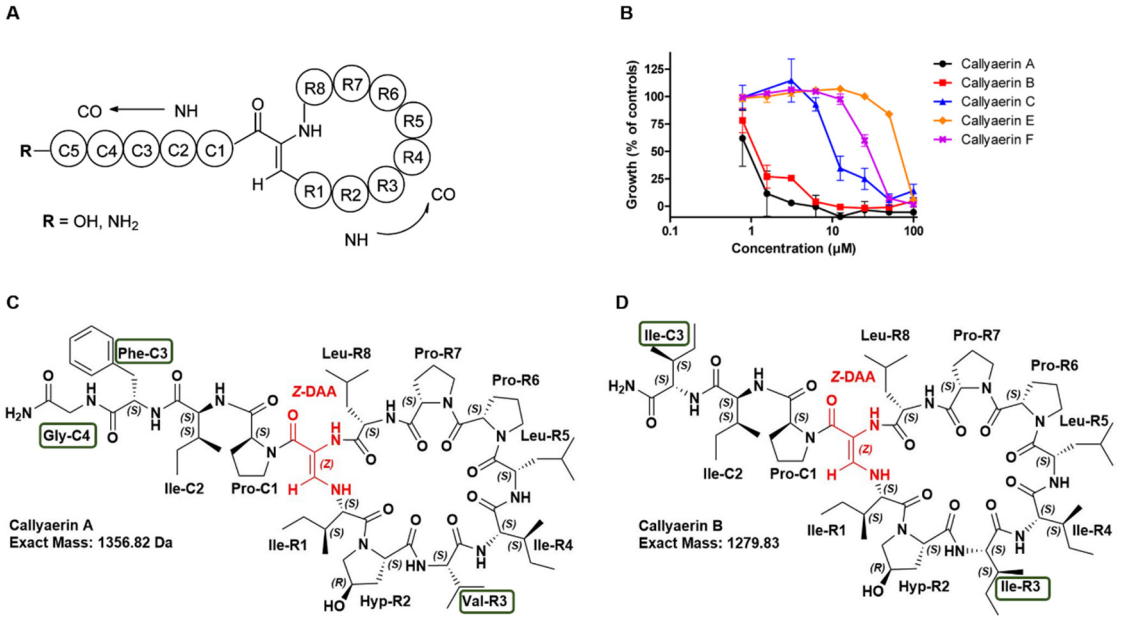

Figure 5: Structure and activity against *M. tuberculosis* of natural callyaerins. The basic structure of callyaerins consist of a cyclic peptide ring (R1 to R8) and a peptide sidechain (C1 to C5), connected by a DAA moiety (**A**). The natural callyaerins A-C, E and F were screened against *M. tuberculosis* H37Rv revealing activity of CalA (●) and CalB (■; **B**). The active compounds CalA and CalB differ in three amino acids (edged in green, **C** and **D**). Figure (**A**) and (**B**) are adapted from Daletos *et al.* (2015). Chemical structures shown in (**C**) and (**D**) were obtained from Florian Schulz, University of Duisburg-Essen, Germany and modified.

The first total synthesis of CalA was published by Zhang *et al.* (2018). However, this synthetic CalA exhibited only a low activity against *M. tuberculosis* at a concentration of 32 µM. The authors explained the decrease in activity by 'subtle variations in peptide conformation' (Zhang *et al.*, 2018). It is hypothesized that the DAA moiety of callyaerins is formed via oxidation of a formyl glycine donated by a serine or cysteine undergoing Shiff base formation like it was described for callynormine A. By reacting with the next amino acid of the arising ring structure and followed by double bond migration, the DAA moiety leads to the closure of the specific cyclic structure (Berer *et al.*, 2004). This synthetic scheme could not be conducted by Zhang *et al.* (2018), forcing a different approach by using a fluorenyl-methyloxycarbonyl (Fmoc)-Rink-amide linker as protecting group. To investigate the importance of the DAA moiety, the group from the University of Auckland synthesized a derivative cyclized by a lactam linkage. However, this compound was inactive leading to the hypothesis that the DAA formation is essential for the activity of callyaerins (Li and Brimble, 2019).

1.5 Aim of this study

TB, caused by *M. tuberculosis*, is still the leading cause of deaths from a single infectious pathogen. Although the number of people suffering from TB slightly decreases (WHO 2019), drug resistance is a major problem. Recently, cases of TDR TB have been reported, which are resistant to all drugs currently used in TB treatment. To control the global spread of TB and to afford treatment of TDR TB, new drugs are urgently needed. Therefore, different strategies aiming to identify new compounds with anti-TB activity need to be pursued. Apart from target-directed synthesis, nature and natural products represent a rich source of new structural scaffolds. This thesis aims to reveal further insights into the activity of callyaerins, a group of cyclic peptides from marine source that represent new active compounds against *M. tuberculosis*. In this study, different approaches are conducted to elucidate the mode of action of callyaerins, starting with the generation of SRM for target identification. In cooperation with the research group (RG) of Prof. Dr. Markus Kaiser from the Center of Medical Biotechnology at the University of Duisburg-Essen, Germany, the focus of this thesis was set on the investigation of synthetic callyaerins. The RG of Prof. Dr. Kaiser successfully developed a total synthesis route for callyaerins allowing to perform SAR studies with a comprehensive library of derivatives, thereby enabling identification of structural determinants essential for antibacterial activity and cytotoxicity and revealing the most selective derivatives. Furthermore, the total synthesis of callyearins allows the application of click chemistry by generating azide- or alkyne-containing derivatives. These derivatives are applied for affinity enrichment to identify protein interaction partners of callyaerins. Once a potential target is confirmed, further approaches are conducted to gain additional insights into the revealed mode of action. These approaches include e.g. the cloning of specific genes for generation of merodiploid strains or knock out mutants revealing a putative change in susceptibility. On the long term, a highly selective derivative with a new mode of action in combination with an established, economically feasible synthesis route enables pharmacokinetic studies and efficacy studies in mouse models, paving the way for clinical trials and introduction of callyaerins as a new therapeutic opportunity for TB treatment.

2 Material and Methods

2.1 Kits

Kit	Producer
NucleoSpin® Plasmid Mini Kit	Macherey-Nagel
NucleoSpin® Gel and PCR Clean-up Kit	Macherey-Nagel
RNeasy Mini Kit	Qiagen
RNase-Free DNase Set	Qiagen
SuperScript™ III First-Strand Synthesis SuperMix	Invitrogen
GoTaq® qPCR Master Mix	Promega
BacTiter-Glo™ Microbial Cell Viability Assay	Promega
BCA Protein Assay Kit	Merck Millipore
PD midiTrap™ G-25	GE Healthcare Life Sciences

All kits were used as specified by the manufacturer.

2.2 Enzymes

Enzyme	Producer
Phusion® High Fidelity DNA Polymerase *Go-Taq* DNA Polymerase	New England Biolabs

DNA polymerases for polymerase chain reaction (PCR) were used in combination with Failsafe™ PCR Premix Buffers (epicentre®) as specified by the manufacturer.

Enzyme	Restriction site	Producer
T4 DNA ligase		New England Biolabs
*Cla*I	5'…ATCGAT…3'	
*Pac*I	5'…TTAATTAA…3'	
*Nde*I	5'…CATATG…3'	
*Xho*I	5'…CTCGAG…3'	
*Hind*III	5'…AAGTCC…3'	

Ligase and restriction enzymes for cloning purposes were used as specified by the manufacturer.

2.3 Oligonucleotides

Oligonucleotides for gene amplification, sequencing and diagnostic PCR analysis were designed using Clone Manager 9 software and custom-made by Microsynth Seqlab, Germany. Sequences and area of application of oligonucleotides used in this thesis are listed in table 1.

Table 1: Sequences and applications of oligonucleotides used in this study.

#	Name	Sequence	Application
1	*Pac*I-*hrp1*	5'-TTTTTTTAATTAATGAC CACCGCACGCGACATC-3'	*mycobacteria* shuttle plasmid for *hrp1* expression
2	*Cla*I-*hrp1*	5'-TTTTTATCGATCTAGCTGG CGAGGGCCATGGGC-3'	
3	*Nde*I-Hrp1	5'-TTTTTCATATGATGACCACC GCACGCGACATCATG-3'	*hrp1* expression in pET28a
4	*Xho*I-Hrp1	5'-TTTTTCTCGAGGCTGGCGAG GGCCATGGG-3'	
5	*Hind*III-Rv2113	5'-TTTTTAAGCTTCTAGTCATC GACGTGACCGGCGTCAAC-3'	*mycobacteria* shuttle plasmid for Rv2113 expression
6	*Pac*I-Rv2113	5'-TTTTTTTAATTAATGAGCCTTTC CGTCCGTCGC-3'	
7	pMV261/361 (Kan) FW	5'-CAGCGTAAGTAGCGGGGTTG-3'	sequencing of *mycobacteria* shuttle plasmids
8	pMV261-361 (Apra) Rev	5'-CTGATGGAGCTGCACATGAAC-3'	
9	pMV261/361 (Kan) rev	5'-GCCTCGAGCAAGACGTTTCC-3'	
10	T7probis	5'-TCCCGCGAAATTAATACG-3'	sequencing of pET28 plasmids (Microsynth Seqlab Standard Primer List)
11	T7terbis	5'-AACCCCTCAAGACCCG-3'	
12	*16SrRNA*_ qPCR	5'-GGGTTCTCTCGGATTGACG-3'	primer for qPCR housekeeping gene *16SrRNA*
13	*16SrRNA*_ qPCR	5'-GGCTGCTGGCACGTAGTT-3'	
14	Rv2113 qPCR fwd	5'-ATCGTGCTACTGACGGCATTG-3'	primer for qPCR validation of Rv2113/BCG_2130 expression
15	Rv2113 qPCR rev	5'-GCGATGGCGAGCAGAAAAAC-3'	

2.4 Devices

Device	Producer
Tecan infinite F200 Pro	Tecan
Bio-Rad Gene Pulser Xcell™	Bio-Rad
Sonoplus mini20	Bandelin electronic GmbH & Co.KG
UVP Gel Studio	Analytic Jena AG
Thermal cycler FlexCycler²	Analytic Jena AG
Mx3005P QPCR System	Agilent Technologies
TissueLyser LT	Qiagen
Precellys® 24 Homogenisator	BERTIN
Nikon Eclipse TS100	Nikon

2.5 Software

Software	Producer
Office 2016	Microsoft®
GraphPad Prism 7.02	GraphPad Software Inc.
Clone Manager 9	Scientific and Educational Software
i-control™ 1.1	Tecan Trading AG
Fiji (is just ImageJ)	National Institute of Health, USA
NIS-Elements	Nikon
VisionWorks 8.19	Analytik Jena AG
MxPro – Mx3005P	Stratagene
ChemDraw 19	PerkinElmer Informatics

Graphics in this study have been created involving modifications of cartoons provided by Servier Medical Art conferring to Creative Commons Attribution 3.0 Unported License (https://creativecommons.org/licenses/by/3.0/).

2.6 Bacterial growth conditions and determination of minimal inhibitory concentrations

2.6.1 Bacterial growth conditions

Liquid cultures of several mycobacterial strains (table 2-5) were grown aerobically in Middlebrook 7H9 media (BD Diagnostics, see below) at 37°C and 80 rpm. Solid media for growth of mycobacterial colonies consisted of 7H10 media (BD Diagnostics, see below). Plates were incubated at 37 °C. Supplements for selective media are listed in table 2-5.

Liquid cultures of MRSA strain *S. aureus* Mu50 (ATCC 700699) were grown in Mueller Hinton broth (BD Diagnostics) at 37 °C, 180 rpm.

Liquid cultures of several *Escherichia coli* (*E. coli*) strains (table 7) were grown in lysogeny broth (LB, see below) at 37 °C, 180 rpm. For solid LB media, 2% (w/v) bacto agar (BD Diagnostics) was added. Solid cultures were incubated overnight at 37 °C. Supplements for selective media are listed in table 7.

7H9 media	
10 % (v/v)	albumin dextrose salt (ADS)
0.5 % (v/v)	glycerol
0.05 % (v/v)	tyloxapol

7H10 media	
10 % (v/v)	ADS
0.5 % (v/v)	glycerol

ADS	
5 % (w/v)	bovine serum albumin
2 % (w/v)	glucose
0.85 % (w/v)	sodium chloride

LB media	
0.5% (w/v)	yeast extract
1% (w/v)	bacto tryptone
0.5% (w/v)	NaCl

2.6.2 Bacterial strains

Table 2: *M. tuberculosis* strains used in this study.

Strain	Biosafety level	Media complementation	Source/reference	Strain collection and number
H37Rv	3		obtained from William R. Jacobs Jr., PhD, Albert Einstein College of Medicine, Bronx, USA	MTB 1
HN878				MTB 2
CDC1551				MTB 3
XDR KZN06 XDR KZN13 XDR KZN14 XDR KZN16	3		clinical isolates from KZN, South Africa, obtained from William R. Jacobs Jr., PhD, Albert Einstein College of Medicine, Bronx, USA	-
H37Rv pBEN::mCherry (Hsp60)/GFP (Atc)	3	50 µg/mL hygromycin	RG of Prof. Dr. Kalscheuer, University of Düsseldorf, Germany	MTB 359
CDC1551 Tran Mut 1121 (MT2701, *hrp1*)	3		obtained from BEI Resources, NIAID, NIH - TB Vaccine Testing and Research Materials Contract	MTB 402
H37Rv pMV361::Rv2113	3	30 µg/mL apramycin	RG of Prof. Kalscheuer, University of Düsseldorf, Germany	MTB 357
H37Rv ΔRv2113	3	50 µg/mL hygromycin		MTB 378
H37Rv ΔRv2113 pMV361::Rv2113	3	50 µg/mL hygromycin, 30 µg/mL apramycin		MTB 379
H37Rv Cal-res C1-3				MTB 336
mc²6230 Δ*panCD* Δ*RD1*	2	100 mg/L pantothenic acid	obtained from William, R. Jacobs Jr., PhD, Albert Einstein College of Medicine, Bronx, USA	MBOVIS 299

Table 3: *M. smegmatis* strains used in this study.

Strain	Biosafety level	Media complementation	Source/reference	Strain collection and number
mc²155	2		obtained from William R. Jacobs Jr., PhD, Albert Einstein College of Medicine, Bronx, USA	MSMEG 1
mc²155 pMV361 EV	2	30 µg/mL apramycin	this study	MSMEG 238
mc²155 pMV361::Rv2113	2	30 µg/mL apramycin	this study	MSMEG 239
mc²155 pMV261 EV	2	20 µg/mL kanamycin	this study	MSMEG 240
mc²155 pMV261::*hrp1*	2	20 µg/mL kanamycin	this study	MSMEG 241
mc²155 pMV261 + pMV361 EV	2	20 µg/mL kanamycin, 30 µg/mL apramycin	this study	MSMEG 242
mc²155 pMV261::*hrp1* + pMV361::Rv2113	2	20 µg/mL kanamycin, 30 µg/mL apramycin	this study	MSMEG 243

Table 4: *M. marinum* strains used in this study.

Strain	Biosafety level	Media complementation	Source/reference	Strain collection and number
ATCC 927	2		DSMZ-German Collection of Microorganisms and Cell Cultures GmbH	MMAR 1

Table 5: *M. bovis* and *M. bovis* BCG Pasteur strains used in this study.

Strain	Biosafety level	Media complementation	Source/reference	Strain collection and number
AF2122/97	3		obtained from William R. Jacobs Jr., PhD, Albert Einstein College of Medicine, Bronx, USA	MTB 5
BCG Pasteur	2		obtained from William R. Jacobs Jr., PhD, Albert Einstein College of Medicine, Bronx, USA	MBOVIS 1
BCG Pasteur pMV261 EV	2	20 µg/mL kanamycin	RG of Prof. Dr. Kalscheuer, University of Düsseldorf, Germany	MBOVIS 153
BCG Pasteur pMV361 EV	2	30 µg/mL apramycin	this study	MBOVIS 305
BCG Pasteur pMV361::Rv2113	2	30 µg/mL apramycin	this study	MBOVIS 306
BCG Pasteur pMV261::*hrp1*	2	20 µg/mL kanamycin	this study	MBOVIS 307
BCG Pasteur pMV261 + pMV361 EV	2	20 µg/mL kanamycin	this study	MBOVIS 308
BCG Pasteur pMV261::*hrp1* + pMV361::Rv2113	2	30 µg/mL apramycin	this study	MBOVIS 309

Table 6: *S. aureus* strains used in this study.

Strain	Biosafety level	Media complementation	Source/reference	Strain collection and number
MRSA Mu50 ATCC 700699	2		American Type Culture Collection	SAUREUS 1

Table 7: *E. coli* strains used in this study.

Strain	Biosafety level	Media complementation	Source/reference	Genotype	Strain collection number
NEB® 5-alpha F´Iq	1		New England Biolabs	*fhuA2 Δ(argF-lacZ)U169 phoA glnV44 Φ80 Δ(lacZ)M15 gyrA96 recA1 relA1 endA1 thi-1 hsdR17*	
NEB® 5-alpha F´Iq pMV261	1	40 µg/mL kanamycin	RG of Prof. Dr. Kalscheuer, University of Düsseldorf, Germany		ECOLI 15
NEB® 5-alpha F´Iq pMV361	1	20 µg/mL apramycin			ECOLI 278
NEB® 5-alpha F´Iq pMV361::Rv2113	1	20 µg/mL apramycin			ECOLI 455
NEB® 5-alpha F´Iq pET28a	1	40 µg/mL kanamycin			ECOLI 551
NEB® 5-alpha F´Iq pMV261::*hrp1*	1	40 µg/mL kanamycin	this study		ECOLI 566
NEB® 5-alpha F´Iq pET28a::*hrp1*-His6C	1	40 µg/mL kanamycin			ECOLI 568
Rosetta™ (DE3) pLysS	1		Novagen®	*F⁻ ompT hsdS$_B$(r$_B$⁻ m$_B$⁻) gal dcm (DE3) pLysSRARE (Cam^R)*	
Rosetta™ (DE3) pLysS pET28a::*hrp1*-His6C	1	40 µg/mL kanamycin	this study		ECOLI 578

2.6.3 Determination of minimal inhibitory concentration

MIC of slow-growing mycobacteria

MIC values were determined in 96-well round-bottom microtiter plates. Precultured mycobacteria cells were seeded at a density of $1x10^5$ cells in a total volume of 100 µL per well containing twofold serial diluted compounds. Plates were incubated at 37 °C for five days. 10 µL of a 100 µg/mL resazurin solution was added per well and plates were incubated at room temperature (RT) overnight. Afterward, cells were fixed for 30 min with a final concentration of 5% (v/v) formalin. Fluorescence (excitation 540 nm, emission 590 nm) was quantified using a Tecan infinite F200 Pro reader. MIC_{90} values were calculated in relation to dimethyl sulfoxide (DMSO)-d_6 treated (= 100% growth) and RIF treated (= 0% growth) bacteria. MIC_{90} values of fluorophore-tagged callyaerins were determined using the BacTiter-Glo™ Microbial Cell Viability Assay (Promega) as specified by the manufacturer. Briefly, 50 µL of cell suspension was mixed with 50 µL Bac Titer- Glo™ solution in Nunclon 96-well flat-bottom white polystyrene plates (Thermo Fisher Scientific) and luminescence was measured using a Tecan infinite F200 Pro reader.

MIC of fast-growing *Mycobacteria*

MIC values were determined in 96-well round-bottom microtiter plates. Precultured bacteria cells were seeded at a density of $1x10^5$ cells in a total volume of 100 µL per well containing twofold serial diluted compounds. Plates were incubated at 37 °C overnight. 10 µL of a 100 µg/mL resazurin solution was added per well and plates were incubated at 37°C until color change became visible. Afterward, cells were fixed for 30 min with a final concentration of 5% (v/v) formalin. Fluorescence (excitation 540 nm, emission 590 nm) was quantified using a Tecan infinite F200 Pro reader. MIC_{90} values were calculated in relation to DMSO-d_6 treated bacteria (= 100% growth) and medium control (= 0% growth).

MIC of nosocomial pathogens

MIC against MRSA strain *S. aureus* Mu50 ATCC 700699 was determined according to the Clinical and Laboratory Standards Institute (CLSI) guidelines (CLSI, 2012) in 96-well round-bottom microtiter plates using Mueller Hinton broth. Briefly, precultured cells were seeded at a density of $5x10^4$ cells per well in a total volume of 100 µL containing twofold serial diluted compounds. DMSO-d_6 and moxifloxacin were used as controls. Plates were incubated aerobically at 37 °C overnight. MIC_{90} values

were determined using the BacTiter-Glo™ Microbial Cell Viability Assay (Promega) as described above.

2.7 Growth conditions of human cell lines and determination of therapeutic indices

2.7.1 Growth conditions of human cell lines THP-1, HepG2 and HEK293

Cell lines were cultivated at 37 °C in a humidified atmosphere of 5% CO_2. Medium for human monocytic cell line THP-1 (Deutsche Sammlung von Mikroorganismen und Zellkulturen GmbH) consisted of RPMI 1640 medium containing 10% (v/v) fetal bovine serum (FBS). HepG2 cells (CLS Cell Lines Service GmbH) were cultivated using Ham's F12 medium supplemented with 2 mM L-glutamine and 10% (v/v) FBS. HEK293 cells (CLS Cell Lines Service GmbH) were cultivated using EMEM medium supplemented with 2 mM L-glutamine, 1% (v/v) non-essential amino acids, 1 mM sodium pyruvate and 10% (v/v) FBS. For splitting and cytotoxicity assays, cells were harvested by centrifugation (150 x *g*, 5 min). For this, adherent cells were washed with phosphate-buffered saline (PBS) and treated with 0.25% trypsin-ethylenediaminetetraacetic acid (Gibco®) for 5 min at 37 °C. Fresh medium containing 10% (v/v) FBS was added to inactivate trypsin. Centrifuged cells were resuspended in fresh media and split into cell culture flasks or seeded in 96-well plates for cytotoxicity or infection assays. To adjust appropriate cell density, cells were counted using a Neubauer hemocytometer.

2.7.2 Determination of cytotoxicity and selectivity indices

Cytotoxicity was determined by seeding $5x10^4$ cells per well in 96-well flat-bottom microtiter plates in a total volume of 100 µL containing twofold serial dilutions of selected compounds in respective media. Cells were incubated at 37 °C, 5% CO_2 for 48 h. Afterward, 10 µL of a 100 µg/mL resazurin solution was added per well and plates were incubated at 37 °C, 5% CO_2 for two hours. Fluorescence (excitation 540 nm, emission 590 nm) was quantified using the Tecan infinite F200 Pro reader. IC_{50} values were calculated in relation to DMSO-d_6 treated (= 100% growth) and Titron-X 100 treated (= 0% growth) cells. Selectivity indices (SI) were described as the ratio between IC_{50} and MIC_{90} values.

2.8 Molecular and microbiological analytical methods

2.8.1 Extraction of mycobacterial genomic DNA

Genomic DNA from mycobacteria was isolated using the cetyltrimethylammonium bromide (CTAB)-lysozyme method as described by Larsen *et al.* (2017).

2.8.2 Generation and whole-genome sequencing of spontaneous resistant mutants

SRM of *M. tuberculosis* H37Rv wild type (WT) were generated by plating approx. 10^8 to 10^9 CFU on 7H10 agar plates containing four to five times the MIC_{90} of selected compounds. Resistant colonies appeared at a density of $1x10^{-7}$ after six weeks of incubation at 37 °C. Resistances were quantified by determination of MIC as described above (chapter 2.6.3). For whole-genome sequencing of selected clones, genomic DNA was prepared using the CTAB-lysozyme method. Whole-genome sequencing to identify the resistance mediating mutations was performed by Prof. Dr. T. Ioerger (Department of Computer Science, Texas A&M University, College Station, Texas, USA). Briefly, libraries from genomic DNA were prepared for sequencing using the standard paired-end genomic DNA sample prep kit from Illumina. Genomes were sequenced using an Illumina HiSeq 2500 next-generation sequencer (San Diego, CA, USA) and compared with the parent *M. tuberculosis* H37RvMA genome (GenBank accession GCA_000751615.1). Paired-end sequence data was collected with a read length of 106 bp. Base-calling was performed using Casava software, v1.8. The reads were assembled using a comparative genome assembly method, using *M. tuberculosis* H37RvMA as a reference sequence (Ioerger *et al.*, 2010).

For generation of SRM of H37Rv pMV361::Rv2113 merodiploid strains and *M. smegmatis* mc²155 pMV361::Rv2113 strains callyaerin-containing media was supplement with 30 µg/mL apramycin. No resistant colonies could be obtained after 12 weeks or two weeks at 37 °C, respectively.

2.8.3 Isolation of total cytosolic protein of *M. tuberculosis*

M. tuberculosis H37Rv WT cells were grown as liquid culture to late-log phase and collected by centrifugation (4000 x *g*, 10 min, 4 °C). Cells were washed twice with ice-cold PBS and finally resuspended in 1/20th PBS of culture volume. Cells were lysed using Precellys® tubes containing a mixture of 0.5 mm and 0.1 mm glass beads and the Qiagen TissueLyser LT thrice for 3 min at 50 Hz. Samples were cooled on ice between the runs. Afterward, samples were centrifuged at 14000 x *g*, 1 min at 4 °C. Supernatants of the samples were sterilized by threefold filtration using 0.22 µm cellulose acetate low protein binding filters. Total cytosolic protein lysate was stored on ice and used directly for protein quantification assays and affinity enrichment (see 2.8.9).

2.8.4 Macrophage infection assays

For differentiation into macrophage-like cells, THP-1 cells were seeded at a density of 1x10^5 cells per well in a total volume of 100 µL RPMI 1640 supplemented with 10% (v/v) FBS and 50 nM phorbol-12-myristate-13-acetate (PMA) in a 96-well flat-bottom microtiter plate and incubated overnight at 37 °C, 5% CO_2. The next day, cells were washed with PBS twice and medium was replaced with fresh RPMI 1640 medium supplemented with 10% (v/v) FBS containing 3x10^5 cells of precultured H37Rv pBEN::mCherry (Hsp60)/GFP (Atc) resulting in a multiplicity of infection of three (MOI = 3). After three hours, cells were washed with PBS twice and medium was replaced with fresh RPMI 1640 medium supplemented with 10% (v/v) FBS containing either 15.6 µM of CalA or 1.95 µM of CalB respectively, DMSO-d_6 or antibiotics (1 µM of RIF or 20 µM of STREP). After five days of cultivation at 37 °C and 5% CO_2, cells were fixed with a final concentration of 5% (v/v) formalin and incubated for 30 min at RT. Fluorescence was quantified using a Nikon Eclipse TS100 and NIS-Elements (100 x magnification, 500 ms exposure time). Integrated density of red fluorescence was calculated using Fiji (ImageJ).

2.8.5 ATP quantification assay

For quantification of substance-dependent ATP depletion, precultured H37Rv WT cells were seeded at a density of 1x10^6 cells per well in a total volume of 100 µL per well in 96-well round-bottom plates containing twofold serial diluted compounds.

DMSO-d_6, RIF, BDQ and carbonyl cyanide m-chlorophenyl hydrazone (CCCP) were used as controls. Plates were incubated overnight at 37 °C. The next day, ATP measurement was performed using the BacTiter-Glo™ Microbial Cell Viability Assay (Promega) as described above (chapter 2.6.3).

2.8.6 Expression of *hrp1* (Rv2626c) and Rv2113

Gene region of *hypoxic response protein 1 (hrp1)* was amplified using the oligonucleotides #1 and #2 (table 1) and cloned into expression vectors pMV261 containing a kanamycin resistance using *Cla*I and *Pac*I (New England Biolabs) restriction sites by chemically transformation of *E. coli* NEB® 5-alpha (New England Biolabs) as specified by the manufacturer. Sequenced plasmid pMV261::*hrp1* and pMV261 empty vector (EV) were electroporated into *M. smegmatis* mc²155 or *M. bovis* BCG Pasteur according to Larsen *et al.* (2017) and plated on 7H10 selective plates (see table 3 and 5). Single colonies were picked and grown in selective 7H9 media after four days or three weeks of incubation, respectively.

For expression of Rv2113, plasmids pMV361::Rv2113 and pMV361 EV were electroporated into *M. smegmatis* mc²155 or *M. bovis* BCG Pasteur according to Larsen *et al.* (2017) and plated on 7H10 selective plates (see table 3 and 5). Single colonies were picked and grown in selective 7H9 media after four days or three weeks of incubation, respectively.

For Rv2113 and *hrp1* coexpression, both plasmids were electroporated simultaneously into *M. smegmatis* mc²155 or *M. bovis* BCG Pasteur according to Larsen *et al.* (2017) and plated on 7H10 selective plates (see table 3 and 5). Single colonies were picked and grown in selective 7H9 media after four days or three weeks of incubation, respectively.

2.8.7 Recombinant expression and purification of Hrp1

Gene region of *hrp1* was amplified using the oligonucleotides #3 and #4 (table 1) for ligation into pET28a vector containing a kanamycin resistance by usage of the restriction enzymes *Nde*I and *Xho*I (New England Biolabs). The resulting plasmid pET28a::*hrp1* containing the gene sequence with a C-terminal polyhistidine (His)-tag was transformed to *E. coli* NEB® 5-alpha (New England Biolabs) as specified by the manufacturer. For generation of an expression strain, *E. coli* Rosetta (DE3) pLysS

(Novagen®) was electroporated (settings: 2500 V, 200 Ω, 25 µF) using pET28a::*hrp1*. *E. coli* Rosetta (DE3) pLysS pET28a::*hrp1* cultures were grown in LB selective media at 37 °C and 180 rpm to $OD_{600\ nm}$ = 0.6 and induced using 1 mM isopropyl β-D-1-thiogalactopyranoside (Sigma Aldrich). For protein expression, cultures were grown overnight at 37 °C and 180 rpm. Cells were harvested by centrifugation (4000 x *g*, 4 °C, 20 min), resuspended in 10 mL ice-cold lysis buffer (see below) and sonicated on ice (4 x 10 s bursts using 40% amplitude). Lysed cells were centrifuged for 40 min, 16000 x *g* at 4 °C. Proteins were purified by application of batch binding. Supernatant of cell lysate was mixed with 3 mL Ni-NTA agarose (Qiagen, previously equilibrated in lysis buffer) and rotated on ice for one hour. Pierce™ Disposable Columns (Thermo Scientific™) with porous polyethylene discs were equilibrated with buffer A. Ni-NTA-lysate suspension was loaded onto the column and washed with at least 100 column volumes of buffer A. His-tagged Hrp1 was eluted using 500 mM imidazole in buffer A in a total volume of 10 mL. Protein eluate was concentrated using Vivaspin 20 centrifugal concentrators (MWCO 10 kDA, Sigma) for approximately 15 min, 4000 x *g* at 4 °C. Finally, buffer was exchanged to buffer B or PBS using PD MidiTrap G-25 (GE Healthcare) as specified by the manufacturer. Samples were analyzed by sodium dodecyl sulfate–polyacrylamide gel electrophoresis (SDS-PAGE) (Laemmli, 1970). Protein concentrations were determined using the BCA Protein Assay Kit (Merck Millipore) as specified by the manufacturer. Purified protein was stored at 4 °C. Co-crystallization with Biotin-CalB was performed by Stefanie Kobus and Dr. Sander Smits at the Center for Structural Studies (CSS), University of Düsseldorf, Germany.

Lysis buffer

20 mM	Hepes-HCl pH 7.5
150 mM	NaCl
10 mM	Imidazole
0.5% (v/v)	Triton X-100
1% (v/v)	Protease inhibitor cocktail
10% (w/v)	Lysozyme

Buffer A

20 mM	Hepes-HCl pH 7.5
150 mM	NaCl
30 mM	Imidazole
5 mM	β-mercaptoethanol

Buffer B

20 mM	Hepes-HCl pH 7.5
150 mM	NaCl
5 mM	β-mercaptoethanol

2.8.8 Quantitative real-time PCR (RT-qPCR)

For preparation of RNA, $1x10^9$ CFU/mL of precultured mycobacteria were used. Cells were centrifuged (4000 x *g*, 10 min), resuspended in 2 mL RNA protection reagent (Qiagen) and incubated overnight at RT. RNA was isolated using the RNeasy Kit (Qiagen) as specified by the manufacturer. Cells were lysed using Precellys® tubes containing a mixture of 0.5 mm and 0.1 mm glass beads and the Precellys® 24 Homogenisator (BERTIN). Complementary DNA was synthesized using the SuperScript™ III First-Strand Synthesis SuperMix Kit (Thermo Fisher). RT-qPCR was performed using the Agilent Technologies Mx3005P qPCR system and the GoTaq® qPCR Master Mix (Promega) as specified by the manufacturer. Oligonucleotides used for qPCR are listed in table 1. Quantification of RT-qPCR was performed following the ΔΔCt method. Expression of mRNA was calculated in relation to amplification of reference gene *16sRNA*, resulting in ΔCt values. ΔCt values were calibrated to control cells (BCG Pasteur WT or BCG Pasteur pMV361 EV) for calculation of ΔΔCt values. Relation of expression was shown as $2^{-\Delta\Delta Ct}$ values.

2.8.9 Pull down affinity enrichment coupled with LC-MS/MS using biotinylated callyaerins

In order to identify potential protein interaction partners of callyaerins, pulldown affinity enrichment experiments were done employing biotinylated callyaerin derivatives provided by the RG of Prof. Dr. Markus Kaiser from the Center of Medical Biotechnology at the University of Duisburg-Essen, Germany. After providing freshly prepared *M. tuberculosis* H37Rv protein lysates (see 2.8.3), pull down affinity enrichment as well as subsequent identification of enriched proteins employing liquid chromatography tandem mass spectroscopy (LC-MS/MS) was done by Florian Schulz and David Podlesainski (RG of Prof. Dr. Kaiser, University of Duisburg-Essen, Germany).

Briefly, the lysate was aliquoted into 15 samples (300 µg total protein per sample). The five conditions with three replicates each were: 1. DMSO, 2. trifunctional fluorophosphonate (Tri-FP; 2 µM), 3. Biotin_CalA (2 µM), 4. Biotin_CalA (2 µM) + bead washing with 20 µM CalA in washing solution, and 5. Biotin_CalB (2 µM). To each Eppendorf tube was added 1352 µL of either DMSO, Tri-FP (1 mM), Biotin_CalA (1 mM) or Biotin_CalB (1 mM) (all dissolved in DMSO resulting in a total DMSO concentration of 0.2 %). The samples were incubated for 60 min at 4 °C and 600 rpm. Pierce Avidin-Agarose beads (bed volume ~ 50 µL) were aliquoted into each sample Eppendorf-tube

and incubated for 30 min at 4 °C and 1100 rpm and for 30 min at RT and 1100 rpm. After centrifugation for 5 min at 600 x *g*, the beads were washed thrice with 1 mL PBS at RT (each time shaking at 1100 rpm followed by centrifugation for 5 min at 600 x *g* and discarding the supernatant). Samples of condition 4 (see above) were washed with PBS containing 20 µM CalA in washing steps 2 and 3. The beads were taken up in 100 µL 6 M urea (in 50 mM ammonium bicarbonate (ABC) containing 10 mM dithiothreitol (DTT)) followed by incubation for 30 min at RT shaking at 1100 rpm. Iodoacetamide was added (6 µL of 0.5 M stock solution in 50 mM ABC) followed by incubation for 30 min at RT shaking at 1100 rpm. DTT was added (6 µL of 0.5 M stock solution in 50 mM ABC) followed by incubation for 5 min at RT shaking at 1100 rpm. Samples were diluted with 470 µL 50 mM ABC. 1 µg trypsin was added per sample (10 µL of 100 ng/µL stock solution in 50 mM acetic acid) followed by incubation for 16 h at 37 °C shaking at 1100 rpm for in-solution digestion. The digestion was stopped by adding 10 µL 50% formic acid (FA) followed by incubation for 10 min at 37 °C shaking at 1100 rpm, and peptides were desalted on home-made C18 StageTips (Rappsilber *et al.*, 2007). Briefly, the peptide solution was passed over the methanol pre-conditioned and 0.5% FA equilibrated StageTip. Immobilized peptides were then washed twice with 0.5% (v/v) FA. Washed peptides were eluted from the StageTips with 80% (v/v) acetonitrile (ACN) 0.5% (v/v) FA and dried using a vacuum concentrator (Eppendorf). Before LC-MS/MS, peptide samples were resuspended in 10 µl 0.1% (v/v) FA.

LC–MS/MS experiments were performed on an Orbitrap Elite instrument (Michalski *et al.*, 2012) (Thermo) that was coupled to an EASY-nLC 1000 LC system (Thermo). The LC was operated in the one-column mode. The analytical column was a fused silica capillary (75 µm × 45 cm) with an integrated PicoFrit emitter (15 µm, New Objective) packed in-house with Reprosil-Pur 120 C18-AQ 1.9 µm resin (Dr. Maisch). The analytical column was encased by a column oven (Sonation) and attached to a nanospray flex ion source (Thermo). The column oven temperature was adjusted to 45 °C during data acquisition. The LC was equipped with two mobile phases: solvent A (0.1% FA, in water) and solvent B (0.1% FA in ACN). All solvents were of UPLC grade (Sigma). Peptides were directly loaded onto the analytical column with a maximum flow rate that would not exceed the set pressure limit of 980 bar (usually around 0.5-0.6 µl min^{-1}). Peptides were subsequently separated on the analytical column by running a 140 min gradient of solvent A and solvent B at a flow rate of 300 nL min^{-1} (gradient: start with 7% B; gradient 7 to 35% B for 120 min; gradient 35–100% B for 10 min and 100% B for 10 min). The mass spectrometer was operated using Xcalibur software, Thermo Fischer Scientific, UK (version 2.2 SP1.48) and was set in the positive ion mode. Precursor ion scanning was performed in the Orbitrap analyzer (fourier

transform mass spectrometry (FTMS)) in the scan range of m/z 300–1800 and at a resolution of 60000 with the internal lock mass option turned on (lock mass was 445.120025 m/z, polysiloxane) (Olsen *et al.*, 2005). Product ion spectra were recorded in a data dependent fashion in the ion trap (ion trap mobility spectrometry (ITMS)) in a variable scan range and at a rapid scan rate. The ionization potential (spray voltage) was set to 1.8 kV. Peptides were analyzed using a repeating cycle consisting of a full precursor ion scan (1.0×10^6 ions or 50 ms) followed by 15 product ion scans (1.0×10^4 ions or 100 ms), where peptides are isolated based on their intensity in the full survey scan (threshold of 500 counts) for tandem mass spectrum (MS2) generation that permits peptide sequencing and identification. Collision-induced dissociation (CID) energy was set to 35% for the generation of MS2 spectra. During MS2 data acquisition, dynamic ion exclusion was set to 120 s with a maximum list of excluded ions consisting of 500 members and a repeat count of one. Ion injection time prediction, preview mode for the FTMS (the orbitrap), monoisotopic precursor selection and charge state screening were enabled. Only charge states higher than one were considered for fragmentation. RAW spectra were submitted to an Andromeda (Cox *et al.*, 2011) search in MaxQuant (version 1.5.3.30) using the default settings (Cox and Mann, 2008). Label-free quantification was activated (Cox *et al.*, 2014). MS/MS spectra data were searched against the Uniprot *Mycobacterium tuberculosis* (strain ATCC 25618 / H37Rv) reference proteome database (UP000001584; 3,993 entries). All searches included a contaminants database (as implemented in MaxQuant, 245 sequences). The contaminants database contains known MS contaminants and was included to estimate the level of contamination. Andromeda searches allowed oxidation of methionine residues (16 Da), acetylation of the protein N-terminus (42 Da) as dynamic modifications and the static modification of cysteine (57 Da, alkylation with iodoacetamide). Enzyme specificity was set to “Trypsin/P”. The instrument type in Andromeda searches was set to Orbitrap and the precursor mass tolerance was set to ±20 ppm (first search) and ±4.5 ppm (main search). The MS/MS match tolerance was set to ±0.5 Da. The peptide spectrum match FDR and the protein FDR were set to 0.01 (based on target-decoy approach). Minimum peptide length was seven amino acids. For protein quantification unique and razor peptides were allowed. Modified peptides with dynamic modifications were allowed for quantification. The minimum score for modified peptides was 40. Further data analysis and filtering of the MaxQuant output was done in Perseus v1.5.5.3 (Tyanova *et al.*, 2016). MS/MS counts were loaded into the matrix from the proteinGroups.txt file and potential contaminants as well as reverse hits, hits only identified by site and protein groups with less than two identified unique peptides were removed. For the statistical calculations samples technical replicates were grouped in categorical groups and filtered. Only those

protein groups were kept that contained three valid values in a minimum of one categorical group. The missing values in the remaining protein groups were then imputed and the t-test performed (number of randomizations 250; initial FDR 0.05 and S0 0.1).

3 Results

This study aimed to investigate the activity and mode of action of callyaerins against *M. tuberculosis*. To overcome the challenge of product availability and to allow a wide range of various analyses, the Kaiser group successfully established a straightforward total synthesis of callyaerins based on a standard robot automized SPPS (unpublished). Briefly, amino acids are protected by Fmoc and *tert*-butyl alcohol. For oxidation of serine, deprotection is conducted by trifluoroacetic acid giving access to electrons for serine aldehyde formation resulting in the cyclic structure of callyaerins. In contrast to Zhang *et al.* (2018), where ring closure using a serine moiety failed, this approach represents the cyclization predicted for natural callyaerins. The synthesis delivers up to 20 mg of corresponding callyaerins in 30 min at RT and allows the generation of different derivatives. In the following, a comprehensive library of synthetic callyaerins was examined using SAR studies and approaches for target identification. All synthetic callyaerin derivatives used and analyzed in this study were produced by Florian Schulz or David Podlesainski (RG of Prof. Dr. Kaiser, University of Duisburg-Essen, Germany).

First, the activity of the synthetic CalA and CalB against *M. tuberculosis* strain H37Rv WT was evaluated to ensure the comparability of the two lead structures to the previous results published by Daletos *et al.* (2015). To distinguish between natural and synthetic CalA and CalB, naturally isolated callyaerins are henceforth referred to as ‘nat CalA’ and ‘nat CalB’ whereas synthetic compounds are directly abbreviated as ‘CalA’ and ‘CalB’. MIC assays were used to determine the activity of natural and synthetic callyaerins resulting in very similar dose response curves (fig. 6) and the same MIC_{90} values for CalA and nat CalA (= 3.125 µM). A small shift was observed in the activity of CalB (MIC_{90} = 0.39 µM) compared to nat CalB (MIC_{90} = 0.78 µM), most likely due to a higher chemical purity of the synthetic compound.

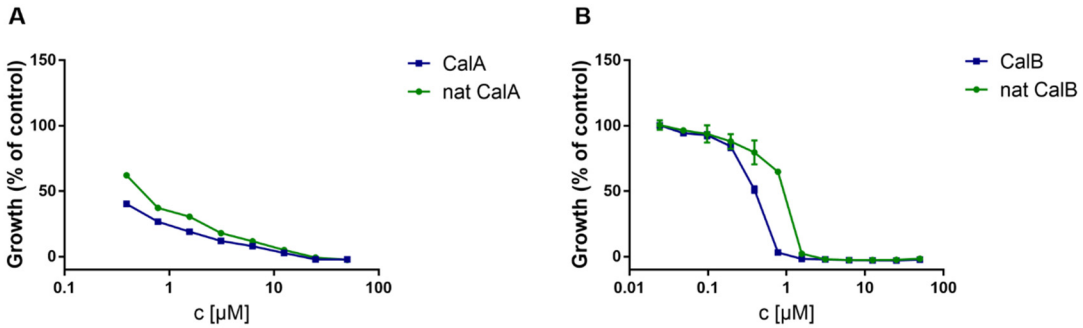

Figure 6: Comparison of the *in vitro* activity of natural and synthetic callyaerins. Dose-response curves of synthetic (■) and natural (●) CalA (**A**) and CalB (**B**) against *M. tuberculosis* H37Rv WT. Data are shown as means of n = 3 ± SEM.

3.1 Callyaerins selectively inhibit growth of *M. tuberculosis*

To investigate the selectivity of both, CalA and CalB, compounds were tested for potential cytotoxicity against human cells. Different human cell lines were used, namely THP-1, HepG2 and HEK293 allowing to exclude potential hepatotoxic and nephrotoxic side effects. Dose-response curves of CalA and CalB against the respective cell lines (fig. 7) revealed a strong selectivity of both compounds. Neither CalA nor CalB showed cytotoxic activity at low micromolar concentrations. Growth inhibition of human cell lines was observed at 50 or 25 µM, resulting in SI of 16 or 64 for CalA or CalB, respectively (table 8). Noticeable, the previously published data described a cytotoxic potential of nat CalB (Daletos *et al.*, 2015) whereas a strong cytotoxic activity is missing for the synthetic substance resulting in a greater therapeutic window compared to CalA (table 8). This specific property of CalB was likely achieved due to higher quality and chemical purity of the synthetic compound by comparison with the isolated natural substance.

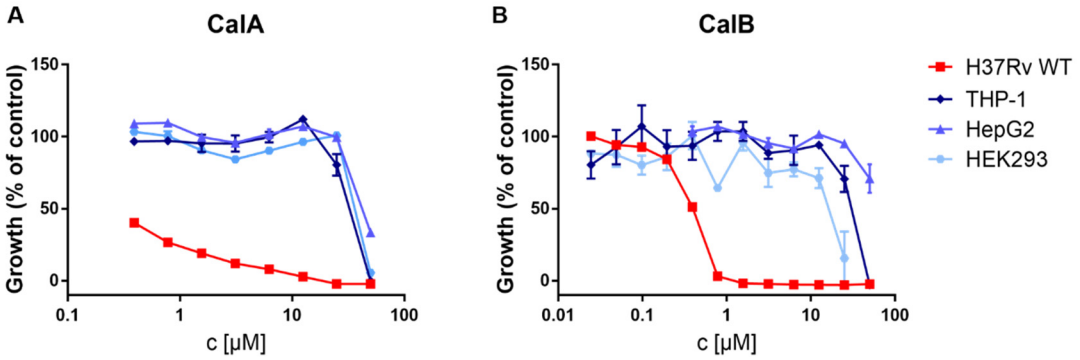

Figure 7: Selectivity of callyaerins. Dose-response curves of CalA (**A**) and CalB (**B**) against *M. tuberculosis* H37Rv WT (■) are compared to several human cell lines (♦-THP-1, ▲-HepG2 and ●-HEK293). Data are shown as means of n = 3 ± SEM.

Table 8: MIC_{90} and IC_{50} values [µM] of CalA and CalB screened against *M. tuberculosis* H37Rv WT and respective cell lines. MIC_{90} and IC_{50} values were determined in triplicates. SI were calculated as ratio between IC_{50} and MIC_{90} values. SI of CalB was determined using IC_{50} value of HEK293 cells.

	H37Rv (MIC_{90})	**THP-1** (IC_{50})	**HepG2** (IC_{50})	**HEK293** (IC_{50})	**SI** (IC_{50}/MIC_{90})
CalA	3.125	50	50	50	16
CalB	0.39	50	>50	25	64

After evaluation of selectivity, callyaerins were screened against other bacteria, in particular further mycobacteria. As further slow-growing mycobacteria, susceptibility of callyaerins was determined against virulent *M. bovis* and attenuated *M. bovis* BCG Pasteur. Compared to *M. tuberculosis*, a clear shift was observed regarding both strains (fig. 8A and 8B). The same was observed for *M. bovis* BCG Danish, Copenhagen and Birkhaug (data not shown). To evaluate the effect on fast-growing mycobacteria, screens were performed against *M. smegmatis* (fig. 8C) and *M. marinum* (fig. 8D). However, no clear activity of both compounds could be detected. Last, to investigate a potential activity of CalA and CalB against nosocomial pathogens, the MRSA *S. aureus* strain Mu50 was used as a representative for gram-positive bacteria. Again, neither CalA nor CalB inhibited growth of MRSA up to a concentration of 50 µM (fig. 8E).

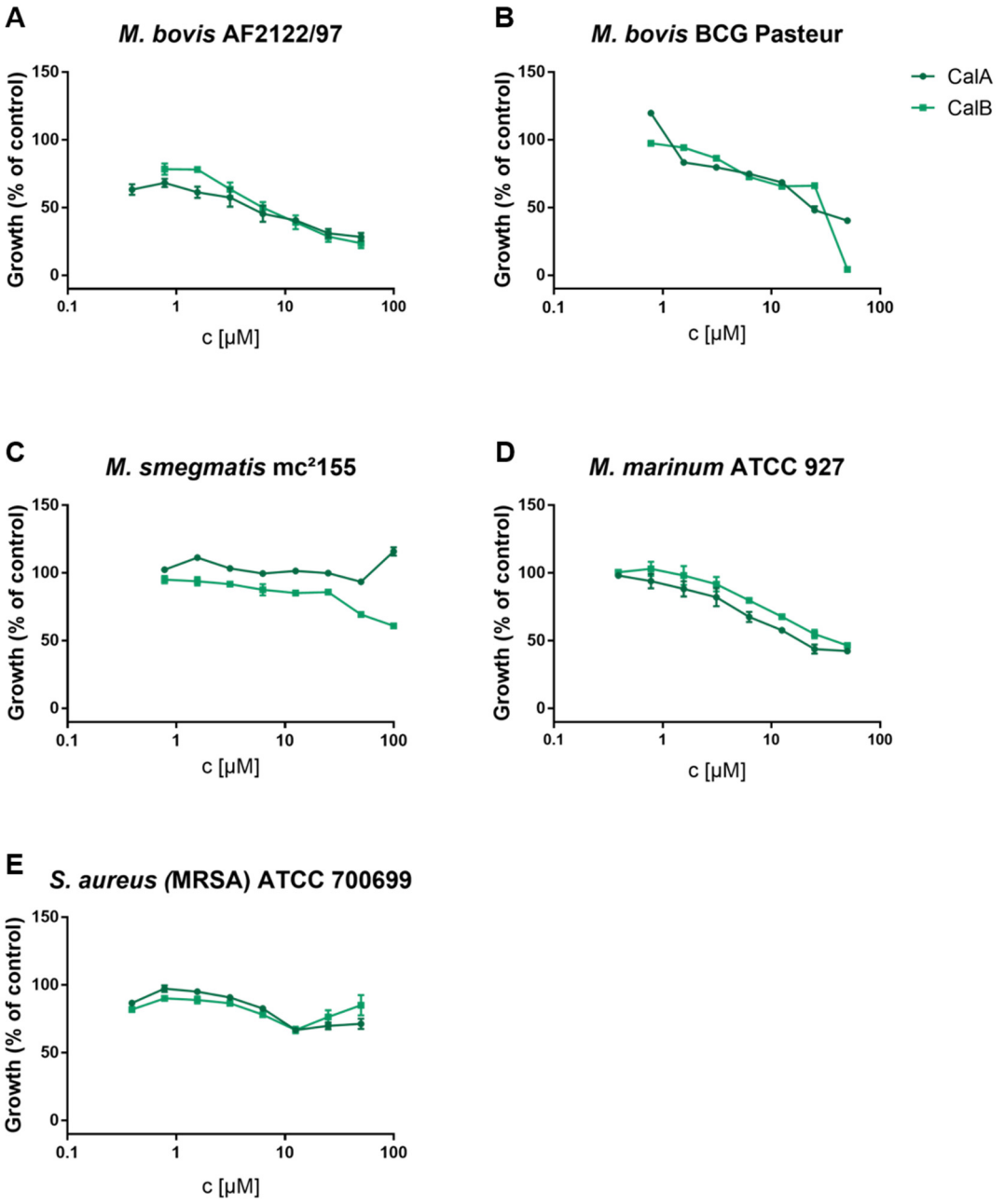

Figure 8: Susceptibility of further bacteria against callyaerins. Dose-response curves of CalA (●) and CalB (■) against further mycobacteria including virulent *M. bovis* (**A**), *M. bovis* BCG Pasteur (**B**), *M. smegmatis* (**C**) and *M. marinum* (**D**). Figure (**E**) shows dose-response curves of a MRSA *S. aureus* strain Mu50 (ATCC 700699) representative for gram-positive bacteria. Data are shown as means of n = 3 ± SEM.

Summarizing the previously described results, callyaerins seem to specifically inhibit growth of *M. tuberculosis*. However, to substantiate this hypothesis, further *M. tuberculosis* strains were used to exclude a limited activity only against the laboratory strain H37Rv. Figure 9A shows a representative screening of CalA against different

M. tuberculosis strains including CDC1551, HN878 and the attenuated strain mc²6230 *ΔpanCD ΔRD1*. Activity could be detected against all the strains; however, a shift was observed for *M. tuberculosis* HN878 WT (MIC_{90} = 12.5 µM). HN878 represents a strain of the Beijing lineage of *M. tuberculosis* and is known for increased virulence, altered regulation of the DosR (Domenech *et al.*, 2017) and a specific lipid profile (Huet *et al.*, 2009). In contrast, for the avirulent auxotrophic strain mc²6230 Δ*panCD* Δ*RD1*, the MIC_{90} was reduced to 0.78 µM (see table 9). In a final step, activity of callyaerins was determined against different *M. tuberculosis* XDR clinical isolates from KZN (Ioerger *et al.*, 2009). Albeit the potency of CalA and CalB was lower compared to their activity against H37Rv WT and CDC1551 WT (table 9), dose-dependent growth inhibition was observed for both compounds (fig. 9B and 9C).

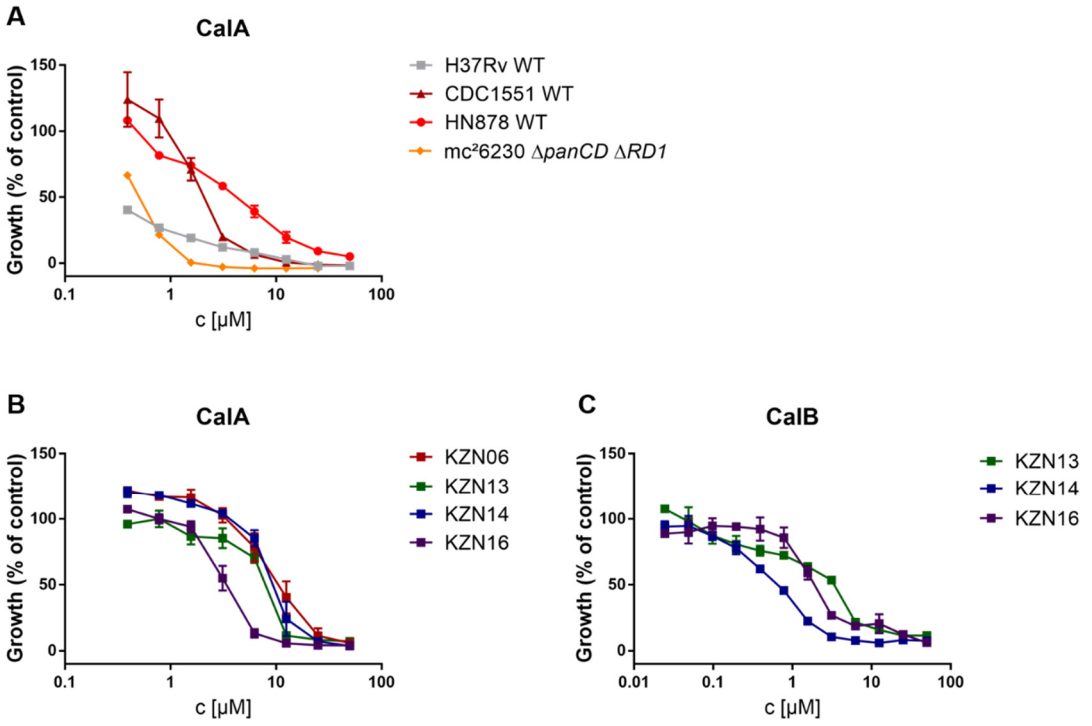

Figure 9: Activity of callyaerins against different *M. tuberculosis* strains including XDR clinical isolates. Dose-response curves of CDC1551 WT (▲), HN878 WT (●) and mc²6230 Δ*panCD* Δ*RD1* (♦) as compared to H37Rv WT (■) against CalA are shown in (**A**). Several XDR clinical isolates (■-KZN06, ■-KZN13, ■-KZN14, ■-KZN16) were screened against CalA (**B**) and CalB (**C**). Corresponding MIC_{90} values are listed in table 9. Data are shown as means of n = 3 ± SEM.

Table 9: MIC_{90} values [µM] of CalA and CalB screened against several *M. tuberculosis* WT strains and *M. tuberculosis* XDR clinical isolate KZN06-16. MIC_{90} values were determined in triplicates. MIC_{90} values of CalB against CDC1551 WT, HN878 WT and KZN06 were not determined (n.d.).

	CalA (MIC_{90})	**CalB** (MIC_{90})
H37Rv WT	3.125	0.39
CDC1551 WT	3.125	n.d.
HN878 WT	12.5	n.d.
mc²6230 Δ*panCD* Δ*RD1*	0.78	< 0.78
KZN06	12.5	n.d.
KNZ13	12.5	> 50
KZN14	12.5	3.125
KZN16	6.25	25

To assess whether the growth-inhibiting activity of callyaerins is accompanied by decreased energy metabolism, the effects on energy-generating pathways like the branched electron transport chain were evaluated. The electron transport chain is an energy-generating machinery for energy production by oxidative phosphorylation and thereby maintains the membrane potential. Effects on the energy-generating pathways were determined by measurement of ATP in a whole-cell assay of antibiotic-treated *M. tuberculosis* cells. When treated with CalA or CalB, cellular ATP concentration decreased in a concentration-dependent manner, indicative of a reduced energy level of the cells (fig. 10). A similar but slightly less potent effect was observed for CCCP, an efflux pump inhibitor that depolarizes the cell membrane and thereby leads to a reduced membrane potential (Lamprecht *et al.*, 2016). A stronger reduction in ATP concentration was determined for BDQ, which directly targets the ATP synthase (electron transport chain complex V) by binding to subunit c (Preiss *et al.*, 2015). In contrast, RIF, which is a bactericidal drug that targets the DNA-dependent RNA polymerase (see chapter 1.2.2), did not substantially affect intracellular ATP levels as expected. The observed effect of CalA and CalB indicates that energy metabolism in *M. tuberculosis* is impaired when treated with callyaerins and might give a hint that energy-generating pathways are involved in the mode of action. However, a direct effect on ATP synthase seems rather unlikely due to the much weaker influence of callyaerins compared to BDQ.

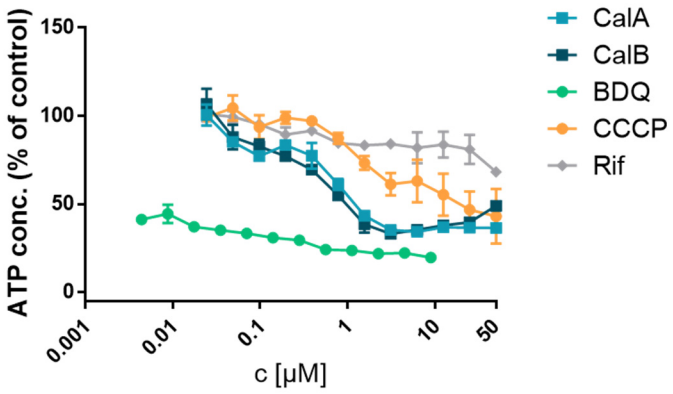

Figure 10: Effects of callyaerins on energy metabolism, as quantified by measurement of ATP concentration. Treatment of *M. tuberculosis* H37Rv WT with CalA (■) and CalB (■) leads to a reduced ATP concentration and a decrease in energy metabolism. BDQ (●) and CCCP (●) were used as positive controls, by targeting ATP synthase or inhibition of efflux pumps, respectively (Lamprecht *et al.*,2016, Preiss *et al.*, 2015). RIF (♦) was used as negative control. Data are shown as means of n = 3 ± SEM.

3.2 Structure-activity relationship studies of synthetic callyaerins

The two cyclic peptides CalA and CalB were identified as active compounds and lead structures. The established chemical synthesis route for callyaerins allows a batched production of a comprehensive library of derivatives for SAR studies giving insights into essential structural characteristics and possible modifications of callyaerins. CalA (fig. 5C) consists of seven amino acids that are distributed to eight ring positions and four positions in the sidechain: isoleucine, hydroxyproline, valine, leucine, phenylalanine, glycine and proline. In contrast, CalB is composed of five different amino acids: isoleucine, hydroxyproline, valine, leucine and proline. CalB could be described as a less complex structure than CalA, with a reduced sidechain due to the missing glycine at position C4 (fig. 5D). However, it is active at lower concentrations than CalA resulting in a higher selectivity (table 8). Both compounds consist of three prolines and one hydroxyproline. These amino acids contain a secondary amino group contributing to a rigid conformation of the peptides and reduced formation of hydrogen bridge linkages caused by a missing amide hydrogen. To complete the screenings and the library of callyaerins, the naturally occurring callyaerins C to L were synthesized. Nevertheless, none of them showed a growth-inhibiting activity against *M. tuberculosis* (table 10E). To verify the importance of the specific cyclic structure of callyaerins, a linearized CalA (non_cyc, fig 11B) was provided for activity studies. A linearized peptide structure of

CalA resulted in a complete loss of its activity, which is in conformity with the results published by Li and Brimble (2019) where a modified ring closure by a lactam linkage leads to a loss of activity as well. Both results emphasize the importance of the typical cyclization by the DAA moiety. Since ring closure is an essential step for callyaerin activity, is was next focused on the length of the sidechain. A reduction of the sidechain of CalA at positions C3 and C4 (CalA_C3+C4X) led to decreased activity of this specific compound (fig. 11B). However, more derivatives are needed for a final evaluation of the putative impact of the sidechain, for instance CalA_C2+C3+C4X or a derivative missing the complete sidechain. Remarkably, the extension of the sidechain of CalA with an additional alanine residue at position C5 (table 10A) resulted in a maintained activity of the derivative, implying that the specific composition of the sidechain in combination with its length is essential for the activity.

Focusing on the similarities between CalA and CalB, several CalA derivatives were synthesized introducing amino acid exchanges that converge to the amino acid composition of CalB (CalA/CalB intermediates, table 10C). Reduction in the sidechain (C4X) or substitution of isoleucine at different positions (R3I and C3I) led to an increase in activity resulting in a lower MIC_{90} value. Interestingly, activity was maintained for the combined CalA derivative (C3I+C4X), despite resembling CalB the most (fig 11A). The strongest reduction in the MIC_{90} was observed for derivative CalA_R3I, implying that isoleucine at this ring position either increases affinity of callyaerin to its target or facilitates uptake or both.

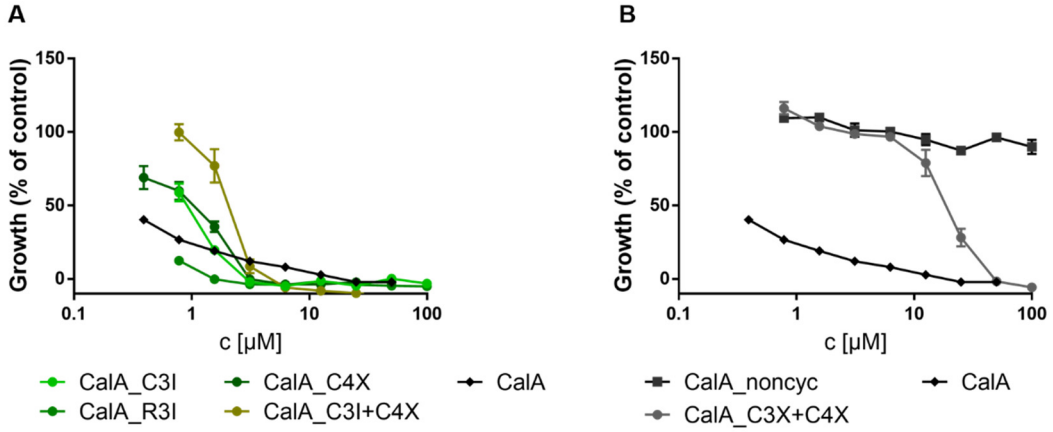

Figure 11: Dose-response curves of different callyaerin derivatives against *M. tuberculosis* H37Rv WT. Activity of different CalA derivatives harboring amino acid exchanges to CalB are shown in (**A**). Reduced activity was observed for a noncyclic derivative (■) and a shortened sidechain (●; **B**). Dose-response curve of CalA is shown for comparison (♦). Data are shown as means of n = 3 ± SEM.

The main part concerning the synthesis of derivatives focused on modifications of CalA in both, in ring and sidechain positions. While the substitution of isoleucine at positions where it occurs in CalB increased the activity, a replacement with isoleucine at position R5 reduced the activity of the compound (table 10A). At this specific position, the replacement with another aliphatic branched-chain amino acid already resulted in an unfavorable change in activity. Substitutions of other amino acids naturally occurring in CalA at different ring positions like R2P, R3L, R3F or R8V eventuated in an unaltered activity (MIC_{90} = 3.125 µM). Repeatedly, reduced activity was observed for an isoleucine derivative, here substituted at position R8, giving a hint that an additional steric center near the DAA moiety putatively leads to steric hindrance of interaction with the target. Individual substitution of all ring positions of CalA with alanine resulted in an increased MIC_{90} value, except for the derivative R4A (table 10A). This implies that a less complex configuration of CalA is accompanied by a reduction in activity. To further investigate the maintained activity of CalA_R4A, additional derivatives of position R4 need to be studied. Those studies will reveal whether position R4 can be modified in general giving a hint that this position might not be involved in target interaction. The modification with a hydrophilic acidic amino acid like aspartic acid (R5D) or with an aromatic amino acid like tryptophan (R8W) caused a complete loss of activity (table 10). Thus, the hydrophobic character of callyaerins seems to be essential for their ability to pass the mycobacterial membrane and conceivably for interaction with the target. Analogous to the results of alanine substitution at different ring positions, a reduced activity was observed for all derivatives containing alanine at different sidechain positions (C1A, C2A, C3A and C4A, table 10). This, in fact, supports the hypothesis that a certain complexity is required for the growth-inhibiting activity of callyaerins. Intensified studies on position C3 revealed that substitution by tryptophan resulted in a lower MIC_{90} value, whereas leucine led to maintained activity. Special about the amino acid composition of both, CalA and CalB, is the occurrence of hydroxyproline, a post-translationally modified amino acid at ring position R2. From a chemical point of view, hydroxyproline mirrors a cost-intensive part in synthesis. Therefore, successful replacement with proline (R2P) accompanied by maintained activity of the compound (table 10) allows the synthesis of a more affordable and economic derivative in multi gram-scale permitting studies in animal models of infection.

Table 10: Heatmap showing MIC_{90} [µM] values of different callyaerin derivatives. Substances are grouped in CalA (**A**) and CalB (**B**) derivatives and CalA/B intermediates (**C**). Click chemistry derivatives are listed in (**D**). (**E**) shows MIC_{90} values of a linearized CalA derivatives and callyaerins C-L. Amino acid exchanges are shown in one-letter code (expect for Hyp), exchanges based on non-natural amino acids are shown in three-letter code (**A**, **B** and **D**). MIC_{90} of unsubstituted CalA and CalB are 3.125 µM or 0.39 µM, respectively. MIC_{90} were determined in triplicates. All callyaerin derivatives were synthesized by Florian Schulz or David Podlesainski, University of Duisburg-Essen, Germany. Heatmap shows color code of MIC_{90} values in µM. The structure scheme of callyaerins (Daletos *et al.*, 2015) displays positions of substitutions of derivatives. Amino acids of unsubstituted CalA and CalB are listed below.

A

CalA derivatives

aa-exchanges in ring structure	MIC_{90} [µM]
R1A	12.5
R2A	12.5
R2P	3.125
R2P+R3I	3.125
R3A	>50
R3F	3.125
R3L	3.125
R3Cpg	3.125
R3Abu	12.5
R4A	3.125
R5A	6.25
R5D	>100
R5I	12.5
R6A	12.5
R7A	6.25
R8A	12.5
R8W	>100
R8V	3.125
R8I	25

aa-exchange in side chain	MIC_{90} [µM]
C1A	12.5
C2A	>50
C3A	>50
C3L	3.125
C3W	1.56
C3X+C4X	25
C4A	12.5
C5A	3.125

aa-exchange in both	MIC_{90} [µM]
R2P+C3I+C4X	6.25

B

CalB derivatives

aa-exchange in side chain	MIC_{90} [µM]
C3PrGly	25
C3Abu	>50
C3Bpa	6.25
C3Tle	6.25

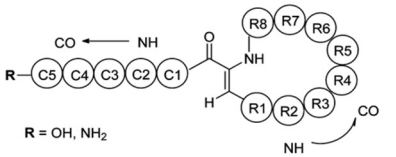

	R1	R2	R3	R4	R5	R6	R7	R8	DAA	C1	C2	C3	C4
CalA	I	Hyp	V	I	L	P	P	L		P	I	F	G
CalB	I	Hyp	I	I	L	P	P	L		P	I	I	

C

CalA/B intermediates

aa-exchange	MIC_{90} [µM]
R3I	0.78
C3I	1.56
C3I+C4X	3.125
C4X	1.56

D

Click chem derivates

	MIC_{90} [µM]
CalA_C4Pra	1.56
CalA_C4Aha	3.125
CalB_C4Pra	3.125
Cy3_CalA	0.004
Biotin_CalA	12.5
Biotin_CalB	6.25

E

others

	MIC_{90} [µM]
noncyc	>100
CalC-CalL	25-100

µM
<0.39
0.39
0.78
1.56
3.125
6.25
12.5
25
>50

It needs to be emphasized that from all tested derivatives substituted with natural amino acids, the natural, unsubstituted CalB still has the strongest growth-inhibiting activity. The studies with alanine substitutions described above revealed a favorable effect of bulky hydrophobic amino acids. Based on these results, different bulky amino acids have been substituted to both, CalA and CalB. With similarity to leucine, 2-aminobutyric acid (Abu) and *tert*-leucine (Tle) have been substituted to CalA (R3Abu) and CalB (C3Abu and C3Tle), respectively. Additionally, cycloproylglycine (PrGly), an amino acid composed of a hydrophobic ring residue, has been substituted to chain position C3 of CalB. Last, representing the bulkiest amino acid, a benzophenone (Bpa) analogue that allows photoaffinity labeling of proteins by cross-linking induced by

application of UV-light, was used to synthesize a CalB derivative at position C3 (table 10B). However, all of these comprehensive modifications led to a decreased growth-inhibiting activity.

3.2.1 Callyaerin derivatives for click chemistry approaches

The term click chemistry was introduced by Kolb *et al.* (2001). The substitution of CalA and CalB by amino acids like propargylglycine (Pra) and azidohomoalanine (Aha) allows the application of click chemistry via azide-alkyne-cycloaddition. Using this simple and fast method, different chemical approaches could be conducted to gain further insights into the mode of action of callyaerins and thereby elucidating its target. Different derivatives for click chemistry approaches have been synthesized by the Kaiser group, like CalA_C4Aha, CalA_C4Pra and CalB_C4Pra (fig 12). Those azide- and alkyne-containing derivatives could be used for specific labeling of biomolecules via, for instance, alkyne- or azide-tagged fluorophores, thus allowing to determine the intracellular or membrane-bound location of callyaerins. Additionally, 'clicking' of residues for specific capturing of molecules allows the application of affinity enrichment approaches like it was shown for biotin-tagged callyaerins (see chapter 3.5).

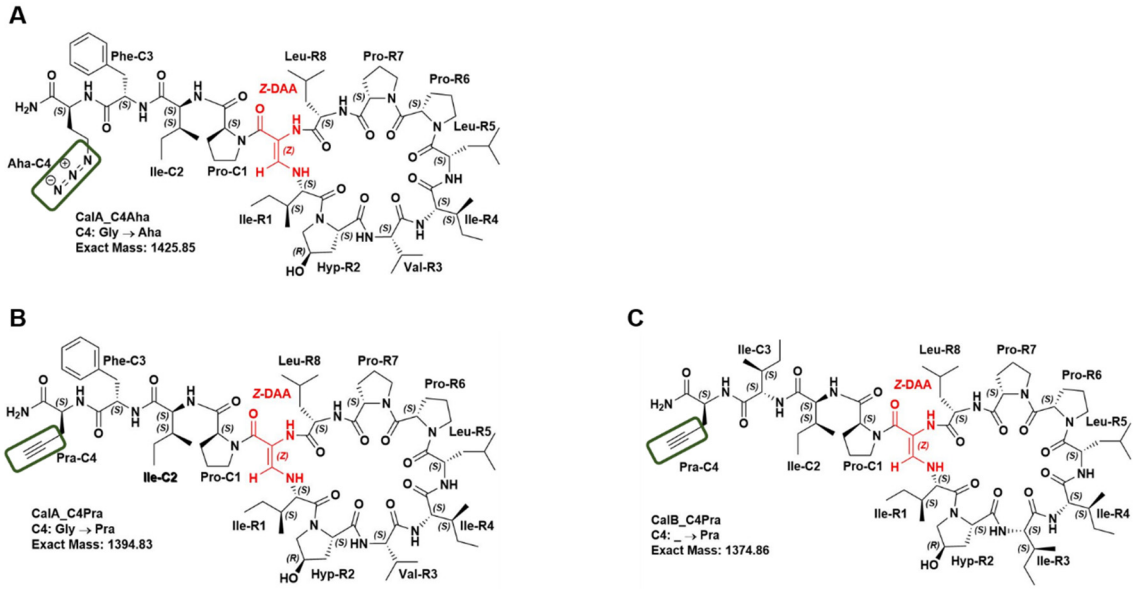

Figure 12: CalA and CalB derivatives comprising azide- or alkyne-containing amino acids Aha or Pra. CalA was substituted with Aha at position C4 resulting in a free azide residue (**A**). Additionally, CalA (**B**) and CalB (**C**) were substituted with Pra at position C4 generating a free alkyne-residue. Azide and alkyne residues are edged in green. All derivatives show a dose-depended growth-inhibiting activity against *M. tuberculosis* (fig. 13). Chemical structures were obtained from Florian Schulz, University of Duisburg-Essen, Germany.

To exclude that these modifications have an impact on the activity of callyaerins, click chemistry derivatives were screened for growth-inhibiting effects in MIC assays. Comparable to CalA, all three derivatives showed a dose-dependent growth inhibition of *M. tuberculosis* resulting in activity in micromolar concentrations (fig 13A). Additionally, a callyaerin-resistant (Cal-res) clone (see chapter 3.4) was utilized to prove that all tested derivatives are subject to the same uptake-based mechanism for entering the bacterial cells (fig. 13B).

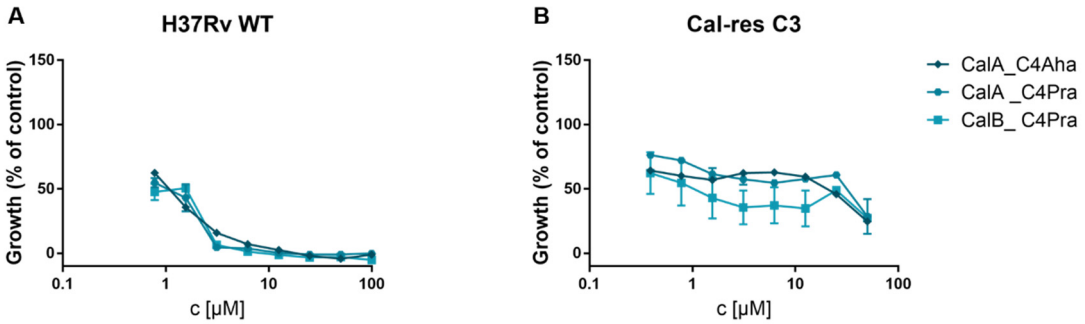

Figure 13: Growth-inhibiting activities of callyaerin derivatives containing Pra or Aha residues for click reactions. Dose-response curves of CalA_C4Aha (♦), CalA_C4Pra (⬢) and CalB_C4Pra (■) against *M. tuberculosis* H37Rv WT are shown in (**A**). Resistance of a Cal-res mutant is represented in growth patterns shown in (**B**). Data are shown as means of n = 3 ± SEM.

3.2.2 Fluorophore-tagged callyaerin derivatives

Special derivatives were designed by ‘clicking’ fluorophores to the callyaerins CalA_C4Pra and CalB_C4Pra. Those fluorophore-tagged callyaerin derivatives could be used for fluorescence microscopy approaches to identify an intracellular location of the compounds or might be utilized as *M. tuberculosis*-specific probes in terms of diagnosis. Proceeding from the C4_Pra derivatives, two different compounds were synthesized using a Cy3-triethylenglycol (PEG3)-azide or a Cy5-PEG3-azide, respectively, resulting in Cy3_CalA and Cy5_CalB (fig. 14D and 14E). Both compounds were screened for their growth-inhibiting properties with respect to the fluorophore alone (fig. 14A and 14B). The combination of Cy3 and CalA led to a very strong, dose-dependent growth inhibition resulting in a MIC_{90} at nanomolar concentration (5 nM). In contrast, the Cy5_CalB derivative showed only a slight growth-inhibiting effect. However, the same effect was observed for the unconjugated fluorophore alone. This strong discrepancy in activities is surprising comparing the high structural similarity between CalA and CalB as well as Cy3

and Cy5. Since the activity of Cy3_CalA is three order of magnitudes higher than the activity of CalA itself, potential cytotoxic effects were evaluated. However, no cytotoxicity could be detected for Cy3_CalA against THP-1 and HEK293 cell lines (fig. 14C). Additionally, a Cal-res clone was screened against Cy3_CalA resulting in a clear shift in the MIC_{90} (fig. 14C), implying that this compound underlies the same mode of resistance although there is a vigorous increase in activity. Based on the slight activity of the Cy3-PEG3-azide, which might be due to a poor cell penetration rate of the charged fluorophore, it can be assumed that Cy3_CalA could have two independent targets giving a first hint of potential callyaerin derivatives used as multi-targeting drugs. Comparable to CalA, Cy3_CalA has no growth-inhibiting effect on *M. smegmatis* (data not shown), enabling the application of fluorescent callyaerins in terms of diagnosis of TB disease.

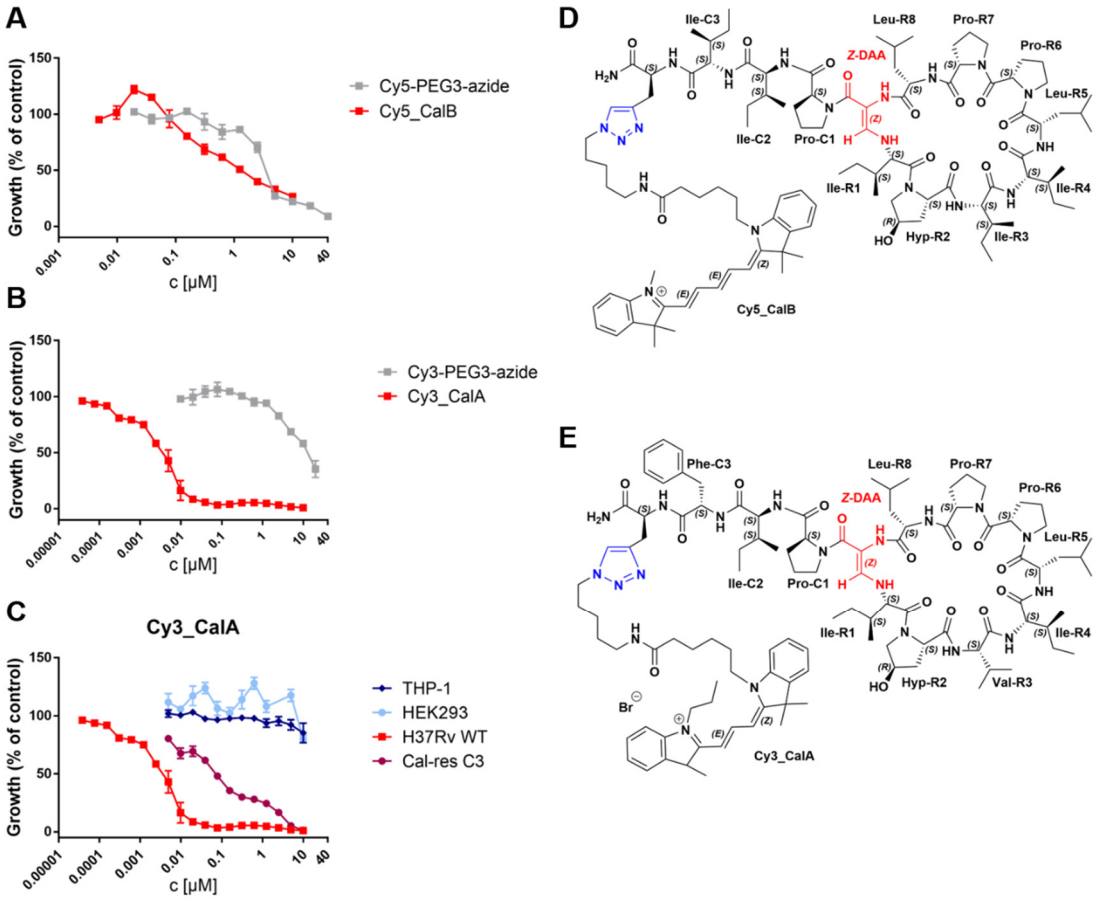

Figure 14: Growth-inhibiting activity of fluorophore-tagged callyaerin derivatives. A Cy5-PEG3-azide and a Cy3-PEG3-azide were clicked to CalB_C4Pra or CalA_C4Pra, respectively. Dose-response curves of the callyaerin derivatives (■) and fluorophores alone (■) against *M. tuberculosis* H37Rv WT are shown in (**A**) and (**B**). The Cy3_CalA derivative was screened against THP-1 (♦) and HEK293 (●) cells as well as a *M. tuberculosis* Cal-res clone (●;**C**). Cy5_CalB (**D**) and Cy3_CalA (**E**) were synthesized by 'clicking' a fluorophore PEG3-azide via cycloaddition (blue) to Pra residues at position C4. Data are shown as means of n = 3 ± SEM.

3.3 Callyaerins inhibit intracellular replication of *M. tuberculosis* in a macrophage infection assay

Since *M. tuberculosis* is an intracellular phagocytosed pathogen, the growth-inhibiting activity of new potential drugs against bacteria internalized by macrophages is of particular interest. In this study, a macrophage infection assay was applied by differentiation of THP-1 cells to macrophage-like cells upon PMA stimulation. Cells were infected with a reporter strain of *M. tuberculosis* constitutively expressing mCherry for fluorescence evaluation as a correlate of growth. Three hours post infection, cells were treated with CalA, CalB or the clinically used antibiotics RIF and STREP. Efficiency of antibiotics was evaluated five days post infection (dpi). Cells treated with control solvent (DMSO, fig. 15A-A`) exhibited a heavy intracellular bacterial burden, appeared clumpy and started to detach from the surface. A high intensity in red fluorescence documented a strong infection with the reporter strain. In contrast, cells treated with CalA (fig. 15B-B`) and CalB (fig. 15C-C`) exhibited a healthy morphology further supported by a low integrated red fluorescence density (fig 16) with only around 1% of that of the DMSO-treated control. Treatment with RIF resulted in a healthy cell morphology of the cells (fig. 15D-D`) and an even stronger intracellular growth inhibition of *M. tuberculosis* evident from measurement of red fluorescence density (fig. 16). Remarkably, STREP exhibited a lower effect on internalized *M. tuberculosis*. The cells already started to detach from the surface (fig. 15E), and the determined red fluorescence density was around 20% of the DMSO-treated control (fig. 16).

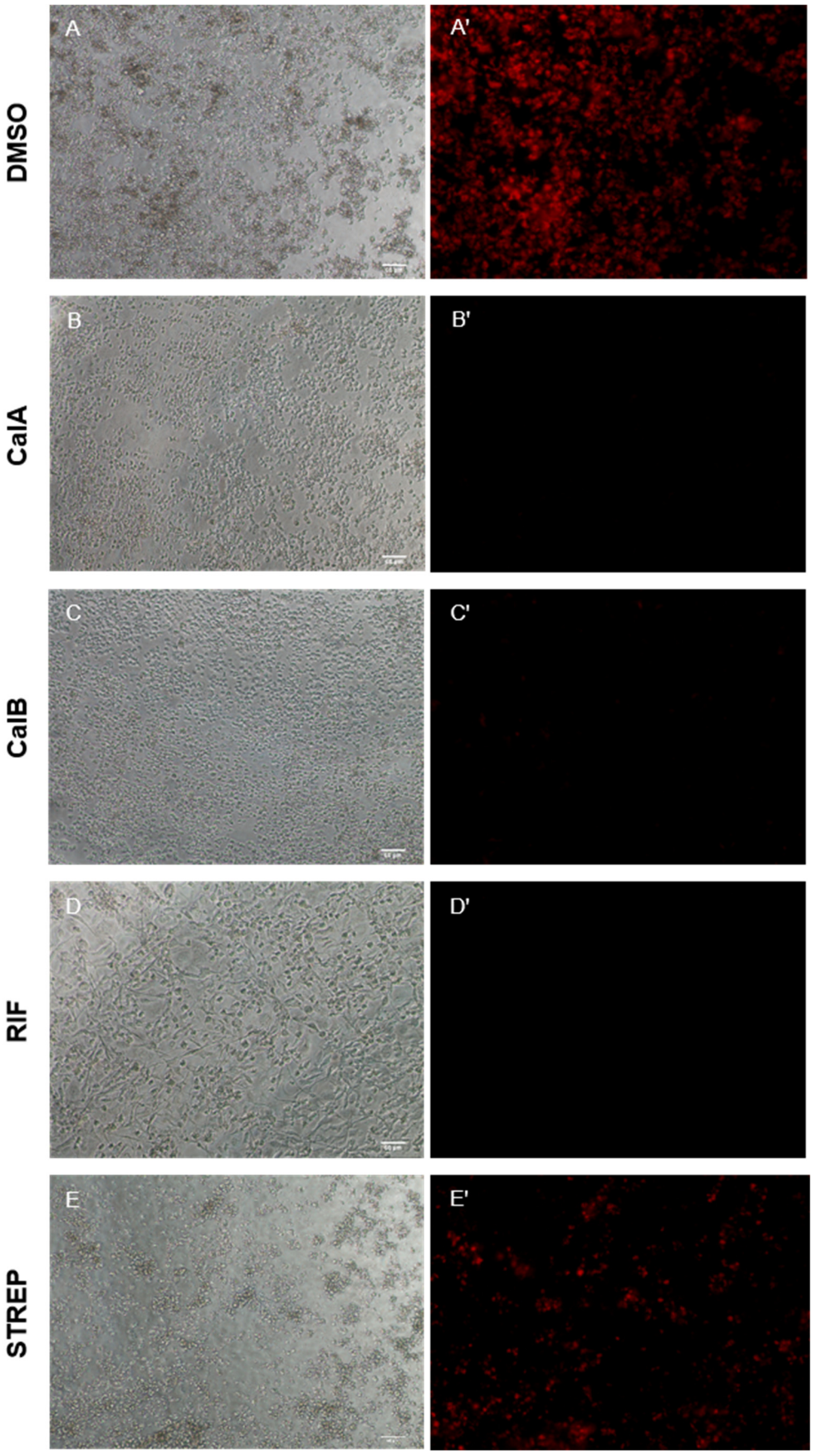

Figure 15: Intracellular activity of CalA and CalB in a macrophage infection assay. THP-1 cells were differentiated into macrophage-like cells using PMA. Cells were infected with a mCherry expressing strain of H37Rv (MOI = 3) for three hours and treated with 15.6 µM CalA, 1.95 µM CalB or antibiotics (1 µM RIF or 20 µM STREP). Control cells were treated with 0.15 % (v/v) DMSO. Cells were fixed 5 dpi and analyzed by fluorescence microscopy. Data show representative images of two independent experiments. A-E: brightfield. A'-E': red channel. Scale bar represents 50 µm.

The results indicate that CalA and CalB are able to penetrate the macrophages and strongly inhibit growth of *M. tuberculosis* in the phagosome by impaired replication of the bacteria. Additionally, evaluation of these results led to exclusion of a mode of action of callyaerins based on metabolic mechanisms synthesizing nutrients that could be incorporated from the host cell environment.

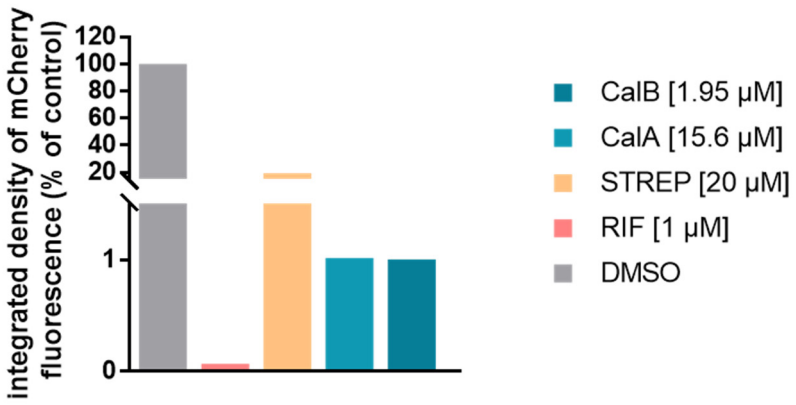

Figure 16: Integrated density of red fluorescence as percent of DSMO-treated control. After three hours of infection, cells were treated with 1.95 µM CalB (■), 15.6 µM CalA (■), 20 µm STREP (■) or 1 µM RIF (■). Cells were used for microscopy and evaluation of red fluorescence 5 dpi. For each condition, three fields per view were evaluated and means were normalized to DMSO-treated control (■; = 100 %). Integrated density of red fluorescence was calculated using Fiji (ImageJ).

3.4 Single point mutations in the membrane protein Rv2113 mediate resistance against callyaerins

To gain insights into the mode of action of callyaerins, SRM of *M. tuberculosis* H37Rv WT were generated. For this, bacterial cells were plated on 7H10 agar supplemented with nat CalA at fourfold MIC. Plates were incubated aerobically until single colonies appeared. After approx. six weeks, single colonies on selective media were obtained resulting in a resistance frequency of 10^{-7}. Several independent clones were grown in liquid culture to verify their resistance against callyaerins. Resistance profiles of clones C1 to C3 determined by MIC assays against CalA and CalB are shown in fig. 17. Clones C1 to C3 (henceforth referred to as Cal-res C1-C3) displayed a strong resistance since virtually no dose-dependent growth inhibition could be detected up to a concentration of 100 µM. Cross-resistance was also detected against several active

CalA derivatives harboring amino acid exchange in both, ring or sidechain position (such as CalA_R2P, CalA_R4A, CalA_R5A and CalA_C4A; see fig. S2).

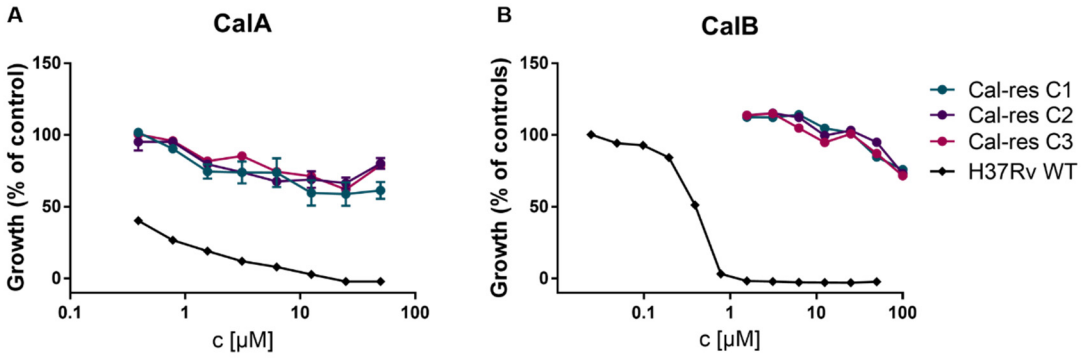

Figure 17: Resistance pattern of SRM against callyaerins. Dose-response curves of *M. tuberculosis* H37Rv Cal-res clones C1 (●), C2 (●) and C3 (●) against CalA (**A**) and CalB (**B**). *M. tuberculosis* H37Rv WT (♦) is shown for comparison. Data are shown as means of n = 3 ± SEM. Data of Cal-res clones in (**B**) represent single measurements.

Whole-genome sequencing of the three resistant clones revealed mutations in the gene Rv2113 engendering single amino acid substitutions (table 11). The gene Rv2113 codes for a putative nonessential transmembrane protein with so far unknown function. Secondary structure prediction employing a Hidden Markov Model (online tool available at http://www.cbs.dtu.dk/services/TMHMM/) revealed eight predicted transmembrane domains of the protein Rv2113. Only in one resistant mutant, Cal-res C3, a second gene harboring a mutation was identified. This essential gene, *aftD,* encodes an arabinofuranosyltransferase synthesizing parts of the mycobacterial cell wall, namely the arabinan domain of arabinogalactan and lipoarabinomannan (Škovierová *et al.*, 2009).

Table 11: Whole-genome sequencing of *M. tuberculosis* H37Rv CalA-res mutants C1-C3 revealed amino acid exchanges in the protein Rv2113. Resistant mutants of H37Rv were generated on 7H10 agar containing four times the MIC of nat CalA and appeared at a density of 10^{-7} after six weeks of incubation. Amino acid exchanges are listed in one-letter code. Whole-genome sequencing was performed by T. Ioerger (Department of Computer Science, Texas A&M University, College Station, Texas, USA).

Resistant mutant	Mutations
CalA-res C1	**Rv2113**: T185A
CalA-res C2	**Rv2113**: L28P
CalA-res C3	**Rv2113**: L341P, Rv0236c/AftD:G882G

Both proteins are putatively involved in cell wall processes of *M. tuberculosis*, which implies a potential mode of action affecting the composition of the mycobacterial cell wall. However, only mutations in Rv2113 were found in all three resistant clones. As a consequence, the mutation in the gene *aftD* seemed to appear independently from acquired resistance. The different mutations in CalA-res C1-C3 were spread across the nucleotide sequence of the gene Rv2113 suggesting a loss-of-function mediated mechanism of resistance. Therefore, the impact of this specific gene on growth of *M. tuberculosis* and on susceptibility against callyaerins was investigated. By application of specialized transduction and homologous recombination, merodiploid overexpressing strain and knock out mutant strain of Rv2113 were generated by Dr. Nidja Rehberg (Institute of Pharmaceutical Biology and Biotechnology, University of Düsseldorf, Germany). These strains were screened in MIC assays against CalA. A second copy of the gene Rv2113 in the merodiploid clones harboring pMV361::Rv2113 led to enhanced susceptibility toward CalA (fig. 18A). The integrative vector pMV361::Rv2113 integrates into the *attB* site on the genome in single copy and maintains stably inside the bacteria through multiple generations. In contrast, deletion of the Rv2113 gene conferred resistance to CalA since the anti-TB activity was completely lost against the H37Rv ΔRv2113 knock out mutant clones (fig. 18B). Complementation of the gene deletion mutant restored the phenotype of the ΔRv2113 knock out mutant, resulting again in a dose-dependent growth inhibition of CalA consistent with the parental H37Rv WT (fig. 18B), which unequivocally proves that the observed phenotype is specifically linked to Rv2113. In summary, the described studies on the recombinant *M. tuberculosis* strains suggest an uptake-based mechanism of resistance against callyaerins based on mutations in the gene Rv2113.

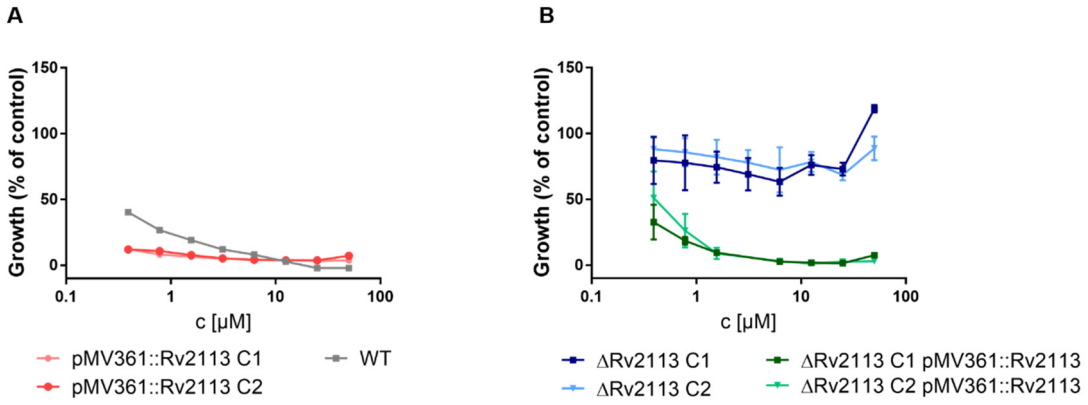

Figure 18: Susceptibility of recombinant *M. tuberculosis* H37Rv strains of the membrane protein Rv2113. Dose-response curves of Rv2113 merodiploid strain pMV361::Rv2113 (●, ●) against CalA are compared to parental WT strain (●; **A**). Loss of activity of CalA was observed against Rv2113 knock out strain (**B**) ΔRv2113 (■, ▼). The effect was restored in the complemented mutant ΔRv2113 pMV361::Rv2113 (■, ▼). For each condition, two independent clones were screened. Data are shown as means of n = 3 ± SEM. Mutant strains were generated by Dr. N. Rehberg, University of Düsseldorf, Germany.

Proceeding from these results, it seems unlikely that Rv2113 is the direct target of callyaerins in *M. tuberculosis* but rather seems to be involved in uptake of the compounds across the cytoplasm membrane. To force mutations to occur in other loci and gain further insights into the mode of action, Rv2113 overexpressing strains were applied for a second approach to generate SRM. For this, the H37Rv Rv2113 merodiploid strain and a recombinant *M. smegmatis* mutant strain expressing the Rv2113 gene of *M. tuberculosis*, which exhibits increased sensitivity toward CalA and CalB (see chapter 3.6), were exposed to solid media containing CalA at onefold or fourfold MIC (see table 12). Additionally, the recombinant *M. smegmatis* strain was also cultivated on agar containing the derivative CalA_R3I at twofold MIC to increase a potential growth of single resistant colonies. However, no further single colonies resistant to callyaerins could be selected even after prolonged incubation times, suggesting that once callyaerins have entered the cells via Rv2113-mediated uptake, single mutations are not sufficient to mediate resistance toward the compounds, indicative of a complex and pleiotropic antibacterial mechanism underlying their antibacterial activity.

Table 12: Resistance frequency of different mycobacteria against CalA or CalA derivatives. Slow development of resistance in *M. tuberculosis* H37Rv WT occurred after six weeks of incubation at a frequency of 10^{-7}. Frequency for a merodiploid Rv2113 overexpressing H37Rv strain and a recombinant *M. smegmatis* strain expressing Rv2113 were lower than the respective detection limit.

Strain	7H10 medium supplementation	Time	Resistance frequency
H37Rv WT	4x MIC nat CalA	6 weeks	10^{-7}
H37Rv pMV361::Rv2113	1x and 4x MIC CalA; 30 µg/mL apramycin	12 weeks	$<5x10^{-7}$
mc²155 pMV361::Rv2113	1x and 4x MIC CalA or 2x MIC CalA_R3I; 30 µg/mL apramycin	2 weeks	$<10^{-8}$

3.5 Application of an affinity enrichment approach for identification of proteins putatively interacting with callyaerins

The comprehensive library of callyaerins and the availability of derivatives containing a Pra amino acid that contains an alkyne residue allow the application of click chemistry for target-fishing approaches. Proceeding from the derivatives CalA_C4Pra and CalB_C4Pra, affinity probes were synthesized by cycloaddition of a PEG3 conjugated biotin to the alkyne residue of Pra. The two designed compounds Biotin_CalA and Biotin_CalB (fig. 19A and B) were utilized for an affinity enrichment approach with protein lysate extracted from *M. tuberculosis*. Biotin-based affinity enrichment studies were performed in cooperation with the Kaiser group and the Analytics Core Facility (ACF, University of Duisburg-Essen, Germany). Briefly, total cytosolic protein lysate of a late-log culture of *M. tuberculosis* H37Rv WT was prepared applying bead-beating to induce cell damage and lysis by high-speed agitating movement. Filter-sterilized lysate was incubated with Biotin_CalA or Biotin_CalB, respectively, allowing binding to putative target proteins. Enriched proteins were separated by avidin-agarose capture following on-bead digest for identification based on LC-MS/MS. By this approach, an easy and fast method for identification of cytosolic protein interactions with the labeled compounds was established. However, this assay does not allow covalent binding of the target to the appended probes, hence excluding the identification of membrane-bound targets or the evaluation of lipids putatively involved in the mode of action. In two independent experiments, six different proteins were identified as potential targets of callyaerins. With

respect to the negative control, the strongest fold-change was observed for a protein identified as Hrp1 utilizing both, Biotin_CalA or Biotin_CalB (fig. 19C and D, Hrp1 edged in red in volcano plots).

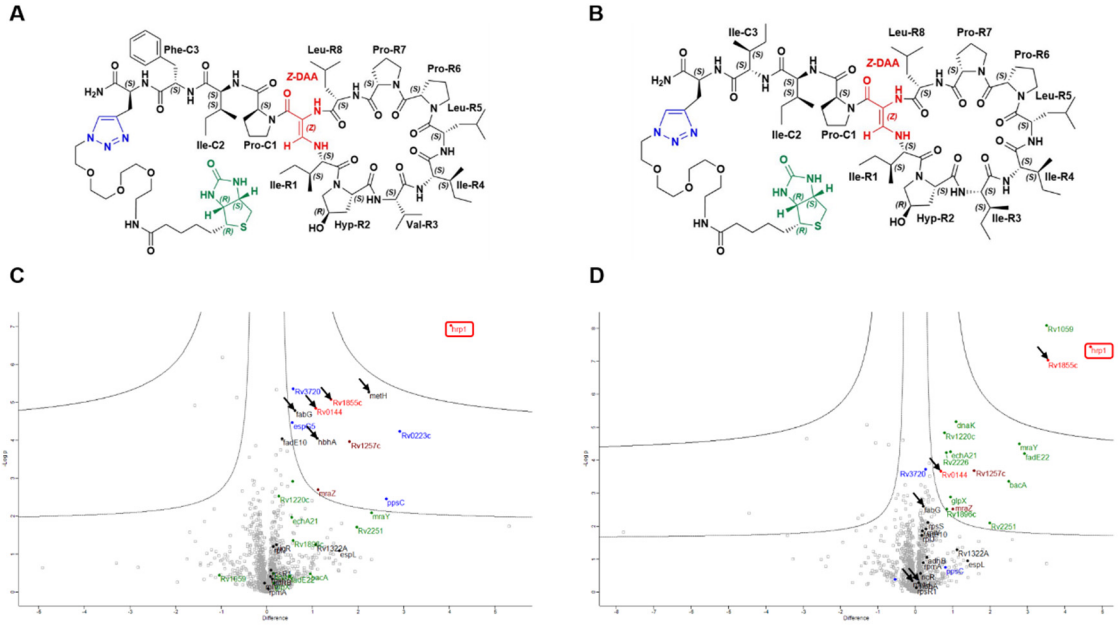

Figure 19: Affinity enrichment using biotin-tagged callyaerins and cytosolic protein lysate of *M. tuberculosis*. Putative proteins interacting with callyaerins were enriched using biotin-tagged callyaerin probes of CalA_C4Pra (**A**) or CalB_C4Pra (**B**) respectively. Biotin (green) was 'clicked' to C4Pra applying an azide-PEG3 conjugate as linker by cycloaddition (blue). Biotin-tagged peptides were immobilized on avidin agarose beads and identified by LC-MS/MS. Enriched proteins using either Biotin_CalA (**C**) or Biotin_CalB (**D**) were illustrated as volcano plots showing means of n = 4 runs with respect to the negative control. Proteins listed in table 13 are marked with black arrows, Hrp1 is edged in red. Experiments were performed in cooperation with the Kaiser group at the ACF (University of Duisburg-Essen, Germany).

All reproduced hits of the two independent approaches are listed in table 13. Although MS-based evaluation of the proteins revealed FabG1, an essential protein involved in fatty acid biosynthesis, as a putative target of callyaerins, the most distinct fold-change in enrichment was observed for Hrp1. Hence, Hrp1 is particularly interesting for further studies that shall provide insights into the activity of callyaerins.

Table 13: Confirmed proteins identified by two independent affinity enrichment approaches using biotin-tagged callyaerin probes and total cytosolic protein lysate of *M. tuberculosis.* Biotin-tagged peptides were identified by LC-MS/MS. Corresponding proteins are either marked with black arrows or edged in red in volcano plots illustrated in figure 19. Essential genes for *in vitro* growth *M. tuberculosis* H37Rv are marked with ☑, non-essential genes with ☒ (Sassetti *et al.*, 2003, DeJesus *et al.*, 2017). Experiments were performed in cooperation with the Kaiser group at the ACF (University of Duisburg-Essen, Germany).

Protein	Locus	Background	Essential gene
Hrp1	Rv2626c	regulated by DosR	☒
FabG1	Rv1483	involved in fatty acid biosynthesis	☑
HbhA	Rv0475	heparin-binding hemagglutinin; extrapulmonary dissemination	☒
MetH	Rv2124c	methionine synthase	☒
	Rv0144	potential transcriptional regulatory protein	☒
	Rv1855c	potential oxidoreductase	☒

Hrp1 is part of the DosR regulon in *M. tuberculosis* which consists of approx. 50 genes, organized in nine blocks (Selvaraj *et al.*, 2012). Located in block eight, *hrp1* is known as the most strongly induced transcript by DosR (Sun *et al.*, 2017). Consequently, *hrp1* is highly upregulated in *M. tuberculosis* strains belonging to the Beijing lineage, which is in conformity with the reduction in callyaerin activity observed for the strain HN878 (fig. 9). This strengthens the hypothesis of Hrp1 as a potential target. Several stress conditions like hypoxia or nitric oxide stress lead to the upregulation of Hrp1 (Boon *et al.*, 2001). Its ability to bind to the surface of murine macrophages and the activation of a strong immune response proven by an enhanced production of TNFα substantiate the important role of Hrp1 in infection and interaction with the host cell (Davidow *et al.*, 2005, Bashir *et al.*, 2010). Furthermore, increased expression of *hrp1* is accompanied by promoted host cell necrosis (Danelishvili *et al.*, 2016). Although Hrp1 is non-essential for *in vitro* growth, the potential regulatory function controlling further proteins involved in stress response might be involved in the mode of action of callyaerins.

3.5.1 Co-crystallization of Hrp1 and Biotin_CalB

To further study the putative interaction of callyaerins with Hrp1 a C-terminal His-tagged protein was recombinantly expressed and purified by application of a batch-binding approach captured on a Ni-NTA agarose affinity chromatography matrix. Protein purification and a partial crystal structure of Hrp1 (Hrp1-Δ128-143) have previously been published by Sharpe *et al.* (2008), however, they failed to obtain crystals of full-length Hrp1. The identified structure of Hrp1-Δ128-143 by Sharpe *et. al*, revealed that the protein is an example of a cystathionine-β-synthase (CBS) domain only protein which consists of two CBS domains. Additionally, the structural analysis shows that Hrp1-Δ128-143 forms strong dimers that are stabilized by disulfide bonds. In agreement with these reported findings, the protein purified in the current study is present as dimer in solution as estimated by the migration pattern in SDS-PAGE (fig. S3). The Hrp1 protein was obtained in high yields and subjected to co-crystallization with both, Biotin_CalA and Biotin_CalB. Crystallization was performed in cooperation with Stefanie Kobus and Dr. Sander Smits at the CSS (University of Düsseldorf, Germany). Commercial screens were employed to identify conditions yielding crystals using NexTal tubes (Qiagen). Homogenous Hrp1 was mixed with Biotin_CalA or Biotin_CalB, respectively, and equilibrated against reservoir solution. It should be noted, that protein crystallization in combination with Biotin_CalA was unsuccessful. In contrast, two promising conditions were identified for co-crystallization with Biotin_CalB applying the vapor-diffusion method and yielding diffraction-quality crystals. Crystals were obtained in sitting-drop MRC3 plates at 12 °C after three days or three weeks for the two different conditions (a) and (b). Reservoir solution for condition (a) consisted of Mb Class II, A12 (1 M di-ammonium phosphate / ammonium dihydrogen phosphate pH 6.5) or ProComplex C4 (0.2 M lithium sulfate, 0.1 M MES pH 6 and 20% PEG 4000) for condition (b). Crystals reached a maximum size of 61x18x15 µM for condition (a) or 150x10x8 µM for condition (b) and emerged in miscellaneous shapes (fig. 20). Grid screens were examined to prove initial crystals resulting in favorable conditions by applying 6-8 µg Hrp1 to 0.5 mM Biotin_CalB and 1 µL reservoir solution equilibrated against 300 µL of respective reservoir solution. Obtained crystals were determined at 1.4-1.8 Å resolution for condition (a) or 1.2-1.4 Å resolution for condition (b) collecting data by application of synchrotron radiation at ‘Deutsches Elektronen-Synchrotron’ DESY (European Molecular Biological Laboratory (EMBL), Hamburg, Germany). Diffraction data (fig. 20) of protein measurements did not allow 3D structural elucidation caused by occurring phase problems. Heavy metals were applied for molecular replacement by adding mercury(II)chloride or platinum directly to the crystals obtained by condition (a). Measurements with heavy metals allow

retrograded calculation of phases and thereby support structure elucidation of Hrp1. Currently, calculations are ongoing. However, structural measurements already permit the hypothesis that the protein crystals are composed of two monomers, most likely as a functional dimer, albeit, final calculations need to be accomplished for distinct evidence.

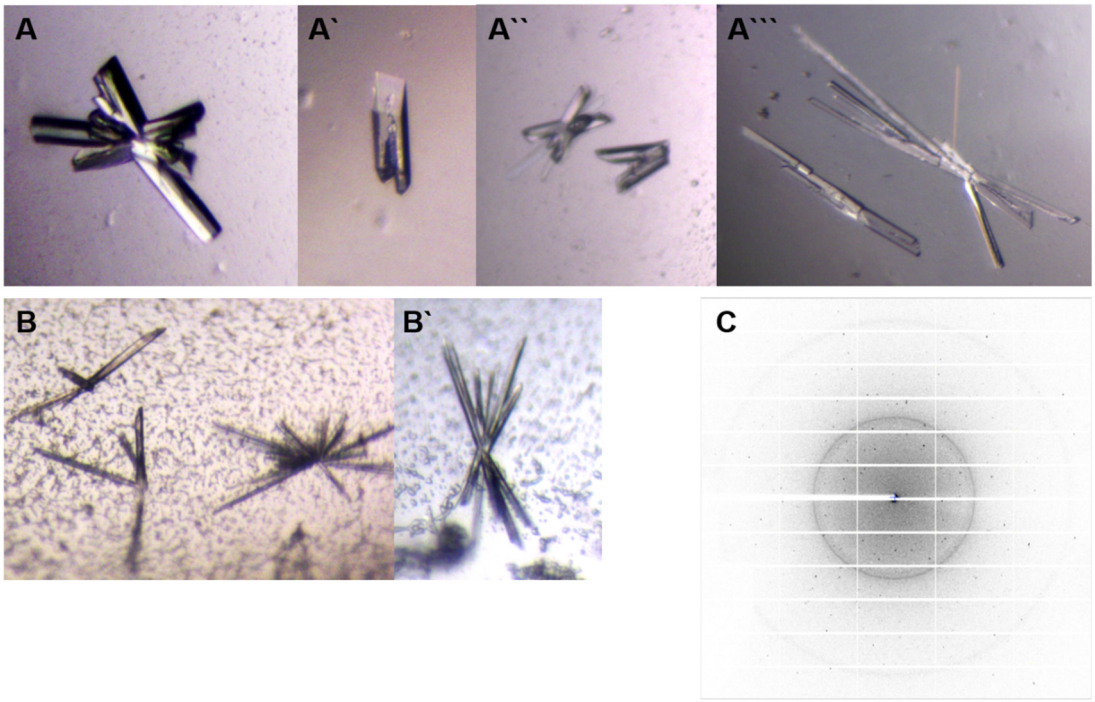

Figure 20: Protein crystals of Hrp1, co-crystalized with Biotin_CalB. Crystals of Hrp1 were obtained at two different conditions in sitting-drop position by applying vapor-diffusion method. Crystals of various shapes were spawned by reservoir solutions consisting of Mb Class II, A12 (**A-A**```) or ProComplex C4 (**B-B**`). Crystals reached a maximum size of 61x18x15 µM or 150x10x8 µM. Obtained crystals were overlaid with mineral oil before harvesting and flash frozen in liquid nitrogen. Representative diffraction pattern of crystal structure measurements by synchrotron radiation at DESY (EMBL, Hamburg, Germany) are shown in (**C**). Crystallization were performed at the CSS (University of Düsseldorf, Germany) in cooperation with Stefanie Kobus and Dr. Sander Smits. Pictures were taken by Stefanie Kobus.

3.6 Studies on proteins potentially involved in the mode of action of callyaerins

As described previously, CalA and CalB selectively inhibit growth of *M. tuberculosis* in a dose-dependent manner (chapter 3.1). Two proteins have been identified to be involved in the mechanism of resistance and potentially in the mode of action of callyaerins: Rv2113 and Hrp1. To gain further insights into the effect of these two proteins and to elucidate the missing activity against other mycobacterial species, potentially associated with those two genes, protein sequences were blasted to identify orthologues between the species. No orthologues were found in both, *M. smegmatis* and *M. marinum*, neither to Rv2113 nor to Hrp1 (table 14). In terms of *M. bovis*, orthologues were found to both, Rv2113 and Hrp1, in virulent *M. bovis* as well as in *M. bovis* BCG Pasteur. Amino acid sequences of the Hrp1 orthologues Mb2659c and BCG_2653c both were identical to the H37Rv protein (table 14 and fig. S5). Regarding Rv2113 orthologues, substitutions in the amino acid sequences were found. A substitution of threonine to proline was detected in the sequence of *M. bovis* (Mb2317) and *M. bovis* BCG Pasteur (BCG_2130). For the membrane protein Mb2317 of the virulent *M. bovis* strain, an additional amino acid exchange was identified (serine to leucine, table 14).

Table 14: Orthologous proteins to Rv2113 and Hrp1 in different mycobacteria. Amino acid exchanges in protein sequences of corresponding proteins to Rv2113 in *M. bovis* and *M. bovis* BCG Pasteur are marked in red. No exchanges were found in the protein sequences of orthologues to Hrp1. No orthologues (--) were detected in genome sequences of *M. smegmatis* and *M. marinum*. Sequences were blasted and analyzed for exchanges using Clone Manager 9 (fig. S5).

Strain	Rv2113	Hrp1 (Rv2626c)
M. bovis AF2122/97	Mb2317: T207P; S278L	Mb2659c
M. bovis BCG Pasteur	BCG_2130: T207P	BCG_2653c
M. smegmatis mc²155	--	--
M. marinum ATCC 927	--	--

First, the effect of the expression of both genes, *hrp1* and Rv2113, in *M. smegmatis*, a well-established model organism in TB research, was evaluated concerning a potential effect in callyaerin susceptibility. Expression of the gene encoding the membrane protein Rv2113 led to dose-dependent growth inhibition with both compounds, CalA and CalB. Albeit, this effect could only be achieved at high concentrations (fig. 21A and B). For CalB, growth inhibition at 100 µM was also observed for the EV control (pMV361 EV). Even though, dose-dependent growth curves of Rv2113 expressing recombinant clones were clearly different. In contrast, expression of the DosR regulated gene *hrp1* did not lead to a change in the activity of CalA (fig. 21C). Again, for CalB growth inhibition was observed at 100 µM. Since this effect was detected for both, *hrp1* expressing recombinant strain and EV control (pMV261 EV), a specific effect caused by expression of *hrp1* could be excluded (fig. 21D). As described previously, mutations in the gene Rv2113 confer resistance in *M. tuberculosis* against callyaerins (chapter 3.4), suggesting that the missing membrane protein in *M. smegmatis* prevents callyaerin entrance. Therefore, a recombinant strain of *M. smegmatis* was generated expressing both genes, Rv2113 and *hrp1*. However, no additive effect was observed regarding the susceptibility of CalA and CalB, resulting in a dose-dependent growth inhibition comparable to the recombinant strain expressing only Rv2113 (fig. 21E and F). This leads to the hypothesis, that expression of Rv2113 in *M. smegmatis* allows uptake of callyaerins and growth inhibition at high concentrations. Albeit, the real target might be missing in *M. smegmatis*. Moreover, in case of Hrp1, the protein might interact in a different way compared to *M. tuberculosis* or is regulated as distinguished from DosR and therefore is not involved in the mode of action of callyaerins.

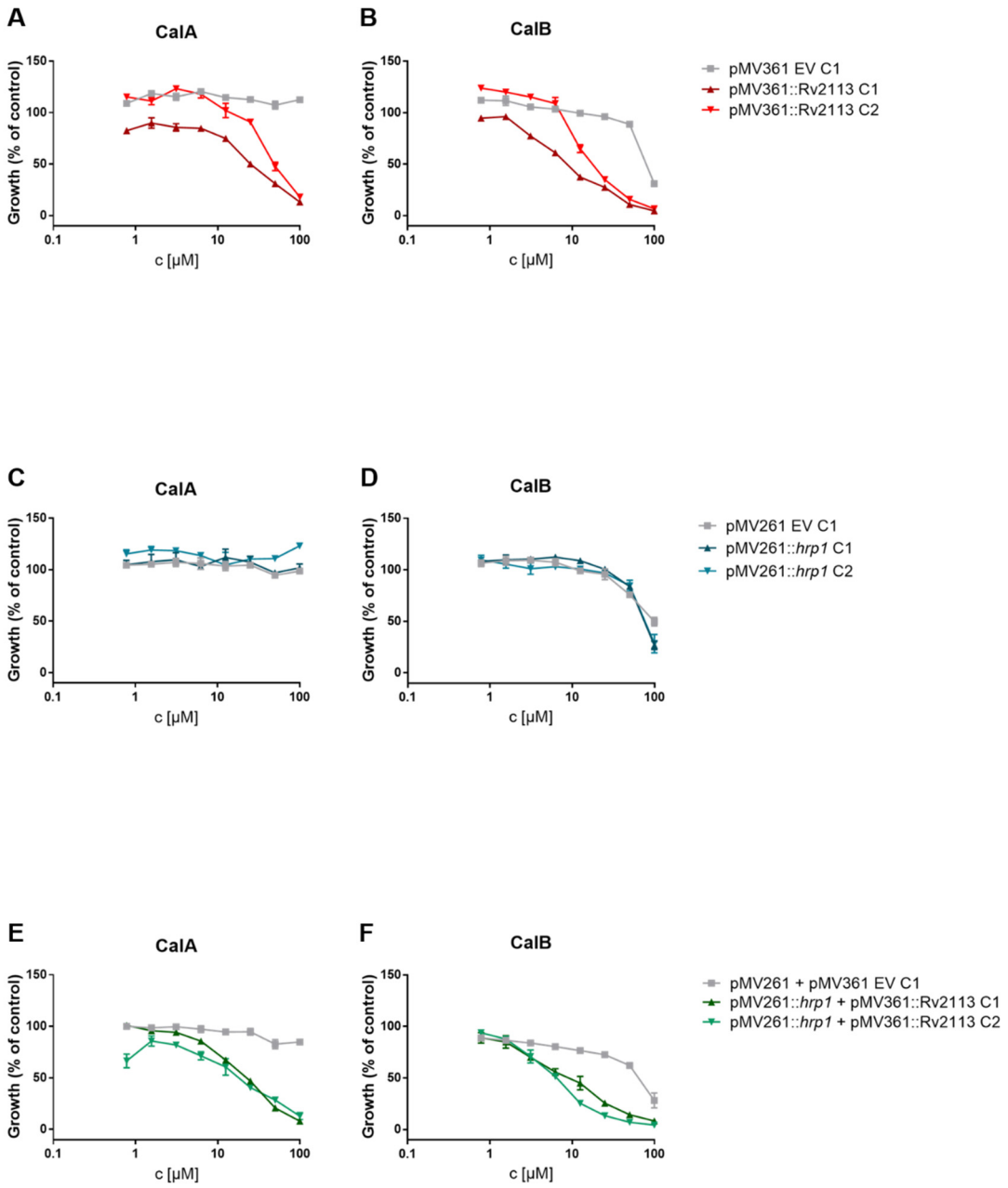

Figure 21: Susceptibility of *M. smegmatis* recombinant strains expressing genes putatively involved in the mode of action of callyaerins. Dose-response curves of strains expressing Rv2113 (▲,▼) against CalA (**A**) or CalB (**B**) or expressing *hrp1* (▲,▼) against CalA (**C**) or CalB (**D**). Screening of *M. smegmatis* recombinant strain expressing both *hrp1* and Rv2113 simultaneously (▲,▼) against CalA and CalB are shown in (**E**) and (**F**). Two independent clones were screened for each condition. In all experiments, an EV was used as control (■). Data are shown as means of n = 3 ± SEM.

Orthologues to both proteins were found in *M. bovis* BCG Pasteur, however, the amino acid sequence of BCG_2130 harbors a single amino acid substitution compared to Rv2113. To study the effect of both proteins in a second model organism, the corresponding gene sequence of *M. tuberculosis* was expressed in *M. bovis* BCG

Pasteur. Expression of Rv2113 resulted in a strong shift in callyaerin susceptibility showing a clear dose-dependent growth inhibition for CalA (fig. 22A). In contrast, overexpression of *hrp1* had no specific effect (fig. 22B). This, in fact, supports the hypothesis that callyaerins can only enter the bacterial cell by passing the specific membrane protein Rv2113. To evaluate the effect of Hrp1 in *M. bovis* BCG Pasteur cells susceptible to callyaerins, a recombinant strain expressing both *hrp1* and Rv2113 simultaneously was generated. Here, a strong growth-inhibiting effect of CalA was observed dependent on the exposed dose (fig. 22C). Bacterial growth could be detected at low concentrations (0.78 µM) whereas growth of Rv2113 (over-) expressing strain was still inhibited (compare fig. 22A). However, whether this effect is caused by *hrp1* overexpression needs further evaluation. Supposing that Hrp1 is the target of callyaerins, a stronger effect might be expected, although regulation and composition of DosR might differ in *M. bovis* BCG Pasteur and *M. tuberculosis*.

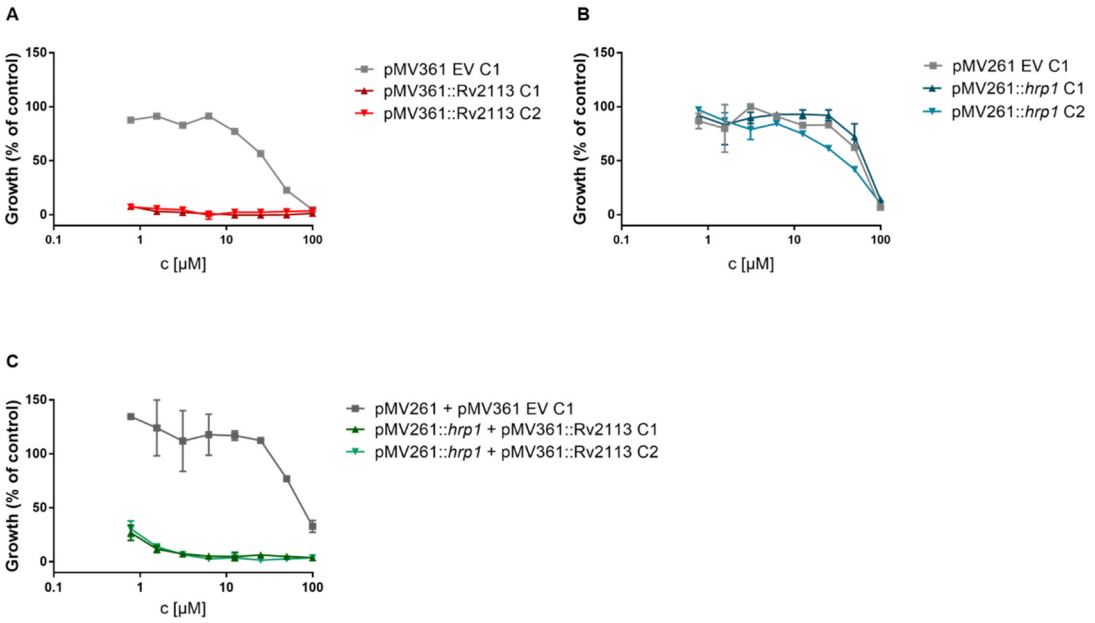

Figure 22: Susceptibility of *M. bovis* BCG Pasteur recombinant strains expressing *M. tuberculosis* genes putatively involved in the mode of action of callyaerins. Dose-response curves of recombinant strains expressing Rv2113 (▲,▼; **A**) or *hrp1* (▲,▼; **B**) against CalA. Screenings of a recombinant *M. bovis* BCG Pasteur strain expressing *hrp1* and Rv2113 simultaneously (▲,▼) against CalA are shown in (**C**). Two independent clones were used in each condition. In all experiments, an EV was used as control (■). Data are shown as means of n = 3 ± SEM.

The general missing activity of callyaerins against *M. bovis* BCG Pasteur WT is strongly connected to the membrane protein Rv2113/BCG_2130. As the protein sequence differs in one single amino acid, it might be obvious that this substitution confers resistance, especially since single amino acid exchanges in *M. tuberculosis* led to resistance as well (chapter 3.4). However, it might also be possible that the orthologue BCG_2130 is not constitutively expressed in *M. bovis* BCG Pasteur. Gene expression of Rv2113 and BCG_2130 was therefore evaluated by RT-qPCR. Expression of the membrane protein in *M. tuberculosis* H37Rv WT was calibrated to expression in *M. bovis* BCG Pasteur WT resulting in a fourfold higher expression level of Rv2113 compared to BCG_2130 (fig. 23A). Additionally, expression level of Rv2113 (over-) expressing mutants were calibrated to pMV361 EV control in *M. bovis* BCG Pasteur, revealing a fourfold or ninefold induction for the two independent clones (fig. 23B). The increase in expression of Rv2113 in *M. tuberculosis* was comparable to expression of Rv2113 mutants in *M. bovis* BCG Pasteur. This implies that rather a missing constitutive expression of BCG_2130 than a single amino acid substitution is responsible for missing activity of callyaerins in *M. bovis* BCG Pasteur. Nevertheless, SRM in *M. tuberculosis* verified that a single amino acid exchange is sufficient to confer resistance. Application of overexpression of BCG_2130 in *M. bovis* BCG Pasteur or mutagenesis of the sequence of Rv2113 in *M. tuberculosis* will reveal greater details in the intrinsic resistance of *M. bovis*.

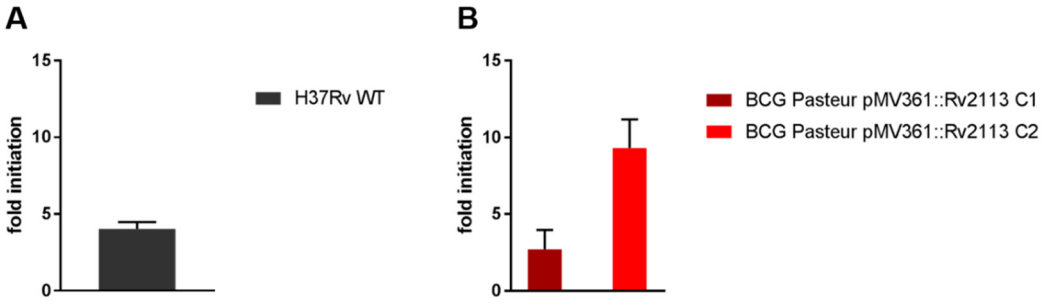

Figure 23: Quantitative analysis of Rv2113 and BCG_2130 expression using RT-qPCR. RT-qPCR was performed using complementary DNA synthesized from RNA samples of *M. bovis* BCG Pasteur WT, recombinant strain expressing Rv2113, pMV361 EV control and *M. tuberculosis* H37Rv WT. *16sRNA* was used as reference gene. Expression of Rv2113 in H37Rv WT (■) was calculated with reference to BCG_2130 expression in BCG Pasteur WT (**A**). Expression level of BCG Pasteur strain heterologously expressing Rv2113 (■,■) were normalized to pMV361 EV control (**B**). Data in (**A**) show means of n = 4 ± SEM, data in (**B**) show means of n = 2 ± SEM obtained in two independent experiments.

4 Discussion

4.1 Callyaerins as new antibiotic lead structures against *M. tuberculosis*

With increasing resistance of *M. tuberculosis* against currently used drugs, the urgency to find new drugs to control the global spread of TB rises alarmingly. The recently reported emergence of TDR TB (Velayati *et al.*, 2009) with missing treatment opportunities exacerbates the critical situation of the TB epidemic. In the last 60 years, only three new drugs have reached the market and have been introduced to TB therapy for the treatment of drug-resistant TB (see chapter 1.2.2-1.2.3). Against two of them, BDQ and delamanid, clinical resistance has already been reported (Hartkoorn *et al.*, 2014, Fujiwara *et al.*, 2018). This study aimed to gain further insights into the activity and the underlying mode of action of callyaerins against *M. tuberculosis*. Callyaerins were previously identified in a bioactivity guided screening (Daletos *et al.*, 2015). The identification of natural products as new antibiotics is often accompanied by the problem of product availability. In cooperation with the Kaiser group, an efficient and quick total synthesis of callyaerins was established (unpublished). This facilitated the application of SAR studies and approaches based on click chemistry, of the one part, and formed a basis to consider callyaerins as available new antibiotic lead structures, of the other part. In order for newly identified active compounds against *M. tuberculosis* to offer beneficial treatment opportunities, it needs to be proven that these compounds inhibit growth of relevant clinical *M. tuberculosis* strains including XDR clinical isolates. Therefore, CalA was screened against different *M. tuberculosis* strains that represent different lineages and consequently genetic diversity (Portevin *et al.*, 2011). CalA was also active against *M. tuberculosis* strains HN878 and CDC1551 (fig. 9A). This shows, that callyaerins are active against different lineages of *M. tuberculosis* and rules out a limited growth-inhibiting effect on the laboratory strain H37Rv. Furthermore, CalA and CalB were screened against *M. tuberculosis* XDR clinical isolates (fig. 9B and 9C). The activity of both compounds was decreased when compared to the H37Rv WT strain. However, dose-dependent growth inhibition in the low micromolar range was still detectable. The observed shift is most likely induced by a decreased fitness of the XDR strains in absence of the antibiotics they are resistant to (Gagneux *et al.*, 2006). This implies, that the shift in the MIC values of callyaerins might not be due to a lower activity against drug-resistant *M. tuberculosis*. Therefore, it is unlikely that callyaerins address the same molecular targets as currently used antibiotics. Further CalA derivatives were screened against those XDR clinical isolates. The CalA/CalB intermediate derivatives CalA_R3I

and CalA_C3I showed dose-dependent inhibition of drug-resistant *M. tuberculosis*, likewise (fig. S1). Especially the derivative CalA_R3I displayed a strong activity against XDR strains (table S1). The different growth-inhibiting properties of callyaerin derivatives might allow unique treatment strategies for either drug-susceptible or drug-resistant TB. Following CalB, CalA_R3I hast the second lowest MIC of the different callyaerins, when excluding the exceptional chemical properties of the Cy3_CalA derivative. The SAR studies performed in frame of this dissertation so far did not reveal a minimal core pharmacophore of callyaerins. However, with certainty, it was shown that the cyclic structure of callyaerins is essential (fig. 11B). Furthermore, the combination of the length and chemical composition of amino acids in the sidechain seems to be essential for callyaerin activity. In general, the hydrophobic character of callyaerins plays an important role in passing the mycobacterial membrane and in growth inhibition, since amino acid exchanges to alanine resulted in decreased activity (see table 10). The strong activity of CalB and CalA_R3I implies that isoleucine at position R3 might be significant for target interaction. Other amino acids exchanges at this position did not lead to a positive effect on the activity. Since the natural amino acid composition of CalB shows the strongest activity against *M. tuberculosis* and the greatest therapeutic window, it would be beneficial to further focus on CalB derivatives for further medicinal chemical optimization. With a focus on an economic and cost-efficient synthesis route, it would be advantageous to study a CalB_R2P derivative, with hydroxyproline exchanged to proline. A maintained activity of this compound would allow a more cost-efficient synthesis for gram-scale production in reference to pharmacokinetics and mouse models of infection. The application of mouse models needs to be performed to evaluate the activity of callyaerins in the host environment. In this study, callyaerins were applied in a macrophage infection assay to evaluate an effect on intracellular phagocytosed *M. tuberculosis*. In this approach, CalA and CalB displayed a strong inhibition of replication of incorporated bacteria (see fig. 15). However, a macrophage infection assay can only mimic the host environment and *in vivo* conditions during infections will likely differ.

Antibiotics or antimicrobials need to accomplish different properties to ensure a successful and secure treatment of pathogenic diseases. The ‘ideal’ antibiotic combines strong growth inhibition of the disease-causing pathogen with missing toxicity in the host and without affecting the beneficial human microbiome. Furthermore, resistance frequency should be low (Singh *et al.*, 2017). Potential toxic effects of callyaerins were excluded employing cytotoxicity assays using different human cell lines (fig. 7). In conclusion, hepato- or nephrotoxic side effects of callyaerins are scarcely expected. Especially for CalB, cytotoxicity assays yielded in a large therapeutic window, which

promises a great beneficial effect of the drug (Singh *et al.*, 2017). Remarkably, studies on the derivative Cy3_CalA yielded in an exceptional great therapeutic window, giving a hint that functionalized callyaerin conjugates might be used as multi-targeting drugs (see chapter 4.3.1). Resistance frequency of *M. tuberculosis* to callyaerins was determined by the generation of SRM (table 12). Resistance in *M. tuberculosis* occurred at a frequency of 10^{-7}. Compared to currently used antibiotics, resistance to callyaerins is lower than resistance to delamanid or INH (~10^{-5} to 10^{-6}) (Fujiwara *et al.*, 2018). Resistance to callyaerins is mediated by mutations in the membrane protein Rv2113 (chapter 3.4). Further approaches to generate SRM failed, implicating that resistance is limited to mutations in this specific membrane protein. Various currently used antibiotics for treatment of bacterial infections are broad-spectrum antibiotics. Broad-spectrum antibiotics allow to immediately start the antibacterial therapy without the previous identification of the distinct pathogen causing the infection. By targeting different bacterial species, broad-spectrum antibiotics, as a consequence, cause side effects by also affecting gut microbes of the human microbiome (Singh *et al.*, 2017). In the case of a TB disease, the beneficial effect of broad-spectrum antibiotics is irrelevant, since *M. tuberculosis* is the only causative agent in humans. For treatment of TB, narrow-spectrum antibiotics are preferable, especially since drug therapy is continued over several months (see chapter 1.2.2). Callyaerins have been shown to selectively inhibit growth of *M. tuberculosis*, without affecting other mycobacteria and gram-positive bacteria like *S. aureus* (fig. 8). This implies that serious side effects on the human microbiome during callyaerin treatment are unlikely to occur. Since combination therapy in TB is well established (Kerantzas and Jacobs, 2017), approaches to identify synergistic effects of callyaerins and currently used first-line and second-line drugs should be conducted. A synergistic killing effect of callyaerins with current drugs would allow establishing alternative combination treatment regiments, which in the best case might lead to a reduction in treatment duration. In conclusion, the availability of callyaerins by an established total synthesis, in combination with their specific anti-TB properties and the great therapeutic window qualify them as new lead structures for TB therapy. Although the mode of action of callyaerins has not been identified in detail so far (4.2), pharmacokinetics and infection studies will reveal their applicability in treatment of TB.

4.2 Mode of action of callyaerins

In this study, two proteins have been identified that are involved in the *in vitro* activity of callyaerins. The first protein was elucidated by generating SRM and thereby identifying the mechanism of resistance. The membrane protein Rv2113 is involved in an uptake-based mechanism of resistance, which demonstrates that callyaerins enter the mycobacterial cell by passing the transmembrane domains. The specific membrane-passing mechanism of callyaerins and the protein Rv2113 might be exploited as a carrier system for drug conjugates (see chapter 4.3.1). However, in addition to mediating uptake, the membrane protein might also be involved in the direct mode of action of callyaerins. Second, the protein Hrp1 was identified as a direct interaction partner of callyaerins by application of an affinity enrichment approach. So far, the underlying mode of action based on both or either one of the proteins is not revealed in detail. As described previously, different cyclic peptides have been analyzed for their anti-TB activity, initiated by different molecular mechanisms and interactions with different targets. Tuberactinomycins, for instance, target protein synthesis by interacting with tRNA (Modolfll and Vázquez, 1977, Stanley *et al.*, 2010), while griselimycin inhibits mycobacterial growth by targeting DnaN (Kling *et al.*, 2015). Teixobactin, in turn, targets the mycobacterial cell wall synthesis (Ling *et al.*, 2015). ADEPs and lassomycin both target ClpP1, although the precise mode of action differs between the two compounds (Gavrish *et al.*, 2014, Brötz-Oesterhelt *et al.*, 2005). Callyaerins, as further cyclic peptides with anti-TB activity, might have a related mode of action comparable to the already known cyclic peptides. Nevertheless, it is rather likely that the activity of callyaerins is based on a new unique mode of action, highly probably mediated by interactions with the two identified proteins Rv2113 and/or Hrp1. In the following, the potential mode of actions involving either Rv2113 or Hrp1 are discussed.

4.2.1 Rv2113 as a potential target of callyaerins

While the essential role of Rv2113 in the mechanism of resistance to callyaerins has clearly been demonstrated in the current thesis, it is still possible that Rv2113 might also be involved in the mode of action. MIC assays showed that callyaerins are not active against *M. bovis* and *M. smegmatis,* based on modifications or absence of the membrane protein (table 14). Therefore, callyaerins are not able to enter the bacterial cell and reach their target. Nevertheless, the missing activity might also be explained by

lack of Rv2113 as the target itself. Studies with ADEPs and ClpP protease in *S. aureus* (Brötz-Oesterhelt *et al.*, 2005) or lassomycin and ClpC in *M. tuberculosis* (Gavrish *et al.*, 2014) show in exemplary ways that cyclic peptides are able to dysregulate enzymatic processes. Likewise, a potential mode of action of callyaerins might be associated with toxic deregulation of Rv2113 function. Interaction of callyaerins with Rv2113 as a target might also induce conformational changes of the protein followed by an altered cell wall composition. This, in turn, might lead to loss of the membrane potential and/or pore formation in the cell wall. To gain further insights into this potential mode of action, different approaches need to be pursued. Fluorophore-labeling of Rv2113 will enable to colocalize the protein with fluorophore-tagged callyaerins and will allow to study interactions by application of approaches based on Förster resonance energy transfer (Agrawal *et al.*, 2016). Additionally, experiments revealing changes in the membrane potential (Chawla and Singh, 2013) will give a hint on a cell wall-based mode of action of callyaerins. Pore formation in the mycobacterial cell wall triggered by callyaerin treatment could be verified by scanning electron microscopy like it was shown for treatment with INH which leads to an altered cell wall morphology (Takayama *et al.*, 1973).

4.2.2 Hrp1 as a potential target of callyaerins

By application of an affinity enrichment approach, Hrp1 was identified as a direct interaction partner of callyaerins. As described previously, *hrp1* is regulated by DosR and is therefore associated with several processes connected to dormancy and stress responses (Sun *et al.*, 2017). Since Hrp1 is non-essential for *in vitro* growth, the mode of action cannot simply be based on inhibition of an essential protein. In this case, the mode of action would rather be explained by disturbed protein-protein interactions and an altered function of Hrp1 or an overactivity induced by callyaerins, that might start a cascade activating further proteins regulated by Hrp1. This will lead to downregulation of the metabolism and suppression of replication resulting in bacterial dormancy and thereby causing a bacteriostatic effect of callyaerins. This hypothesis is based on a potential regulatory function of Hrp1, which is corroborated by the identification of CBS domains in the protein structure (Sharpe *et al.*, 2008). CBS domains contain potential binding cavities and might regulate the activity of associated functional domains (Baykov *et al.*, 2011). In general, DosR is the transcriptional regulator that induces *hrp1* upon stress conditions like hypoxia (Park *et al.*, 2003). Contingent upon callyaerin treatment,

hrp1 then might be induced independently from DosR and hypoxic or further stress signals. This theory is further supported by the determined ATP reduction in CalA and CalB treated cells (fig. 10), which shows that the metabolism of *M. tuberculosis* is reduced by callyaerin treatment. Bactericidal effects of antibiotics are often associated with targeting the cell wall, whereas bacteriostatic compounds most likely inhibit replication (Leekha *et al.*, 2011). So far, no bactericidal effect of callyaerins was observed, supporting a bacteriostatic effect induced by inhibition of replication via targeting Hrp1. This potential mode of action of callyaerins needs to be further evaluated. Genetic modification of *hrp1* expression will reveal further insights. Therefore, knock out mutants and merodiploid strains of *M. tuberculosis* overexpressing *hrp1* need to be generated. In this study, a *hrp1* transposon mutant (Tn Mut) of *M. tuberculosis* CDC1551 (CDC1551 Tn Mut 1121) (Lamichhane *et al.*, 2003) was analyzed to gain further insights into the role of Hrp1. Gene sequence of *hrp1* is interrupted by insertion of a transposon most likely leading to an altered protein translation. However, the susceptibility of this *hrp1* Tn Mut was equal to the susceptibility of the *M. tuberculosis* CDC1551 WT (fig. S4). In the case of an altered protein structure of the target Hrp1, a loss of activity of callyaerins might be expected. The missing impact of transposon disruption of Hrp1 could have different reasons. First, callyaerins might have more than one intracellular target in *M. tuberculosis*. In this case, at least a reduction of the activity would be expected. Second, the active center and interaction site of callyaerins with Hrp1 potentially is not hampered by transposon insertion. The transposon is inserted after 243 bases which equals approx. half the gene sequence of *hrp1*. The N-terminal portion of the protein might be solely essential for callyaerin interaction and for induction of protein-protein interactions that lead to dormancy. Co-crystallization will finally contribute to elucidate details into the interaction between callyaerins and Hrp1. Indeed, callyaerins seem to stabilize Hrp1, since crystals of the full-length protein could not be obtained alone, neither in this study nor by Sharpe *et al.* (2008). The determined shift in the susceptibility of the *M. tuberculosis* strain HN878, in turn, supports the hypothesis of Hrp1 as the target of callyaerins. *M. tuberculosis* strain HN878 belongs to the Beijing lineage of *M. tuberculosis*. Strains of this lineage constitutively overexpress genes regulated by DosR, independent from external signals induced by mutations in the promoter region of DosR. As a consequence, *hrp1* is increased significantly in the active-replicating metabolism of HN878 compared to H37Rv (Domenech *et al.*, 2017). Overexpression of *hrp1* could explain the reduced activity of callyaerins (fig. 9A). However, the *M. tuberculosis* Beijing lineage is also described as hypervirulent harboring a different lipid profile that could play a role in reduced activity of callyaerins (Huet *et al.*, 2009). To investigate the potential mode of action of callyaerins, mutant strains of

M. smegmatis and *M. bovis* BCG Pasteur have been generated and examined in this study (chapter 3.6). Since the activity of callyaerins is based on uptake via the membrane protein Rv2113, the missing effect of *hrp1* (over) expression on the activity of callyaerins is neglectable. First, the susceptibility of *M. smegmatis* recombinant strain expressing both, Rv2113 and *hrp1* will be discussed. No additional effect of *hrp1* expression was detectable. Susceptibility was comparable to the Rv2113-only expressing recombinant strain of *M. smegmatis* (fig. 21), while it was expected that the activity of callyaerins should be increased in the double recombinant strain if Hrp1 was the target. However, it should be considered that dormancy and the genetic mechanisms involved in dormancy are regulated and organized differently in *M. smegmatis* and *M. tuberculosis*. This concerns both, the composition of the genes regulated by DosR and the regulation and organization of DosR itself. Two homologous copies to DosR have been identified in *M. smegmatis* (Berney and Cook, 2010). Therefore, based on the theory that the underlying mode of action of callyaerins targeting Hrp1 is induced by the regulatory function of the protein, it is most likely that expression of *hrp1* in *M. smegmatis* does not lead to regulation of proteins inhibiting replication. With regard to the *M. bovis* BCG Pasteur recombinant strain expressing both *hrp1* and Rv2113, a small difference in susceptibility was observed compared to the Rv2113-only expressing strain (fig. 22). At low concentrations (1.56 µM), growth of the double recombinant strain was detectable whereas growth of the Rv2113-only expressing strain was still inhibited. It might be assumed that overexpression of the target gene *hrp1* leads to reduced activity of CalA at low concentrations. However, this hypothesis needs to be further evaluated. Similar to *M. tuberculosis*, the ortholog to *hrp1* in *M. bovis* is one of the strongest induced transcripts under stress conditions (Boon *et al.*, 2001). Nevertheless, in *M. bovis* BCG Pasteur more than 100 genes in the genome are deleted compared to *M. tuberculosis* (Rosenkrands *et al.*, 2002). It is likely, that some of the gene products might be regulated by Hrp1 and are therefore essential for the complex mode of action underlying the activity of callyaerins. A distinct evidence on the impact of *hrp1* expression can only be concluded by studies of merodiploid *M. tuberculosis* H37Rv strains overexpressing *hrp1* and *hrp1* knock out mutants. Since the here introduced potential mode of action of callyaerins is based on the predicted regulatory function of Hrp1, protein interaction partners need to be revealed to support this theory. Approaches applied as part of this study aiming to ‘fish’ proteins from *M. tuberculosis* protein lysate that interact with purified His-tagged Hrp1 did not result in clear outcomes. Comparable studies of proteomic approaches of *M. tuberculosis* H37Rv WT, *hrp1* knock out mutants and *hrp1* overexpressing mutants could be applied to identify differences in their respective protein profile. Once potentially regulated proteins are identified, further studies will reveal the

interaction with Hrp1. The bacterial two-hybrid approach (Wang *et al.*, 2010) or a modified approach considering three different genes (Tharad *et al.*, 2011) are established tools to study protein-protein interactions. Additionally, a bacterial adenylate cyclase-based two-hybrid system was successfully applied by Datta *et al.* (2006) to prove interactions of *M. tuberculosis* FtsW with penicillin-binding protein 3. However, these methods are limited, since they are not qualified to study complex protein-protein interactions like it is estimated for Hrp1. With reference to Płociński *et al.* (2014), a single-step affinity purification technique could be used to study protein interactions with Hrp1 that also allows the isolation and purification of protein complexes.

In general, Hrp1 might be a 'privileged' target strengthened by its role in infection. Hrp1 has been shown to interact with macrophages (Bashir *et al.*, 2010) and to contribute to host cell necrosis (Danelishvili *et al.*, 2016). Mutations that mediate resistance are less likely to occur in genes that are involved in infection, reducing the risk of clinical target-based resistance against callyaerins. Summarizing the potential mode of actions underlying either Rv2113 or Hrp1, it is most likely that Hrp1 is the target of callyaerins while Rv2113 plays an essential role in the uptake of the compounds.

4.2.3 Strategies to reveal greater details in the mode of action of callyaerins

In this study, two proteins that are involved in the mode of action of callyaerins have been identified and discussed. Since the precise underlying mode of action has not been revealed in detail, further investigations need to be performed to understand the genetic and molecular mechanisms that play a role in callyaerin activity. The presented affinity enrichment approach applying biotin-tagged probes represents a useful and easy tool to identify potential interaction partners of active compounds. However, this approach has its limitations. The application of biotin-tagged probes does not allow a covalent linkage of the compound to its potential target. Therefore, proteins of the cell membrane, for instance, are not traceable in this approach, since their isolation requires the usage of detergents which interrupt noncovalent bonds. Application of approaches based on photoaffinity labeling will allow studies that include cell membrane proteins. Photoaffinity labeling is based on a covalent linkage of the compound to its target by assimilation of a photoreactive group (Wright and Sieber, 2016). The established total synthesis of callyaerins and the opportunity to draw on click chemistry derivatives allowed the design of a callyaerin-based photoaffinity labeling probe. This probe needs to combine both, a photoaffinity labeling group and an azide or alkyne moiety allowing

enrichment of target proteins by application of click chemistry. The Kaiser group successfully has designed a probe of CalB that contains both Bpa, a photoaffinity labeling group that allows covalent binding to the target by cross-linking via excitation by UV light (Wright and Sieber, 2016), and an alkyne function. Although there was a significant drop in the activity of this specific CalB_R3Bpa_C4Pra probe, a dose-dependent effect on growth of *M. tuberculosis* was detectable (fig. S6) and still allows its application in photoaffinity labeling approaches. To increase the activity of the probe, further derivatives could be designed. Since the integration of Bpa at position C3 of CalB only led to a small shift in the activity, the design of a CalB_C3Bpa_C4Pra derivative might be advantageous for photoaffinity labeling approaches. In general, Bpa probes have already been used successfully for target identification. Eirich *et al.* (2011) investigated the design of vancomycin probes containing Bpa and alkyne residues and successfully identified target proteins in living *S. aureus* and *E. faecalis* cells and proved that vancomycin has further targets besides the established mode of action by binding to D-alanyl-D-alanine motifs of peptidoglycan. Additionally, labeling of Bpa is achieved at approx. 366 nm, while other photoaffinity labeling groups need to be excited at shorter wavelengths increasing the risk of damaging target proteins (Wright and Sieber, 2016, Eirich *et al.*, 2011).

Besides the application of further approaches based on chemical modification of callyaerins, studies that reveal specific genetic responses of *M. tuberculosis* to stress induced by callyaerin treatment could be performed. Sequencing of transposon mutant libraries (Tn Seq) is an established tool to study effects on growth of *M. tuberculosis* for the identification of genes that are essential under different conditions (Griffin *et al.*, 2011, DeJesus *et al.*, 2017). Therefore, Tn mutant libraries of *M. tuberculosis* can be subjected to treatment with sub-lethal concentrations of callyaerins. A comparable approach was successfully demonstrated by Xu *et al.* (2017). Tn mutant libraries were exposed to sub-lethal concentrations of current first-line drugs and analyzed for mutations that provide fitness advantages resulting in the identification of the cell wall as a key player in intrinsic resistance to common drugs. Application of Tn Seq will reveal intrinsic mechanisms of resistance of *M. tuberculosis* to callyaerins and might also serve as a basis to identify further genes potentially involved in the mode of action. Furthermore, proteomic profiling can be conducted to gain further insights into the stress profile induced by callyaerins on protein level. Comparative proteome studies of *M. tuberculosis* exposed to bactericidal concentrations of known drugs have been described as a useful tool to identify metabolic pathways that are involved in response to the induced stress conditions (Danelishvili *et al.*, 2017). However, none of the described approaches allow conclusions on lipids potentially involved in the mode of action of callyaerins. Therefore, in addition,

experiments based on ^{14}C-acetate labeling of lipids can be applied to reveal a potential lipid-based mode of action referring to the studies on vitamin C affecting the lipid biosynthesis of *M. tuberculosis* (Vilchèze *et al.*, 2013). In summary, the here presented approaches will help to understand the mode of action of callyaerins based on Hrp1 as a target and, in addition to it, might identify further potential targets that play a role in the activity of callyaerins.

4.3 Further potential fields of application of synthetic callyaerins

4.3.1 Application of callyaerins as a carrier system for membrane translocation of drug conjugates of *M. tuberculosis*

The described mechanism of resistance revealed that the activity of callyaerins is based on presence of the membrane protein Rv2113, which has eight predicted transmembrane domains. Callyaerins obviously specifically enter *M. tuberculosis* cells by virtue of the membrane protein Rv2113 reaching their intracellular target. This was proven by a loss of activity of callyaerins against *M. tuberculosis* knock out mutants of Rv2113 (fig. 18B). The complete loss of activity is caused by a hampered uptake of callyaerins engendered by the missing membrane protein. In contrast, the susceptibility of merodiploid strains of *M. tuberculosis* overexpressing Rv2113 was significantly increased (fig. 18A). Further studies on the impact of the expression of Rv2113 gave a hint that callyaerins and the specific membrane protein might serve as a transporter system overcoming the cell wall membrane of *M. tuberculosis*. This theory was successfully proven by enhancing the susceptibility of *M. smegmatis* and *M. bovis* BCG Pasteur cells that express the specific protein sequence of Rv2113 and in consequence, allow callyaerins to pass the membrane (fig. 21 and 22). While studies on Rv2113 clearly prove that uptake of callyaerins is based on expression of this protein, the design of a Cy3_CalA derivative reveals that the active structure of callyaerins is capable of extension without losing its growth-inhibiting properties (fig. 14). Even more, in the case of Cy3_CalA, the attachment of the fluorophore led to an extreme increase in the growth-inhibiting activity, resulting in the lowest MIC value of all screened compounds (table 10). The mode of action of this enhanced CalA derivative still depends on the membrane protein Rv2113 since a strong shift was detected in the susceptibility of a Cal-res *M. tuberculosis* strain harboring mutations in the gene sequence of Rv2113

(fig. 14C). Studies on Cy3_CalA can be considered as a proof of principle indicating the potential shuttle function of callyaerins. Synthesis of further callyaerin derivatives will be based on the design of dual- or multi-targeting drugs resulting in hybrid-callyaerins. Since the cell wall of *M. tuberculosis* represents a natural barrier against many antimicrobial drugs (Jankute *et al.*, 2015), callyaerins might serve as a shuttle for compounds failing to pass this complex structure (fig. 24). With respect to current drug therapy, multi-targeting drugs have a lower likelihood to force the development of target-based resistance and drug-resistant phenotypes (Torfs *et al.*, 2019, Silver, 2007). Combinational therapy against TB aims to address bacteria in different metabolic states and at different sites of infection (Silver, 2007). Therapy applying multi-targeting drugs might be able to achieve equal results and thereby relieve the patients from daily intake of up to four drugs. The activity of multi-targeting drugs can be based on different modes of inhibition. Multi-targeting drugs can inhibit various targets that belong to the same molecular pathway or act independently from each other, defined as serial inhibitors or parallel inhibitors, respectively. Network inhibitors operate in both ways inhibiting serial and parallel targets (Oldfield and Feng, 2014, Li *et al.*, 2014). Concerning the transporter function of callyaerins, further studies need to be performed to determine guidelines for chemical properties of potential attachments. Extension of callyaerins with additional compounds will result in changes regarding size, charging and polarity of the emerging hybrid that might have an impact on its activity, permeability and pharmacokinetic properties. Once guidelines are defined, hybrid-callyaerins can be designed and studied for their *in vivo* activity. The carrier function of callyaerins opens a new field of research and extends the application of callyaerins from new lead structures to multi-targeting drug design building a base for the development of a new TB therapy.

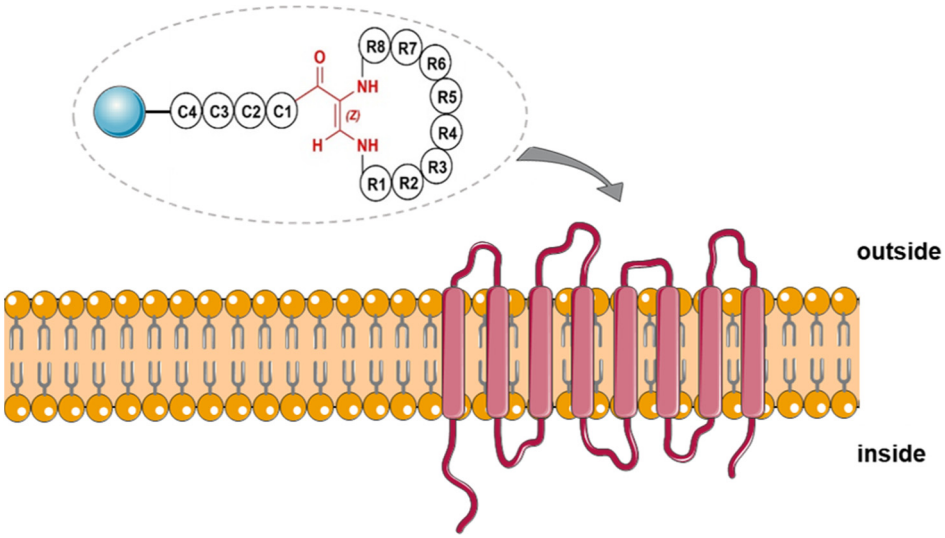

Figure 24: Hybrid-callyaerins enter the mycobacterial cell via the membrane protein Rv2113. Schematic illustration of the potential transporter system composed of callyaerins and the membrane protein Rv2113. Callyaerins are only active in presence of Rv2113 (red), which has eight predicted transmembrane domains and enables transmembrane transport of callyaerins. The fundamental structure of callyaerins can be extended by further chemicals (blue) resulting in hybrid-callyaerins with multi-targeting drug properties.

4.3.2 Application of callyaerins as labeling probes in diagnostic analysis

A rapid and safe diagnosis of TB is still a challenging and critical factor for an urgent start of drug treatment. Therefore, access and reliability of TB diagnostic tools need to be improved to fulfill the aims of the ‘End TB Strategy‘ (WHO, 2015). In addition to classical culture-based methods, diagnosis of TB today can be based on various techniques such as sputum smear microscopy (SSM), immunological quantification like INFγ release assays (e.g. QuantiFERON®-TB Gold by Qiagen), X-ray and, most recently, on the nucleic acid amplification test Xpert MTB/RIF (Pai *et al.*, 2016). However, all these methods have their limitations. Culture-based methods are still the gold-standard for TB diagnosis, although experienced and trained staff and access to biosafety level three facilities are required for SSM. Furthermore, due to the slow generation time, reliable results are only available after several weeks retarding the start of appropriate therapy (Ghiasi *et al.*, 2015). Immunological quantification was observed to be limited in immuno-compromised patients and cannot be utilized to distinguish between active or latent TB infections (Pai *et al.*, 2014). Pulmonary TB is most often detected by X-ray, however, a variety of other pulmonary diseases can cause

abnormalities and yield false-positive results (Ghiasi *et al.*, 2015). Xpert MTB/RIF offers a sensitive method for diagnosis of TB and its resistance to RIF in parallel (Boehme *et al.*, 2010). However, safe application requires comprehensive equipment and well-educated personnel (Pai *et al.*, 2016). Besides several new techniques that are in the pipeline for TB diagnosis (Unitaid, 2017), approaches based on fluorescence microscopy came into the focus of research. Fluorescence-based detection is characterized as more sensitive enabling readouts at lower magnitudes (Steingart *et al.*, 2006). Recently, some studies presented fluorescent-based approaches that are deployable for TB diagnosis. Those approaches are based on metabolic or biosynthetic pathways of mycobacteria, like the incorporation of trehalose derivatives into the mycomembrane for fluorescent-dye detection (Kamariza *et al.*, 2018) or of fluorogenic substrates for the synthesis of the class a beta-lactamase BlaC (Xie *et al.*, 2012, Cheng *et al.*, 2014). Nevertheless, false-positive results in patients immunized with a BCG vaccine cannot be excluded (Swarts *et al.*, 2012, Cheng *et al.*, 2018). Fluorescent callyaerins or substituted callyaerins for intracellular fluorophore labeling based on click chemistry might serve as detection tools in terms of TB diagnosis. Thanks to their high selectivity, false-positive results in case of BCG vaccinated patients will be minimized (chapter 3.1). Sputum of patients that are at risk of TB could be treated with fluorescent callyaerins allowing detection of *M. tuberculosis* by fluorescence microscopy. Additionally, fluorescence screening of biopsy samples is conceivable. Although, access to fluorescence microscopy would be necessary, identification of *M. tuberculosis* cells would be quite simple allowing the investigation of samples by less experienced personnel. So far, application of fluorescent callyaerins in diagnostic terms is just a theoretical outlook. Nevertheless, this theory emphasizes the strong potential and broad application of synthetic callyaerins and their derivatives.

4.4 Conclusion and final remarks

The results presented in this study reveal the great potential of synthetic callyaerins as new lead structures for TB therapy. Callyaerins inhibit growth of *M. tuberculosis* with strong selectivity at low concentrations resulting in favorable therapeutic windows. Their growth-inhibiting properties also affect *M. tuberculosis* cells phagocytosed by macrophages, giving a hint for an effective application in infected organisms. The established synthesis of callyaerins redresses the problem of product availability and enables access for further structural optimization with respect to pharmacokinetic properties and potential administration forms. The distinct mode of action of callyaerins is not revealed in detail. However, it has been proven that callyaerins overcome the mycobacterial cell wall by using the membrane protein Rv2113. It is most likely that interaction of callyaerins with Hrp1 triggers further protein-protein interactions that reduce the metabolism, inhibit replication and thereby lead to a strong bacteriostatic effect of callyaerins. Although the mode of action needs further evaluation, callyaerins qualify for pharmacokinetic studies and animal models of infection since also the mode of action of some of the established drugs in TB therapy used for decades is still under discussion (chapter 1.2.2). The great potential of callyaerins is not only limited to new drug leads but also offers further fields of application. The established mechanisms of resistance depending on the membrane protein Rv2113 revealed a potential transporter function of callyaerins. Synthetic hybrid-callyaerins might be applicable as multi-targeting drugs in TB therapy overcoming the current combinational therapy and thereby reducing the patient's burden to take up to four drugs in parallel. Furthermore, fluorescent callyaerins might be useful tools in terms of diagnosis of TB. To achieve the aims drafted in the WHO's 'End TB Strategy' (2015), better access to new rapid diagnostic technologies need to be provided. It needs to be ensured that patients suffering from TB receive drugs and are monitored during therapy to guaranty the correct process and a successful outcome. Identification of drug-resistant TB needs to be improved and new treatment opportunities need to be discussed with regard to multi-targeting drugs. In all facets, the application of callyaerins might be beneficial. Furthermore, besides antimicrobial therapy, an established vaccine routine which might be based on multi-stage agents combining antigens of early state and latent infections (Aagaard *et al.*, 2011) will help to end the global TB epidemic.

Careless overuse of antibiotics and antimicrobial drugs have led to the development of the current AMR crisis leading to a pre-antibiotic situation (chapter 1.2.1). Optimization of diagnosis and treatment of bacterial infections is essential to counteract the current crisis and set bounds to further development of resistance. To avoid

inappropriate prescribing of antimicrobial drugs, identification of the particular pathogen causing the infection should be ensured. This will also reduce the use of broad-spectrum antibiotics that destroy the human microbiome and allow pathogenic bacteria to gain the upper hand (Fernandes, 2006). Additionally, the use of antibiotics in farming needs to be reduced or terminated to stop the spread of multi-resistant pathogens between humans and animals like it was reported in terms of pig farming (Voss *et al.*, 2005, Mole, 2013). Furthermore, new treatment opportunities need to be considered. Phage therapy, previously developed a century ago, reawakens interest driven by the current AMR crisis (Gordillo Altamirano and Barr, 2019). Recently, it was shown that phage therapy is also applicable to the treatment of infections caused by mycobacteria (Dedrick *et al.*, 2019). In conclusion, staying ahead of AMR will claim all our knowledge, the development of new antimicrobial drugs and treatment opportunities as well as a close collaboration of patients and medics and a reorganized policy of antimicrobial drugs use in farming.

5 Supplement

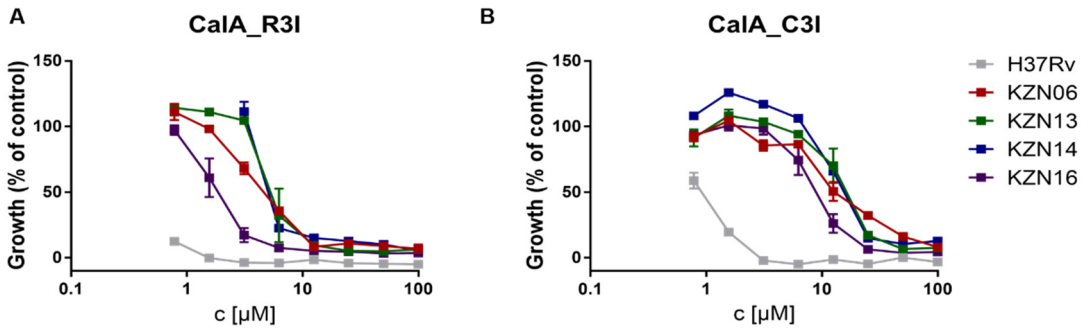

Figure S1: Activity of CalA derivatives against *M. tuberculosis* XDR clinical isolates. Dose-response curves of several *M. tuberculosis* XDR clinical isolates (■-KZN06, ■-KZN13, ■-KZN14, ■-KZN16) against CalA_R3I (**A**) and CalA_C3I (**B**). *M. tuberculosis* H37Rv WT (■) is shown by way of comparison. Data are shown as means of n = 3 ± SEM

Table S1: MIC_{90} values [µM] of CalA_R3I and CalA_C3I screened against *M. tuberculosis* XDR clinical isolate KZN06-16. MIC_{90} values were determined in duplicates.

	CalA_R3I (MIC_{90})	**CalA_C3I** (MIC_{90})
KZN06	6.25	50
KNZ13	6.25	25
KZN14	25	>50
KZN16	3.125	12.5

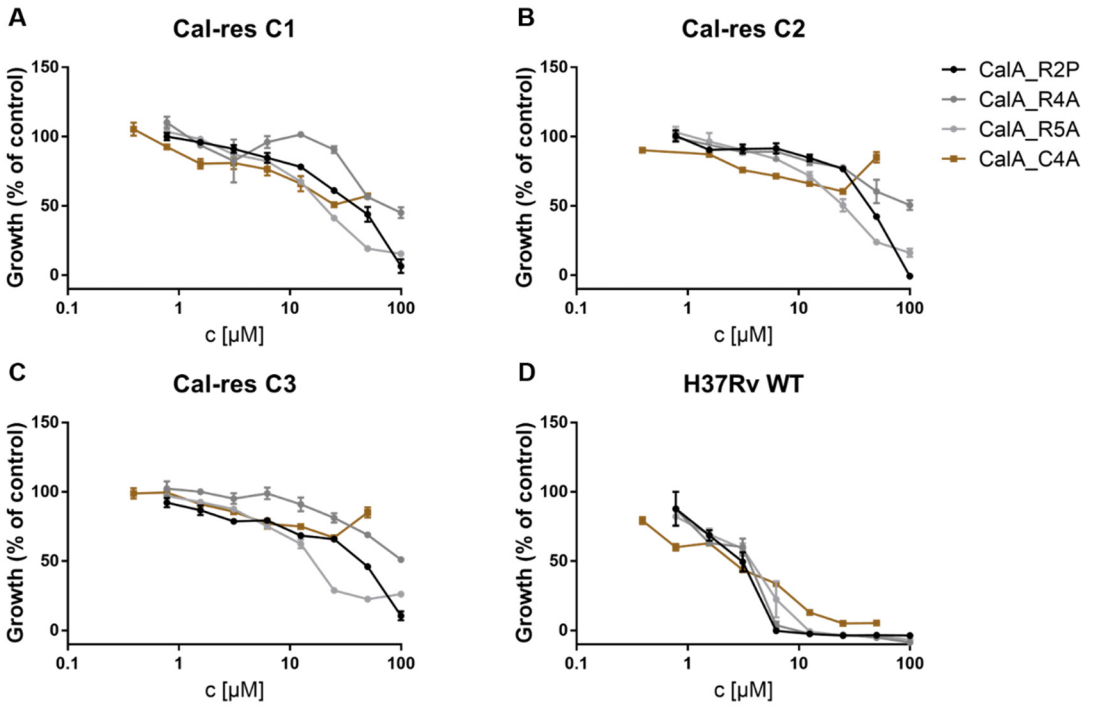

Figure S2: Resistance pattern of the Cal-res strains against further CalA derivatives. Dose-response curves of *M. tuberculosis* H37Rv Cal-res C1 (**A**), C2 (**B**) and C3 (**C**) against several CalA derivatives harboring amino acid exchanges in ring positions (●-R2P, ●-R4A, ●-R5A) or in the sidechain (■-C4A). (**D**) shows dose-response curves of *M. tuberculosis* H37Rv WT against respective CalA derivatives. Data are shown as means of n = 3 ± SEM.

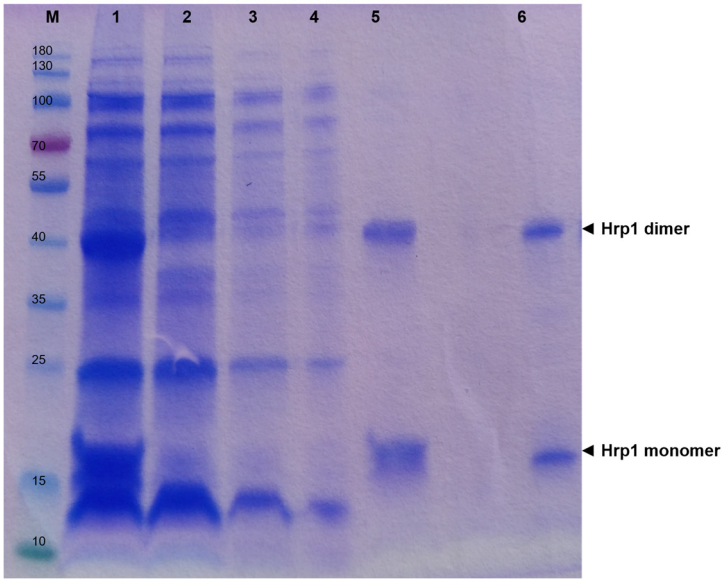

Figure S3: Coomassie-stained SDS-PAGE analysis of recombinant expressed and purified Hrp1. Samples of lysate (**1**), flow through (**2**), washing steps (**3**,**4**) and elution (**5**) were applied on the gel. Purified Hrp1 was concentrated and desalted (**6**). Lane marked with (**M**) shows marker in kDa. Prior to application to a PROTEAN® TGX™ gel, samples were mixed with loading dye and denaturized at 98 °C for 5 min.

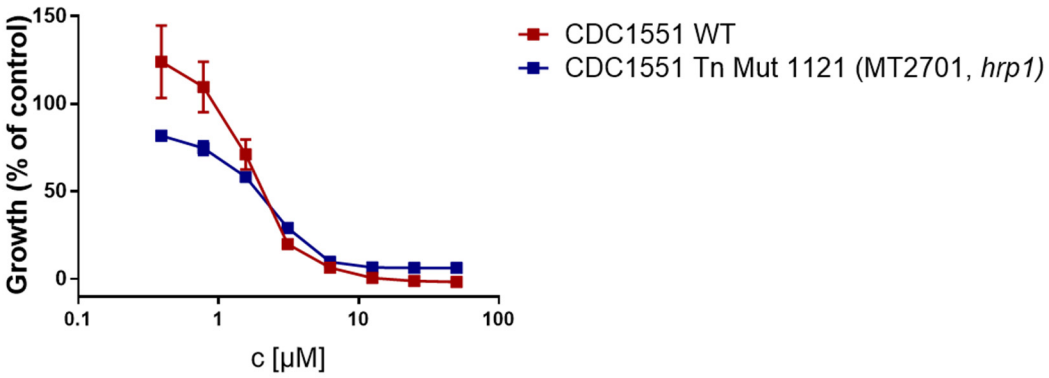

Figure S4: Susceptibility of a *M. tuberculosis* Tn Mut of *hrp1*. Dose-dependent growth inhibition of CalA against *M. tuberculosis* CDC1551 WT (■) and a *M. tuberculosis* CDC1551 Tn Mut of *hrp1* (■). The transposon is inserted into gene sequence of *hrp1* after 234 bases interrupting protein translation. The used *M. tuberculosis* CDC1551 Tn Mut strain was obtained through BEI Resources, NIAID, and generated by Lamichhane *et al.* (2003). Data are shown as means of n = 3 ± SEM.

A

```
Alignment:   Global Protein alignment against reference molecule
Parameters:  Scoring matrix:  BLOSUM 62

Reference molecule: HRP1 (Rv2626c), Region 1 to 143
Number of sequences to align: 3
Total length of aligned sequences with gaps: 143 aas

Sequence                Start     End      Match    NonMatch %Match

HRP1 (Rv2626c)              1     143

Mb2659c                     1     143        143        0       100

BCG_2653c                   1     143        143        0       100


HRP1 (Rv2626c)          1 mttardimnagvtcvgehetltaaaqymrehdigalpicgdddrlhgmltdrdivikgla
Mb2659c                 1 ............................................................
BCG_2653c               1 ............................................................

HRP1 (Rv2626c)         61 agldpntatagelardsiyyvdanasiqemlnvmeehqvrrvpvisehrlvgivteadia
Mb2659c                61 ............................................................
BCG_2653c              61 ............................................................

HRP1 (Rv2626c)        121 rhlpehaivqfvkaicspmalas
Mb2659c               121 .......................
BCG_2653c             121 .......................
```

B

```
Alignment:   Global Protein alignment against reference molecule
Parameters:  Scoring matrix:  BLOSUM 62

Reference molecule: Rv2113, Region 1 to 397
Number of sequences to align: 3
Total length of aligned sequences with gaps: 397 aas

Sequence                Start     End      Match    NonMatch %Match

Rv2113                      1     397

Mb2137                      1     397        395        2        99

BCG_2130                    1     397        396        1        99


Rv2113                  1 mslsvrrppaaraaaiveaeswflkrglpsvltmrgrcrrlwprsapmlaawavvegclm
Mb2137                  1 ............................................................
BCG_2130                1 ............................................................

Rv2113                 61 avffvtdggevfisatpttaqwvilallavalplaslvgwlvsqissgrgqaavatmava
Mb2137                 61 ............................................................
BCG_2130               61 ............................................................

Rv2113                121 faaasdviesgpiqllrtavvvglvllqtgcgvgsvlgwavrmtlehlatvgtlavralp
Mb2137                121 ............................................................
BCG_2130              121 ............................................................

Rv2113                181 ivlltalvffntyvwlmaaningerltlamvfllaiagafvvsktvervrpllrsttvmp
Mb2137                181 ..........................p.....................................
BCG_2130              181 ..........................p.....................................

Rv2113                241 qgsqslagtpfatmgdpspgfpltraerlnvvfllaasqlveilvvasvgaaiylvlgmi
Mb2137                241 ........................................l...........................
BCG_2130              241 ............................................................

Rv2113                301 iltppllrewthydsmtttvlgmtfpapdslirmclflgaltfmyisaravddaeyramf
Mb2137                301 ............................................................
BCG_2130              301 ............................................................

Rv2113                361 ldpliddlhtallarnryrnnvvtapcagvdaghvdd
Mb2137                361 .....................................
BCG_2130              361 .....................................
```

Figure S5: Alignment of amino acid sequences of Hrp1 and Rv2113 and respective orthologues. Sequences of *M. tuberculosis* H37Rv, *M. bovis* AF2122/97 and *M. bovis* BCG Pasteur were aligned using Clone Manager 9. Amino acid exchanges are highlighted in red. Amino acids are shown in single letter code.

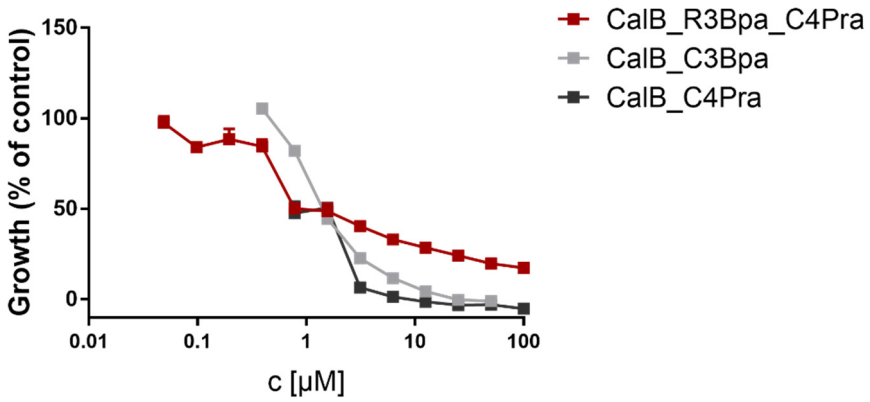

Figure S6: Activity of CalB probes for photo affinity labeling approaches. Dose-response curves of *M. tuberculosis* H37Rv WT against CalB_R3Bpa_C4Pra (■), CalB_C3Bpa (■) and CalB_C4Pra (■). Data are shown as means of n = 3 ± SEM

References

AAGAARD, C., *et al.* 2011. A multistage tuberculosis vaccine that confers efficient protection before and after exposure. *Nature Medicine,* 17**,** 189-194.

AGRAWAL, R., *et al.* 2016. FRET reveals multiple interaction states between two component signalling system proteins of *M. tuberculosis*. *Biochimica et Biophysica Acta (BBA) - General Subjects,* 1860**,** 1498-1507.

AKOPIAN, T., *et al.* 2012. The active ClpP protease from *M. tuberculosis* is a complex composed of a heptameric ClpP1 and a ClpP2 ring. *The EMBO Journal,* 31**,** 1529-1541.

ANDRIES, K., *et al.* 2005. A Diarylquinoline Drug Active on the ATP Synthase of *Mycobacterium tuberculosis*. *Science,* 307**,** 223-227.

ARAI, M., *et al.* 2012. Stylissamide X, a new proline-rich cyclic octapeptide as an inhibitor of cell migration, from an Indonesian marine sponge of Stylissa sp. *Bioorganic & Medicinal Chemistry Letters,* 22**,** 1818-1821.

ARNISON, P. G., *et al.* 2013. Ribosomally synthesized and post-translationally modified peptide natural products: overview and recommendations for a universal nomenclature. *Natural product reports,* 30**,** 108-160.

AUGUSTINIAK, H., *et al.* 1996. Antibiotics from Gliding Bacteria, LXXVIII. Ripostatin A, B, and C: Isolation and Structure and Structure Elucidation of Novel Metabolites from *Sorangium cellulosum*. *Liebigs Annalen,* 1996**,** 1657-1663.

BARKEI, J. J., *et al.* 2009. Investigations into Viomycin Biosynthesis by Using Heterologous Production in *Streptomyces lividans*. *ChemBioChem,* 10**,** 366-376.

BARRY, C. E., *et al.* 2009. The spectrum of latent tuberculosis: rethinking the biology and intervention strategies. *Nature Reviews Microbiology,* 7**,** 845-855.

BARTEK, I. L., *et al.* 2009. The DosR regulon of *M. tuberculosis* and antibacterial tolerance. *Tuberculosis,* 89**,** 310-316.

BARTZ, Q. R., *et al.* 1951. Viomycin, a New Tuberculostatic Antibiotic. *American Review of Tuberculosis,* 63**,** 4-6.

BASHIR, N., *et al.* 2010. *Mycobacterium tuberculosis* conserved hypothetical protein rRv2626c modulates macrophage effector functions. *Immunology,* 130**,** 34-45.

BAYKOV, A. A., *et al.* 2011. The CBS Domain: A Protein Module with an Emerging Prominent Role in Regulation. *ACS Chemical Biology,* 6**,** 1156-1163.

BERER, N., *et al.* 2004. Callynormine A, a New Marine Cyclic Peptide of a Novel Class. *Organic Letters,* 6**,** 2543-2545.

BERNEY, M. & COOK, G. M. 2010. Unique Flexibility in Energy Metabolism Allows Mycobacteria to Combat Starvation and Hypoxia. *PLOS ONE,* 5**,** e8614.

BERNSTEIN, J., *et al.* 1952. Chemotherapy of experimental tuberculosis. V. Isonicotinic acid hydrazide (nydrazid) and related compounds. *American review of tuberculosis,* 65**,** 357-364.

BLAIR, J. M. A., *et al.* 2015. Molecular mechanisms of antibiotic resistance. *Nature Reviews Microbiology,* 13**,** 42-51.

BOEHME, C. C., *et al.* 2010. Rapid Molecular Detection of Tuberculosis and Rifampin Resistance. *New England Journal of Medicine,* 363**,** 1005-1015.

BOON, C., *et al.* 2001. Proteins of *Mycobacterium bovis* BCG Induced in the Wayne Dormancy Model. *Journal of Bacteriology,* 183**,** 2672-2676.

BROENSTRUP, M., *et al.* 2013. Gene cluster for biosynthesis of griselimycin and methylgriselimycin.

BRÖTZ-OESTERHELT, H., *et al.* 2005. Dysregulation of bacterial proteolytic machinery by a new class of antibiotics. *Nature Medicine,* 11**,** 1082-1087.

BROWN, D. G.*, et al.* 2014. New natural products as new leads for antibacterial drug discovery. *Bioorganic & Medicinal Chemistry Letters,* 24**,** 413-418.

CAMBIER, C. J.*, et al.* 2014. Host Evasion and Exploitation Schemes of *Mycobacterium tuberculosis*. *Cell,* 159**,** 1497-1509.

CAPON, R. J.*, et al.* 2002. Phoriospongin A and B: Two New Nematocidal Depsipeptides from the Australian Marine Sponges *Phoriospongia* sp. and *Callyspongia bilamellata*. *Journal of Natural Products,* 65**,** 358-363.

CDC 2006. Notice to readers: revised definition of extensively drug-resistant tuberculosis. . *MMWR Morb Mortal Wkly Rep*.

CEBRAT, M.*, et al.* 1996. Immunosuppressive activity of hymenistatin I. *Peptides,* 17**,** 191-196.

CHAWLA, M. & SINGH, A. 2013. Detection of Membrane Potential in *Mycobacterium tuberculosis*. *Bio-protocol,* 3**,** e785.

CHENG, Y.*, et al.* 2014. Fluorogenic Probes with Substitutions at the 2 and 7 Positions of Cephalosporin are Highly BlaC-Specific for Rapid *Mycobacterium tuberculosis* Detection. *Angewandte Chemie International Edition,* 53**,** 9360-9364.

CHENG, Y.*, et al.* 2018. Rapid and specific labeling of single live *Mycobacterium tuberculosis* with a dual-targeting fluorogenic probe. *Science Translational Medicine,* 10**,** eaar4470.

CLSI 2012. Methods for Dilution Antimicrobial Susceptibility Tests for Bacteria That Grow Aerobically: Approved Standard.

COLDITZ, G. A.*, et al.* 1995. The Efficacy of Bacillus Calmette-Guérin Vaccination of Newborns and Infants in the Prevention of Tuberculosis: Meta-Analyses of the Published Literature. *Pediatrics,* 96**,** 29.

COMAS, I.*, et al.* 2013. Out-of-Africa migration and Neolithic coexpansion of *Mycobacterium tuberculosis* with modern humans. *Nature Genetics,* 45**,** 1176.

CONLON, B. P.*, et al.* 2013. Activated ClpP kills persisters and eradicates a chronic biofilm infection. *Nature,* 503**,** 365.

COPP, B. R. & PEARCE, A. N. 2007. Natural product growth inhibitors of *Mycobacterium tuberculosis*. *Natural Product Reports,* 24**,** 278-297.

COX, J.*, et al.* 2014. Accurate proteome-wide label-free quantification by delayed normalization and maximal peptide ratio extraction, termed MaxLFQ. *Mol Cell Proteomics,* 13**,** 2513-26.

COX, J. & MANN, M. 2008. MaxQuant enables high peptide identification rates, individualized p.p.b.-range mass accuracies and proteome-wide protein quantification. *Nat Biotechnol,* 26**,** 1367-72.

COX, J.*, et al.* 2011. Andromeda: A Peptide Search Engine Integrated into the MaxQuant Environment. *Journal of Proteome Research,* 10**,** 1794-1805.

CROFTON, J. & MITCHISON, D. A. 1948. Streptomycin resistance in pulmonary tuberculosis. *British medical journal,* 2**,** 1009-1015.

DALETOS, G.*, et al.* 2015. Callyaerins from the Marine Sponge *Callyspongia aerizusa*: Cyclic Peptides with Antitubercular Activity. *Journal of Natural Products,* 78**,** 1910-1925.

DANELISHVILI, L.*, et al.* 2016. *Mycobacterium tuberculosis* PPE68 and Rv2626c genes contribute to the host cell necrosis and bacterial escape from macrophages. *Virulence,* 7**,** 23-32.

DANELISHVILI, L.*, et al.* 2017. *Mycobacterium tuberculosis* Proteome Response to Antituberculosis Compounds Reveals Metabolic “Escape” Pathways That Prolong Bacterial Survival. *Antimicrobial Agents and Chemotherapy,* 61**,** e00430-17.

DANIEL, T. M. 2006. The history of tuberculosis. *Respiratory Medicine,* 100**,** 1862-1870.

DATTA, P.*, et al.* 2006. Interaction between FtsW and penicillin-binding protein 3 (PBP3) directs PBP3 to mid-cell, controls cell septation and mediates the formation of a trimeric complex involving FtsZ, FtsW and PBP3 in mycobacteria. *Molecular Microbiology,* 62**,** 1655-1673.

DAVIDOW, A.*, et al.* 2005. Antibody Profiles Characteristic of *Mycobacterium tuberculosis* Infection State. *Infection and Immunity,* 73**,** 6846.

DEBONO, M.*, et al.* 1987. A21978C, a complex of new acidic peptide antibiotics: isolation, chemistry, and mass spectral structure elucidation. *J Antibiot (Tokyo),* 40**,** 761-77.

DEDRICK, R. M.*, et al.* 2019. Engineered bacteriophages for treatment of a patient with a disseminated drug-resistant *Mycobacterium abscessus*. *Nature Medicine,* 25**,** 730-733.

DEJESUS, M. A.*, et al.* 2017. Comprehensive Essentiality Analysis of the *Mycobacterium tuberculosis* Genome via Saturating Transposon Mutagenesis. *mBio,* 8.

DOMENECH, P.*, et al.* 2017. Unique Regulation of the DosR Regulon in the Beijing Lineage of *Mycobacterium tuberculosis*. *Journal of Bacteriology,* 199.

DUTTA, N. K. & KARAKOUSIS, P. C. 2014. Latent Tuberculosis Infection: Myths, Models, and Molecular Mechanisms. *Microbiology and Molecular Biology Reviews,* 78**,** 343.

EIRICH, J.*, et al.* 2011. Unraveling the Protein Targets of Vancomycin in Living *S. aureus* and *E. faecalis* Cells. *Journal of the American Chemical Society,* 133**,** 12144-12153.

ELDHOLM, V. & BALLOUX, F. 2016. Antimicrobial Resistance in *Mycobacterium tuberculosis*: The Odd One Out. *Trends in Microbiology,* 24**,** 637-648.

ELIOPOULOS, G. M.*, et al.* 2004. Antimicrobial Resistance to Linezolid. *Clinical Infectious Diseases,* 39**,** 1010-1015.

FAMULLA, K.*, et al.* 2016. Acyldepsipeptide antibiotics kill mycobacteria by preventing the physiological functions of the ClpP1P2 protease. *Molecular Microbiology,* 101**,** 194-209.

FDA. 2019. *FDA approves new drug for treatment-resistant forms of tuberculosis that affects the lungs* [Online]. https://www.fda.gov/news-events/press-announcements/fda-approves-new-drug-treatment-resistant-forms-tuberculosis-affects-lungs. [Accessed 06.12.2019].

FEDRIZZI, T.*, et al.* 2017. Genomic characterization of Nontuberculous Mycobacteria. *Scientific Reports,* 7**,** 45258.

FERNANDES, P. 2006. Antibacterial discovery and development—the failure of success? *Nature Biotechnology,* 24**,** 1497.

FLEMING, A. 1929. On the Antibacterial Action of Cultures of a Penicillium, with Special Reference to their Use in the Isolation of *B. influenzæ*. *British journal of experimental pathology,* 10**,** 226-236.

FOX, H. H. 1952. The chemical approach to the control of tuberculosis. *Science,* 116**,** 129-134.

FU, L. M. & SHINNICK, T. M. 2007. Genome-wide exploration of the drug action of capreomycin on *Mycobacterium tuberculosis* using Affymetrix oligonucleotide GeneChips. *Journal of Infection,* 54**,** 277-284.

FUJIWARA, M.*, et al.* 2018. Mechanisms of resistance to delamanid, a drug for *Mycobacterium tuberculosis*. *Tuberculosis,* 108**,** 186-194.

GAGNEUX, S. 2018. Ecology and evolution of *Mycobacterium tuberculosis*. *Nature Reviews Microbiology,* 16**,** 202.

GAGNEUX, S.*, et al.* 2006. The Competitive Cost of Antibiotic Resistance in *Mycobacterium tuberculosis*. *Science,* 312**,** 1944-1946.

GANDHI, N. R.*, et al.* 2006. Extensively drug-resistant tuberculosis as a cause of death in patients co-infected with tuberculosis and HIV in a rural area of South Africa. *The Lancet,* 368**,** 1575-1580.

GARCÍA, A.*, et al.* 2012. Recent advances in antitubercular natural products. *European Journal of Medicinal Chemistry,* 49**,** 1-23.

GAVRISH, E.*, et al.* 2014. Lassomycin, a Ribosomally Synthesized Cyclic Peptide, Kills *Mycobacterium tuberculosis* by Targeting the ATP-Dependent Protease ClpC1P1P2. *Chemistry & Biology,* 21**,** 509-518.

GENGENBACHER, M. & KAUFMANN, S. H. E. 2012. *Mycobacterium tuberculosis*: success through dormancy. *FEMS Microbiology Reviews,* 36**,** 514-532.

GERASIMOVA, A.*, et al.* 2011. Comparative genomics of the dormancy regulons in mycobacteria. *Journal of bacteriology,* 193**,** 3446-3452.

GHIASI, M.*, et al.* 2015. Advances in Tuberculosis Diagnostics. *Current Tropical Medicine Reports,* 2**,** 54-61.

GILPIN, C.*, et al.* 2018. The World Health Organization standards for tuberculosis care and management. *European Respiratory Journal,* 51**,** 1800098.

GLAUS, F. & ALTMANN, K.-H. 2012. Total Synthesis of the Bacterial RNA Polymerase Inhibitor Ripostatin B. *Angewandte Chemie,* 124**,** 3461-3465.

GOLDSTEIN, B. P. 2014. Resistance to rifampicin: a review. *The Journal of Antibiotics,* 67**,** 625-630.

GOPAL, P.*, et al.* 2017. Pyrazinoic Acid Inhibits Mycobacterial Coenzyme A Biosynthesis by Binding to Aspartate Decarboxylase PanD. *ACS Infectious Diseases,* 3**,** 807-819.

GORDILLO ALTAMIRANO, F. L. & BARR, J. J. 2019. Phage Therapy in the Postantibiotic Era. *Clinical Microbiology Reviews,* 32**,** e00066-18.

GOUDE, R.*, et al.* 2009. The Arabinosyltransferase EmbC Is Inhibited by Ethambutol in *Mycobacterium tuberculosis*. *Antimicrobial Agents and Chemotherapy,* 53**,** 4138.

GRIFFIN, J. E.*, et al.* 2011. High-Resolution Phenotypic Profiling Defines Genes Essential for Mycobacterial Growth and Cholesterol Catabolism. *PLOS Pathogens,* 7**,** e1002251.

GUGLIELMETTI, L.*, et al.* 2014. Compassionate Use of Bedaquiline for the Treatment of Multidrug-Resistant and Extensively Drug-Resistant Tuberculosis: Interim Analysis of a French Cohort. *Clinical Infectious Diseases,* 60**,** 188-194.

GUO, C.*, et al.* 2018. Chemistry and Biology of Teixobactin. *Chemistry – A European Journal,* 24**,** 5406-5422.

HAMEED, H. M. A.*, et al.* 2018. Molecular Targets Related Drug Resistance Mechanisms in MDR-, XDR-, and TDR-*Mycobacterium tuberculosis* Strains. *Frontiers in Cellular and Infection Microbiology,* 8.

HARTKOORN, R. C.*, et al.* 2014. Cross-Resistance between Clofazimine and Bedaquiline through Upregulation of MmpL5 in *Mycobacterium tuberculosis*. *Antimicrobial Agents and Chemotherapy,* 58**,** 2979.

HEIFETS, L. & LINDHOLM-LEVY, P. 1992. Pyrazinamide Sterilizing Activity In Vitro against Semidormant *Mycobacterium tuberculosis* Bacterial Populations. *American Review of Respiratory Disease,* 145**,** 1223-1225.

HENNINOT, A.*, et al.* 2018. The Current State of Peptide Drug Discovery: Back to the Future? *Journal of Medicinal Chemistry,* 61**,** 1382-1414.

HERR, E. B., JR. 1959. Isolation and characterization of a new peptide antibiotic. *Proceedings Indiana Academy of Sciences,* 69**,** 134.

HERR JR., E. B. & REDSTONE, M. O. 1966. CHEMICAL AND PHYSICAL CHARACTERIZATION OF CAPREOMYCIN. *Annals of the New York Academy of Sciences,* 135**,** 940-946.

HUANG, L.*, et al.* 2019. *Mycobacterium tuberculosis*: Bacterial Fitness within the Host Macrophage. *Microbiology Spectrum,* 7.

HUET, G.*, et al.* 2009. A Lipid Profile Typifies the Beijing Strains of Mycobacterium tuberculosis: IDENTIFICATION OF A MUTATION RESPONSIBLE FOR A MODIFICATION OF THE STRUCTURES OF PHTHIOCEROL DIMYCOCEROSATES AND PHENOLIC GLYCOLIPIDS. *The Journal of Biological Chemistry,* 284**,** 27101-27113.

HUNTER, R. L. 2011. Pathology of post primary tuberculosis of the lung: An illustrated critical review. *Tuberculosis,* 91**,** 497-509.

IBRAHIM, S. R. M.*, et al.* 2008. Callyaerin G, a new cytotoxic cyclic peptide from the marine sponge *Callyspongia arizusa*. *ARKIVOC,* 12**,** 164-171.

IBRAHIM, S. R. M.*, et al.* 2010. Callyaerins A–F and H, new cytotoxic cyclic peptides from the Indonesian marine sponge *Callyspongia aerizusa. Bioorganic & Medicinal Chemistry,* 18**,** 4947-4956.

IOERGER, T. R.*, et al.* 2010. Variation among Genome Sequences of H37Rv Strains of *Mycobacterium tuberculosis* from Multiple Laboratories. *Journal of Bacteriology,* 192**,** 3645.

IOERGER, T. R.*, et al.* 2009. Genome Analysis of Multi- and Extensively-Drug-Resistant Tuberculosis from KwaZulu-Natal, South Africa. *PLOS ONE,* 4**,** e7778.

JACKSON, M. 2014. The Mycobacterial Cell Envelope—Lipids. *Cold Spring Harbor Perspectives in Medicine,* 4**,** a021105.

JANKUTE, M.*, et al.* 2015. Assembly of the Mycobacterial Cell Wall. *Annual Review of Microbiology,* 69**,** 405-423.

JO, K.-W.*, et al.* 2014. Risk factors for 1-year relapse of pulmonary tuberculosis treated with a 6-month daily regimen. *Respiratory Medicine,* 108**,** 654-659.

JOHANSEN, S. K.*, et al.* 2006. Capreomycin Binds across the Ribosomal Subunit Interface Using tlyA-Encoded 2′-O-Methylations in 16S and 23S rRNAs. *Molecular Cell,* 23**,** 173-182.

JOHNSSON, K. & SCHULTZ, P. G. 1994. Mechanistic Studies of the Oxidation of Isoniazid by the Catalase Peroxidase from *Mycobacterium tuberculosis*. *Journal of the American Chemical Society,* 116**,** 7425-7426.

JOURNAL, B. M. 1952. Isoniazid in Pulmonary Tuberculosis. *British Medical Journal,* 2**,** 764.

KALSCHEUER, R.*, et al.* 2019. The *Mycobacterium tuberculosis* capsule: a cell structure with key implications in pathogenesis. *Biochemical Journal,* 476**,** 1995.

KAMARIZA, M.*, et al.* 2018. Rapid detection of *Mycobacterium tuberculosis* in sputum with a solvatochromic trehalose probe. *Science Translational Medicine,* 10.

KERANTZAS, C. A. & JACOBS, W. R. 2017. Origins of Combination Therapy for Tuberculosis: Lessons for Future Antimicrobial Development and Application. *mBio,* 8.

KIRSTEIN, J.*, et al.* 2009. The antibiotic ADEP reprogrammes ClpP, switching it from a regulated to an uncontrolled protease. *EMBO Molecular Medicine,* 1**,** 37-49.

KITA, M.*, et al.* 2013. Stylissatin A, a cyclic peptide that inhibits nitric oxide production from the marine sponge *Stylissa massa*. *Tetrahedron Letters,* 54**,** 6826-6828.

KLING, A.*, et al.* 2015. Targeting DnaN for tuberculosis therapy using novel griselimycins. *Science,* 348**,** 1106-1112.

KOLB, H. C.*, et al.* 2001. Click Chemistry: Diverse Chemical Function from a Few Good Reactions. *Angewandte Chemie International Edition,* 40**,** 2004-2021.

LAEMMLI, U. K. 1970. Cleavage of Structural Proteins during the Assembly of the Head of Bacteriophage T4. *Nature,* 227**,** 680-685.

LAMICHHANE, G.*, et al.* 2003. A postgenomic method for predicting essential genes at subsaturation levels of mutagenesis: Application to *Mycobacterium tuberculosis*. *Proceedings of the National Academy of Sciences,* 100**,** 7213.

LAMPRECHT, D. A.*, et al.* 2016. Turning the respiratory flexibility of *Mycobacterium tuberculosis* against itself. *Nature Communications,* 7**,** 12393.

LARSEN, M. H.*, et al.* 2017. Genetic Manipulation of *Mycobacterium tuberculosis*. *Current Protocols in Microbiology,* 6**,** 10A.2.1-10A.2.21.

LEAR, S.*, et al.* 2016. Total chemical synthesis of lassomycin and lassomycin-amide. *Organic & Biomolecular Chemistry,* 14**,** 4534-4541.

LEEKHA, S.*, et al.* 2011. General principles of antimicrobial therapy. *Mayo Clinic proceedings,* 86**,** 156-167.

LEISTIKOW, R. L.*, et al.* 2010. The *Mycobacterium tuberculosis* DosR Regulon Assists in Metabolic Homeostasis and Enables Rapid Recovery from Nonrespiring Dormancy. *Journal of Bacteriology,* 192**,** 1662-1670.

LI F. F. & BRIMBLE M. A. 2019. Using chemical synthesis to optimise antimicrobial peptides in the fight against antimicrobial resistance. *Pure and Applied Chemistry.*

LI, K.*, et al.* 2014. Multitarget Drug Discovery for Tuberculosis and Other Infectious Diseases. *Journal of Medicinal Chemistry,* 57**,** 3126-3139.

LING, L. L.*, et al.* 2015. A new antibiotic kills pathogens without detectable resistance. *Nature,* 517**,** 455-459.

LIU, J.*, et al.* 1996. Mycolic Acid Structure Determines the Fluidity of the Mycobacterial Cell Wall. *Journal of Biological Chemistry,* 271**,** 29545-29551.

LUCA, S. & MIHAESCU, T. 2013. History of BCG Vaccine. *Maedica,* 8**,** 53-58.

LUCIANA, D. G.-L.*, et al.* 2019. New insights on Ethambutol Targets in *Mycobacterium tuberculosis. Infectious Disorders - Drug Targets,* 19**,** 73-80.

MAEURER, M.*, et al.* 2014. Totally-drug-resistant tuberculosis: hype versus hope. *The Lancet Respiratory Medicine,* 2**,** 256-257.

MANJUNATHA, U.*, et al.* 2009. The mechanism of action of PA-824: Novel insights from transcriptional profiling. *Communicative & integrative biology,* 2**,** 215-218.

MARTIN-GÓMEZ, H. & TULLA-PUCHE, J. 2018. Lasso peptides: chemical approaches and structural elucidation. *Organic & Biomolecular Chemistry,* 16**,** 5065-5080.

MATSUMOTO, M.*, et al.* 2006. OPC-67683, a Nitro-Dihydro-Imidazooxazole Derivative with Promising Action against Tuberculosis In Vitro and In Mice. *PLOS Medicine,* 3**,** e466.

MCDERMOTT, W. 1958. Microbial persistence. *The Yale journal of biology and medicine,* 30**,** 257-291.

MCGREGOR, D. P. 2008. Discovering and improving novel peptide therapeutics. *Current Opinion in Pharmacology,* 8**,** 616-619.

MICHALSKI, A.*, et al.* 2012. Ultra high resolution linear ion trap Orbitrap mass spectrometer (Orbitrap Elite) facilitates top down LC MS/MS and versatile peptide fragmentation modes. *Mol Cell Proteomics,* 11**,** O111 013698.

MICHEL, K. H. & KASTNER, R. E. 1985. *A54556 ANTIBIOTICS AND PROCESS FOR PRODUCTION THEREOF*. USA patent application 423,948.

MIKUSOVÁ, K.*, et al.* 1995. Biogenesis of the mycobacterial cell wall and the site of action of ethambutol. *Antimicrobial Agents and Chemotherapy,* 39**,** 2484.

MODOLFLL, J. & VÁZQUEZ, D. 1977. The Inhibition of Ribosomal Translocation by Viomycin. *European Journal of Biochemistry,* 81**,** 491-497.

MOLE, B. 2013. MRSA: Farming up trouble *Nature News,* 499**,** 398-400.

MUKAMOLOVA, G. V.*, et al.* 2002. A family of autocrine growth factors in *Mycobacterium tuberculosis*. *Molecular Microbiology,* 46**,** 623-635.

NATHAN, C. & GOLDBERG, F. M. 2005. The profit problem in antibiotic R&D. *Nature Reviews Drug Discovery,* 4**,** 887-891.

NEWMAN, D. J. & CRAGG, G. M. 2012. Natural Products As Sources of New Drugs over the 30 Years from 1981 to 2010. *Journal of Natural Products,* 75**,** 311-335.

NICHOLS, D.*, et al.* 2010. Use of Ichip for High-Throughput *In Situ* Cultivation of "Uncultivable" Microbial Species. *Applied and Environmental Microbiology,* 76**,** 2445.

NIEMANN, S.*, et al.* 2000. Differentiation among members of the *Mycobacterium tuberculosis* complex by molecular and biochemical features: evidence for two pyrazinamide-susceptible subtypes of M. bovis. *Journal of clinical microbiology,* 38**,** 152-157.

NJIRE, M.*, et al.* 2016. Pyrazinamide resistance in *Mycobacterium tuberculosis*: Review and update. *Advances in Medical Sciences,* 61**,** 63-71.

O'NEILL, J. 2016. TACKLING DRUG-RESISTANT INFECTIONS GLOBALLY: FINAL REPORT AND RECOMMENDATIONS. *THE REVIEW ON ANTIMICROBIAL RESISTANCE*.

OLDFIELD, E. & FENG, X. 2014. Resistance-resistant antibiotics. *Trends in Pharmacological Sciences,* 35**,** 664-674.

OLLINGER, J.*, et al.* 2012. Validation of the Essential ClpP Protease in *Mycobacterium tuberculosis* as a Novel Drug Target. *Journal of Bacteriology,* 194**,** 663.

OLSEN, J. V.*, et al.* 2005. Parts per million mass accuracy on an orbitrap mass spectrometer via lock mass injection into a C-trap. *Molecular & Cellular Proteomics,* 4**,** 2010-2021.

PAI, M.*, et al.* 2014. Gamma Interferon Release Assays for Detection of *Mycobacterium tuberculosis* Infection. *Clinical Microbiology Reviews,* 27**,** 3.

PAI, M.*, et al.* 2016. Tuberculosis Diagnostics: State of the Art and Future Directions. *Microbiology Spectrum,* 4.

PANNEK, S.*, et al.* 2006. Multidrug efflux inhibition in Acinetobacter baumannii: comparison between 1-(1-naphthylmethyl)-piperazine and phenyl-arginine-β-naphthylamide. *Journal of Antimicrobial Chemotherapy,* 57**,** 970-974.

PARK, H.-D.*, et al.* 2003. Rv3133c/dosR is a transcription factor that mediates the hypoxic response of *Mycobacterium tuberculosis*. *Molecular Microbiology,* 48**,** 833-843.

PETTIT, G. R.*, et al.* 1990. Antineoplastic agents. 193. Isolation and structure of the cyclic peptide hymenistatin 1. *Canadian Journal of Chemistry,* 68**,** 708-711.

PHILLIPS, C. J. C.*, et al.* 2003. The transmission of *Mycobacterium bovis* infection to cattle. *Research in Veterinary Science,* 74**,** 1-15.

PIETERS, J. 2008. *Mycobacterium tuberculosis* and the Macrophage: Maintaining a Balance. *Cell Host & Microbe,* 3**,** 399-407.

PŁOCIŃSKI, P.*, et al.* 2014. Identification of Protein Partners in Mycobacteria Using a Single-Step Affinity Purification Method. *PLoS ONE,* 9**,** e91380.

PONTALI, E.*, et al.* 2017. Cardiac safety of bedaquiline: a systematic and critical analysis of the evidence. *European Respiratory Journal,* 50**,** 1701462.

PORTEVIN, D.*, et al.* 2011. Human Macrophage Responses to Clinical Isolates from the *Mycobacterium tuberculosis* Complex Discriminate between Ancient and Modern Lineages. *PLOS Pathogens,* 7**,** e1001307.

PREISS, L.*, et al.* 2015. Structure of the mycobacterial ATP synthase F_0 rotor ring in complex with the anti-TB drug bedaquiline. *Science Advances,* 1**,** e1500106.

QUAN, D.*, et al.* 2017. New tuberculosis drug leads from naturally occurring compounds. *International Journal of Infectious Diseases,* 56**,** 212-220.

QUEVAL, C. J.*, et al.* 2017. The Macrophage: A Disputed Fortress in the Battle against *Mycobacterium tuberculosis*. *Frontiers in Microbiology,* 8.

RAGHUNANDANAN, S.*, et al.* 2018. Dormant *Mycobacterium tuberculosis* converts isoniazid to the active drug in a Wayne's model of dormancy. *The Journal of Antibiotics,* 71**,** 939-949.

RAJA, A.*, et al.* 2003. Daptomycin. *Nature Reviews Drug Discovery,* 2**,** 943-944.

RAMASWAMY, S. V.*, et al.* 2003. Single Nucleotide Polymorphisms in Genes Associated with Isoniazid Resistance in *Mycobacterium tuberculosis*. *Antimicrobial Agents and Chemotherapy,* 47**,** 1241.

RAPPSILBER, J.*, et al.* 2007. Protocol for micro-purification, enrichment, pre-fractionation and storage of peptides for proteomics using StageTips. *Nature Protocols,* 2**,** 1896-1906.

RAWAT, R.*, et al.* 2003. The isoniazid-NAD adduct is a slow, tight-binding inhibitor of InhA, the *Mycobacterium tuberculosis* enoyl reductase: Adduct affinity and drug resistance. *Proceedings of the National Academy of Sciences of the United States of America,* 100**,** 13881-13886.

REHBERG, N.*, et al.* 2018. Chlorflavonin Targets Acetohydroxyacid Synthase Catalytic Subunit IlvB1 for Synergistic Killing of *Mycobacterium tuberculosis*. *ACS Infectious Diseases,* 4**,** 123-134.

REYRAT, J. M.*, et al.* 1995. The urease locus of *Mycobacterium tuberculosis* and its utilization for the demonstration of allelic exchange in *Mycobacterium bovis* bacillus Calmette-Guérin. *Proceedings of the National Academy of Sciences of the United States of America,* 92**,** 8768-8772.

RICHTER, M. F.*, et al.* 2017. Predictive compound accumulation rules yield a broad-spectrum antibiotic. *Nature,* 545**,** 299-304.
ROSENKRANDS, I.*, et al.* 2002. Hypoxic Response of *Mycobacterium tuberculosis* Studied by Metabolic Labeling and Proteome Analysis of Cellular and Extracellular Proteins. *Journal of Bacteriology,* 184**,** 3485-3491.
ROTH, M. G. 2004. Phosphoinositides in Constitutive Membrane Traffic. *Physiological Reviews,* 84**,** 699-730.
ROZWARSKI, D. A.*, et al.* 1998. Modification of the NADH of the Isoniazid Target (InhA) from *Mycobacterium tuberculosis*. *Science,* 279**,** 98.
RUIZ, P.*, et al.* 2002. Investigation of the In Vitro Activity of Streptomycin Against *Mycobacterium tuberculosis*. *Microbial Drug Resistance,* 8**,** 147-149.
SAKULA, A. 1983. Robert koch: centenary of the discovery of the tubercle bacillus, 1882. *The Canadian veterinary journal = La revue veterinaire canadienne,* 24**,** 127-131.
SASSETTI, C. M.*, et al.* 2003. Genes required for mycobacterial growth defined by high density mutagenesis. *Molecular Microbiology,* 48**,** 77-84.
SCHATZ, A.*, et al.* 1944. Streptomycin, a Substance Exhibiting Antibiotic Activity Against Gram-Positive and Gram-Negative Bacteria.∗†. *Proceedings of the Society for Experimental Biology and Medicine,* 55**,** 66-69.
SCHMITZ, F. J.*, et al.* 1993. Antitumor and Cytotoxic Compounds from Marine Organisms. *In:* ATTAWAY, D. H. & ZABORSKY, O. R. (eds.) *Pharmaceutical and Bioactive Natural Products.* Boston, MA: Springer US.
SCHWARTZ, J. A. 1957. Comparative Efficacy of the Concurrent Use of Pyrazinamide and Isoniazid with That of Other Forms of Therapy in the Treatment of Pulmonary Tuberculosis. *Diseases of the Chest,* 32**,** 455-459.
SCORPIO, A. & ZHANG, Y. 1996. Mutations in pncA, a gene encoding pyrazinamidase/nicotinamidase, cause resistance to the antituberculous drug pyrazinamide in tubercle bacillus. *Nature Medicine,* 2**,** 662-667.
SELVARAJ, S.*, et al.* 2012. In silico analysis of DosR regulon proteins of *Mycobacterium tuberculosis*. *Gene,* 506**,** 233-241.
SENSI, P. 1983. History of the Development of Rifampin. *Reviews of Infectious Diseases,* 5**,** S402-S406.
SHARPE, M. L.*, et al.* 2008. The Structure and Unusual Protein Chemistry of Hypoxic Response Protein 1, a Latency Antigen and Highly Expressed Member of the DosR Regulon in *Mycobacterium tuberculosis*. *Journal of Molecular Biology,* 383**,** 822-836.
SHENOI, S. & FRIEDLAND, G. 2009. Extensively drug-resistant tuberculosis: a new face to an old pathogen. *Annual review of medicine,* 60**,** 307-20.
SILVE, G.*, et al.* 1993. Ethambutol inhibition of glucose metabolism in mycobacteria: a possible target of the drug. *Antimicrobial Agents and Chemotherapy,* 37**,** 1536.
SILVER, L. L. 2007. Multi-targeting by monotherapeutic antibacterials. *Nature Reviews Drug Discovery,* 6**,** 41-55.
SIMEONE, R.*, et al.* 2012. Phagosomal Rupture by *Mycobacterium tuberculosis* Results in Toxicity and Host Cell Death. *PLOS Pathogens,* 8**,** e1002507.
SINGH, S. B.*, et al.* 2017. What is an “ideal” antibiotic? Discovery challenges and path forward. *Biochemical Pharmacology,* 133**,** 63-73.
ŠKOVIEROVÁ, H.*, et al.* 2009. AftD, a novel essential arabinofuranosyltransferase from mycobacteria. *Glycobiology,* 19**,** 1235-1247.
SLAYDEN, R. A.*, et al.* 1996. Antimycobacterial action of thiolactomycin: an inhibitor of fatty acid and mycolic acid synthesis. *Antimicrobial agents and chemotherapy,* 40**,** 2813-2819.
STANLEY, R. E.*, et al.* 2010. The structures of the anti-tuberculosis antibiotics viomycin and capreomycin bound to the 70S ribosome. *Nature Structural & Molecular Biology,* 17**,** 289-293.

STEINGART, K. R., *et al.* 2006. Fluorescence versus conventional sputum smear microscopy for tuberculosis: a systematic review. *The Lancet Infectious Diseases,* 6**,** 570-581.

STOVER, C. K., *et al.* 2000. A small-molecule nitroimidazopyran drug candidate for the treatment of tuberculosis. *Nature,* 405**,** 962-966.

SUN, C., *et al.* 2017. *Mycobacterium tuberculosis* hypoxic response protein 1 (Hrp1) augments the pro-inflammatory response and enhances the survival of Mycobacterium smegmatis in murine macrophages. *Journal of Medical Microbiology,* 66**,** 1033-1044.

SWARTS, B. M., *et al.* 2012. Probing the Mycobacterial Trehalome with Bioorthogonal Chemistry. *Journal of the American Chemical Society,* 134**,** 16123-16126.

TACCONELLI, E., *et al.* 2018. Discovery, research, and development of new antibiotics: the WHO priority list of antibiotic-resistant bacteria and tuberculosis. *The Lancet Infectious Diseases,* 18**,** 318-327.

TAKAYAMA, K., *et al.* 1973. Scanning Electron Microscopy of the H37Ra Strain of *Mycobacterium tuberculosis* Exposed to Isoniazid. *Antimicrobial Agents and Chemotherapy,* 4**,** 62.

TELENTI, A., *et al.* 1993. Detection of rifampicin-resistance mutations in *Mycobacterium tuberculosis. The Lancet,* 341**,** 647-651.

TERLAIN, B. & THOMAS, J. P. 1971. Structure of griselimycin, polypeptide antibiotic extracted Streptomyces cultures. I. Identification of the products liberated by hydrolysis. *Bulletin de la Societe chimique de France,* 6**,** 2349-2356.

THARAD, M., *et al.* 2011. A Three-Hybrid System to Probe In Vivo Protein-Protein Interactions: Application to the Essential Proteins of the RD1 Complex of *M. tuberculosis. PLOS ONE,* 6**,** e27503.

THOMAS, J. P., *et al.* 1961. A New Synthetic Compound with Antituberculous Activity in Mice: Ethambutol (Dextro-2, 2′- (Ethylenediimino)-di-1-Butanol). *American Review of Respiratory Disease,* 83**,** 891-893.

TORFS, E., *et al.* 2019. Opportunities for Overcoming *Mycobacterium tuberculosis* Drug Resistance: Emerging Mycobacterial Targets and Host-Directed Therapy. *International journal of molecular sciences,* 20**,** 2868.

TYANOVA, S., *et al.* 2016. The Perseus computational platform for comprehensive analysis of (prote)omics data. *Nat Methods,* 13**,** 731-40.

UNITAID 2017. Tuberculosis: Diagnostics Technology Landscape. *In:* WHO (ed.) 5 ed.

VALL-SPINOSA, A., *et al.* 1970. Rifampin in the Treatment of Drug-Resistant Mycobacterium tuberculosis Infections. *New England Journal of Medicine,* 283**,** 616-621.

VELAYATI, A. A., *et al.* 2013. The totally drug resistant tuberculosis (TDR-TB). *International journal of clinical and experimental medicine,* 6**,** 307-309.

VELAYATI, A. A., *et al.* 2009. Emergence of New Forms of Totally Drug-Resistant Tuberculosis Bacilli: Super Extensively Drug-Resistant Tuberculosis or Totally Drug-Resistant Strains in Iran. *Chest,* 136**,** 420-425.

VENTOLA, C. L. 2015. The antibiotic resistance crisis: part 1: causes and threats. *P & T : a peer-reviewed journal for formulary management,* 40**,** 277-283.

VEYRIER, F. J., *et al.* 2011. The rise and fall of the *Mycobacterium tuberculosis* genome. *Trends in Microbiology,* 19**,** 156-161.

VILCHÈZE, C., *et al.* 2013. *Mycobacterium tuberculosis* is extraordinarily sensitive to killing by a vitamin C-induced Fenton reaction. *Nature communications,* 4**,** 1881-1881.

VILCHÈZE, C. & JACOBS, W. R. 2019. The Isoniazid Paradigm of Killing, Resistance, and Persistence in *Mycobacterium tuberculosis*. *Journal of Molecular Biology*.

VOSS, A., *et al.* 2005. Methicillin-resistant *Staphylococcus aureus* in pig farming. *Emerging infectious diseases,* 11**,** 1965-1966.

WAKSMAN, S. 1956. Definition of antibiotics. *Antibiotic Med Clin Ther (New York)*

WAKSMAN, S. A. & WOODRUFF, H. B. 1941. Actinomyces antibioticus, a New Soil Organism Antagonistic to Pathogenic and Non-pathogenic Bacteria. *Journal of bacteriology,* 42**,** 231-249.

WAKSMAN, S. A. & WOODRUFF, H. B. 1942. Streptothricin, a New Selective Bacteriostatic and Bactericidal Agent, Particularly Active Against Gram-Negative Bacteria. *Proceedings of the Society for Experimental Biology and Medicine,* 49**,** 207-210.

WANG, Y.*, et al.* 2010. Global Protein−Protein Interaction Network in the Human Pathogen *Mycobacterium tuberculosis* H37Rv. *Journal of Proteome Research,* 9**,** 6665-6677.

WEHRLI, W. & STAEHELIN, M. 1971. Actions of the rifamycins. *Bacteriological reviews,* 35**,** 290-309.

WHO 2013. The use of bedaquiline in the treatment of multidrug-resistant tuberculosis.

WHO 2015. Implementing the end TB strategy: the essentials

WHO 2016. The use of delamanid in the treatment of multidrug-resistant tuberculosis in children and adolescents.

WHO 2019a. Global Tuberculosis Report

WHO 2019b. The Selection and Use of Essential Medicines - Report of the 22nd WHO Expert Committee.

WHO 2019c. WHO consolidated guidelines on drug-resistant tuberculosis treatment.

WINDER, F. G. A.*, et al.* 1970. Effects of isoniazid on mycolic acid synthesis in *Mycobacterium tuberculosis* and on its cell envelope. *Biochemical Journal,* 117**,** 27P.

WOHLLEBEN, W.*, et al.* 2016. Antibiotic drug discovery. *Microbial Biotechnology,* 9**,** 541-548.

WRIGHT, M. H. & SIEBER, S. A. 2016. Chemical proteomics approaches for identifying the cellular targets of natural products. *Natural Product Reports,* 33**,** 681-708.

XIE, H.*, et al.* 2012. Rapid point-of-care detection of the tuberculosis pathogen using a BlaC-specific fluorogenic probe. *Nature Chemistry,* 4**,** 802-809.

XU, W.*, et al.* 2017. Chemical Genetic Interaction Profiling Reveals Determinants of Intrinsic Antibiotic Resistance in Mycobacterium tuberculosis. *Antimicrobial Agents and Chemotherapy,* 61.

YEAGER, R. L.*, et al.* 1952. Pyrazinamide (Aldinamide) in the Treatment of Pulmonary Tuberculosis. *American Review of Tuberculosis,* 65**,** 523-546.

ZHANG, M.*, et al.* 2019a. Anti-inflammatory marine cyclic peptide stylissatin A and its derivatives inhibit differentiation of murine preadipocytes. *Chemical Communications,* 55**,** 5471-5474.

ZHANG, S.*, et al.* 2018. Total Synthesis and Conformational Study of Callyaerin A: Anti-Tubercular Cyclic Peptide Bearing a Rare Rigidifying (Z)-2,3- Diaminoacrylamide Moiety. *Angewandte Chemie,* 130**,** 3693-3697.

ZHANG, S.*, et al.* 2019b. Naturally occurring antitubercular cyclic peptides. *Tetrahedron Letters***,** 151339.

ZIMHONY, O.*, et al.* 2007. Pyrazinoic Acid and *n*-Propyl Ester Inhibit Fatty Acid Synthase Type I in Replicating Tubercle Bacilli. *Antimicrobial Agents and Chemotherapy,* 51**,** 752.

ZONG, Y.*, et al.* 2019. Gram-scale total synthesis of teixobactin promoting binding mode study and discovery of more potent antibiotics. *Nature Communications,* 10**,** 3268.

List of Figures

List of Tables

Contribution to other studies

Minor contributions not described in this thesis have been made to the following publications:

Zaschke-Kriesche, J., Behrmann, L.V., Reiners, J., Lagedroste, M., **Gröner, Y.**, Kalscheuer, R., Smits, S.H. (2019). Bypassing lantibiotic resistance by an effective nisin derivative, Bioorganic and Medicinal Chemistry 27:3454-3462

Ariantari, N. P., Ancheeva, E., Frank, M., Stuhldreier, F., Meier, D., **Gröner, Y.**, Reimche, I., Teusch, N., Wesselborg, S., Muller, W.E.G., Kalscheuer, R., Liu, Z., Proksch, P. (2020). Didymellanosine, a new decahydrofluorene analogue, and ascolactone C from *Didymella* sp. IEA-3B.1, an endophyte of *Terminalia catappa*, RSC Advances 10:7232-7240

Eidesstattliche Erklärung

Ich versichere an Eides Statt, dass die Dissertation von mir selbständig und ohne unzulässige fremde Hilfe unter Beachtung der „Grundsätze zur Sicherung guter wissenschaftlicher Praxis an der Heinrich-Heine-Universität Düsseldorf“ erstellt worden ist.

Düsseldorf, den

Yvonne Gröner

Acknowledgment

First, I would like to express my honest gratitude to Prof. Dr. Rainer Kalscheuer for offering the opportunity for my PhD thesis and for providing such a significant topic. Thank you for your support, for sharing inspiring ideas and all your expertise and for placing your trust in my work.

Likewise, I would like to thank Prof. Dr. Dr. h. c. Peter Proksch for being my co-supervisor, for his commitment to the GRK2158 and for sharing his passion for natural products.

My most profound thanks to Prof. Dr. Markus Kaiser, Florian Schulz and David Podlesainski for such a successful cooperation. Thank you for providing a major contribution to this work.

I am very thankful for being part of the DFG-funded research training group GRK2158. Thanks to all the colleagues for creating such an inspiring scientific environment and for all the opportunities offered by the GRK2158.

Sincere thanks to Dr. Sander Smith and Stefanie Kobus at the CSS for a fruitful cooperation.

To the whole research group in the Kalscheuer lab: thank you for creating an inspiring and pleasant working atmosphere. Major ‘gratefulness in nuts’ to Anna-Lene Ilse Rosemarie ‘Rosie’ Kiffe-Delf, Lasse van Geelen, Steffen Schindler, Dieter Meier, Karina Wolf and Nidja Rehberg. Thank you for not only being colleagues but friends.

Thanks to Prof. Dr. Heiner Schaal and Björn Wefers for all their help and organization in the S3 laboratory.

To my beloved family, significant other and friends: my deepest gratitude for your endless support, for giving hope and for covering my back. Thank you.